Modeling second generation FLIR sensor detection recognition and identification range with polarization filtering

Yildirim, Mehmet

Monterey, California. Naval Postgraduate School

NAVAL POSTGRADUATE SCHOOL
Monterey, California

THESIS

MODELING SECOND GENERATION FLIR SENSOR DETECTION RECOGNITION AND IDENTIFICATION RANGE WITH POLARIZATION FILTERING

by

Mehmet Yildirim

December 2000

Thesis Advisor: Alfred W. Cooper
Second Reader: Ron J. Pieper

Approved for public release; distribution is unlimited.

REPORT DOCUMENTATION PAGE

Form Approved OMB No. 0704-0188

1. AGENCY USE ONLY *(Leave blank)*	2. REPORT DATE	3. REPORT TYPE AND DATES COVERED
	December 2000	Master's Thesis

4. TITLE AND SUBTITLE
Modeling Second Generation FLIR Sensor Detection Recognition and Identification Range With Polarization Filtering.

5. FUNDING NUMBERS

6. AUTHOR(S)
Yildirim, Mehmet.

7. PERFORMING ORGANIZATION NAME(S) AND ADDRESS(ES)
Naval Postgraduate School
Monterey, CA 93943-5000

8. PERFORMING ORGANIZATION REPORT NUMBER

9. SPONSORING / MONITORING AGENCY NAME(S) AND ADDRESS(ES)

10. SPONSORING / MONITORING AGENCY REPORT NUMBER

11. SUPPLEMENTARY NOTES
The views expressed in this thesis are those of the author and do not reflect the official policy or position of the Department of Defense or the U.S. Government.

12a. DISTRIBUTION / AVAILABILITY STATEMENT
Approved for public release; distribution unlimited.

12b. DISTRIBUTION CODE

13. ABSTRACT (maximum 200 words)

The influence of polarization filtering on maximum detection, recognition, and identification ranges of a generic second generation FLIR sensor is examined with a computational model. The scenario studied represents a second generation FLIR sensor mounted on an aircraft in level flight at 300m approaching a ship target. The target ship radiant signature is modeled with an advanced infrared signature prediction program, MuSES (Multi-Service Electro-Optic Signature). A weather file representative of Midlatitude Summer at sea conditions was utilized. Polarized sea background and path radiance calculations are performed with a polarized version of the SEARAD Radiance and Propagation Code. Results showed that there is an improvement in maximum range of the sensor for detection, recognition, and identification tasks when a horizontal filter is included, provided that the target does not have a negative degree of polarization. For detection task the improvements were found to be 33.48%, 35.65%, and 39.78% when the target has 0%, +2%, and +8% degree of polarization respectively. A better modeling of Apparent Temperature Difference (ATD) calculation is also developed. To improve the model use of polarized target model is recommended.

14. Subject Terms
Thermal Imaging Systems, Minimum Resolved Temperature Difference, Polarization Filters.

15. NUMBER OF PAGES
166

16. PRICE CODE

17. SECURITY CLASSIFICATION OF REPORT	18. SECURITY CLASSIFICATION OF THIS PAGE	19. SECURITY CLASSIFICATION OF ABSTRACT	20. LIMITATION OF ABSTRACT
Unclassified	Unclassified	Unclassified	UL

NSN 7540-01-280-5500

Standard Form 298 (Rev. 2-89)
Prescribed by ANSI Std. 239-18298-102

THIS PAGE INTENTIONALLY LEFT BLANK

Approved for pubic release; distribution is unlimited

MODELING SECOND GENERATION FLIR SENSOR DETECTION RECOGNITION AND IDENTIFICATION RANGE WITH POLARIZATION FILTERING

Mehmet Yildirim
1st Lieutenant, Turkish Army
B.S., Turkish War Academy, 1993

Submitted in partial fulfillment of the
requirements for the degree of

MASTER OF SCIENCE IN APPLIED PHYSICS

from the

NAVAL POSTGRADUATE SCHOOL
December 2000

THIS PAGE INTENTIONALLY LEFT BLANK

ABSTRACT

The influence of polarization filtering on maximum detection, recognition, and identification ranges of a generic second generation FLIR sensor is examined with a computational model. The scenario studied represents a second generation FLIR sensor mounted on an aircraft in level flight at 300m approaching a ship target. The target ship radiant signature is modeled with an advanced infrared signature prediction program, MuSES (Multi-Service Electro-Optic Signature). A weather file representative of Midlatitude Summer at sea conditions was utilized. Polarized sea background and path radiance calculations are performed with a polarized version of the SEARAD Radiance and Propagation Code. Results showed that there is an improvement in maximum range of the sensor for detection, recognition, and identification tasks when a horizontal filter is included, provided that the target does not have a negative degree of polarization. For detection task the improvements were found to be 33.48%, 35.65%, and 39.78% when the target has 0%, +2%, and +8% degree of polarization respectively. A better modeling of Apparent Temperature Difference (ATD) calculation is also developed. To improve the model use of polarized target model is recommended.

THIS PAGE INTENTIONALLY LEFT BLANK

TABLE OF CONTENTS

ACKNOWLEDGEMENTS

This research has been supported in part by Naval Sea Systems Command PEO-TSC SEA-53, RADM Mathis.

First of all, I owe many thanks to my advisor, Professor A.W. Cooper for his patience, knowledge, and consultation. The success of this project is largely due to his support. I will always be grateful to him for his generosity, support, and most of all for his friendship.

My special thanks to Professor Ron J. Pieper for his patience and for proofreading this work. I would like to thank the professors in Department of Physics who helped me a lot during my time here at Naval Postgraduate School.

I also would like to thank Turkish Land Forces Command for giving me the opportunity to attend the Naval Postgraduate School, study for this degree, and to serve my country.

Most important, I wish to thank my beloved wife Hulya who always inspired and motivated me for success showing a great patience, time and understanding.

Finally, I dedicate this thesis to my wife and our beautiful baby Bersan Yildirim, who was born during the writing of this thesis and brought happiness to our family.

THIS PAGE INTENTIONALLY LEFT BLANK

I. INTRODUCTION

Infrared systems have been a powerful technique to detect objects in a remote and passive way for some decades. The absence of an active source to perform detection makes this mechanism widely suited for military application. Due to the large number of potential applications, intensive scientific and technological efforts have been made to improve the performance of these systems.

Thermal imaging systems respond to a difference in radiant exitance between a target and its background. They are mostly sensitive enough to detect weak targets, but background radiation hampers the process, making detection difficult. Proper modeling of background and target characteristics is considered as a key factor to develop a successful target detection technique. One such promising model is use of properly polarized filters in sensors for background radiance suppression.

The phenomenon of polarization in the infrared has important potential applications for cueing and detecting targets in forward looking imagery by improving the target-to-background contrast. Previous experiments and analysis

done at the Naval Postgraduate School have shown that sea surface radiance has a vertically polarized characteristic, particularly at viewing angles within a few degrees of the horizon. [Ref. 1, 16]. As a consequence of these studies the concept of improvement in target-to-clutter background contrast ratio by implementing polarization filters gained interest. However having a polarized filter in the sensor also effects the incoming radiation from a target, which may have apparent polarized features.

The main objectives of this project are to determine the effect of degree of polarization on maximum range performance analysis using an advanced signature prediction model, and also to verify previous project results and models which have studied target-background contrast improvement using horizontal polarizers on sensors. In Chapter II some fundamentals of infrared theory are presented. Chapter III is dedicated to background-target radiation theory and polarization theory. In this Chapter beginning from the basic radiation theories, all the known effects, such as environmental radiation components, are studied. The polarization effect on background and target signatures is also studied in detail.

In Chapter IV descriptions of the scenario and the model are given and using the MuSES (Multi-Service Electro-Optic Signature)[Ref. 25] infrared signature prediction program, target signatures for the appropriate conditions are computed.

In Chapter V, computations of Minimum Resolvable Temperature Difference (MRTD) of a second-generation sensor, Apparent Temperature Difference (ATD) between target and background, and sea background radiance are made. Following definition of the degree of polarization, the effect of polarization is included into the overall computations. Having these results, maximum range analysis for a second-generation FLIR (Forward Looking Infrared System) sensor with a horizontally polarized filter is performed by plotting the MRTD and ATD values on the same graph. Finally conclusions and recommendations are provided in Chapter VI.

THIS PAGE INTENTIONALLY LEFT BLANK

II. INFRARED TECHNOLOGY FUNDAMENTALS

This Chapter summarizes the basic infrared theory that includes some important points necessary for full understanding of this work.

A. ELECTROMAGNETIC SPECTRUM

The propagation of electromagnetic energy can be described in terms of spatial and temporal variations in electric and magnetic fields. Typical examples of electromagnetic waves are light rays, radio waves, radar beams and infrared radiation. The optical radiation covers the electromagnetic spectrum from the Ultraviolet (UV) range throughout the visible and up to the Infrared (IR) portion of the spectrum. Figure 2.1 shows the regions of the spectrum.

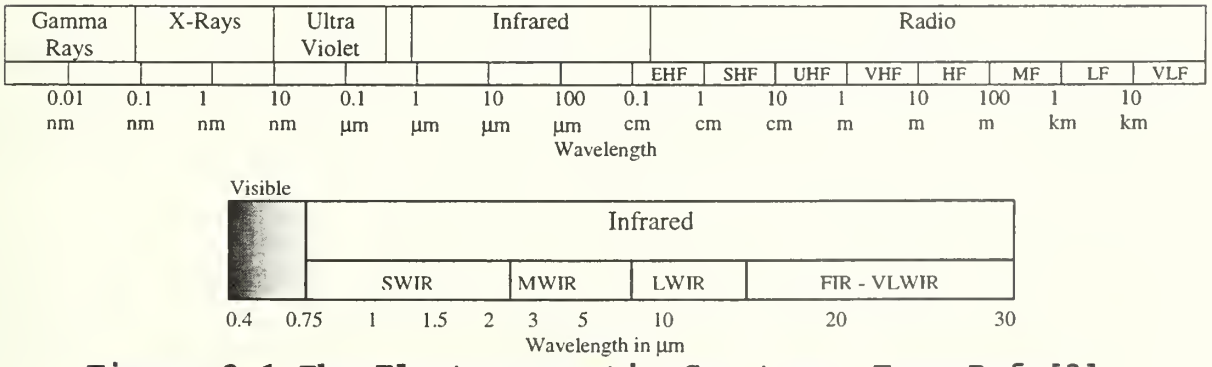

Figure 2.1 The Electromagnetic Spectrum. From Ref.[3].

The infrared portion of the spectrum lies between the visible (shorter wavelength) and the radio frequency (longer wavelength) regions. This region corresponds to the range of wavelengths from approximately 0.7μm to 1000μm. The near infrared (NIR) is characterized by wavelengths from 0.7μm to 0.9μm, and the short-wave infrared (SWIR) is characterized by wavelengths from 0.9μm to 3.0μm. Since the short-wave band includes mostly reflected radiation it can be imaged with night vision devices that collect and amplify the reflected light waves. The mid-wave (MWIR) is characterized by wavelengths from 3.0μm to 6.0μm and the long-wave infrared (LWIR) characterized by wavelengths from 6.0μm to 15.0μm. The long-wave band is called the "thermal radiation region" because thermal emission is greater than the reflection in these wavelengths. Due to this characteristic of the mid-wave and long-wave bands, thermal imaging systems such as FLIR (Forward Looking Infrared System), IRLS (Infrared Line Scan), and IRST (Infrared Search and Track) work in these bands.

The factors such as the form of the radiation, methods of detection, and the atmospheric transmission mostly determine these sub-bands. The region from 5μm to 8μm is

also a part of the infrared spectrum, but it is not used due to the high absorption of the atmosphere in this area.

The infrared radiation complies with the laws of electromagnetism, as stated by Maxwell's Equations.

B. INFRARED DEFINITIONS AND UNITS

Since infrared science makes use of many specific definitions and uses varied units, it is necessary to introduce a terminology for the sake of better understanding. Table 2.1 shows some fundamental radiometric quantities and units associated with infrared radiation. In this table:

- Radiant exitance (emittance) or flux density, M, is the radiant flux density leaving the target surface per unit area.
- Irradiance or radiant flux surface density, E, is the radiant power incident on a unit area of surface.
- Radiant intensity, I, is the radiant power exiting a point source along a given direction within a unit solid angle.
- Radiance, or radiant intensity surface density in a given direction, L, is the radiant power per unit

solid angle per unit area leaving from or incident on an area projected perpendicular to the direction of radiant energy flow.

- In table U represents radiant energy, S represents surface area, and Ω (sr) represents solid angle.

Symbol	Quantity	Units(metric)	Description
U	Radiant Energy	Joules	---
P	Radiant Power	Watts	$\partial U/\partial t$
M	Radiant Exitance	Watt/cm^2	$\partial P/\partial S$
E	Radiant Incidance	Watt/cm^2	$\partial P/\partial S$
I	Radiant Intensity	Watt/sr	$\partial P/\partial \Omega$
L	Radiance	Watt/cm^2 sr	$\partial^2 P/(\partial S \partial \Omega)$

Table 2.1 Radiometric Quantities.

C. LAWS OF THERMAL RADIATION

1. Blackbody Radiation

When we consider the total optical power that is incident on a object, we can distinguish three distinct outcomes. Some fraction of this total radiant energy is absorbed, some is reflected and some is transmitted through the object. Therefore the ratios of each of these to the incident power must add up to unity. [Ref. 4]

$$\alpha + \rho + \tau = 1 \tag{2.5}$$

where:

α (absorptivity) = $P_{absorbed}/P_{incident}$

ρ (reflectivity) = $P_{reflected}/P_{incident}$

τ (transmissivity) = $P_{transmitted}/P_{incident}$

An ideal blackbody can be defined as an ideal emitter and an ideal absorber i.e. absorptivity(α)=emissivity(ε)=1. Thus the blackbody has a reflectivity (ρ) and transmissivity (τ) both of zero. The blackbody radiator is an idealized source of radiant energy having defined properties. It is perfectly diffuse, radiates at all wavelengths, and at all temperatures its spectral radiant exitance is the maximum possible for any actual thermal source at the same temperature. The characteristics of many real sources of radiation approach the ideal quite closely; many others are conveniently described by corrections to the blackbody curve.[Ref. 2] The spectral radiant exitance of a blackbody

is presented in Figure 2.2, as a function of wavelength and source temperature.

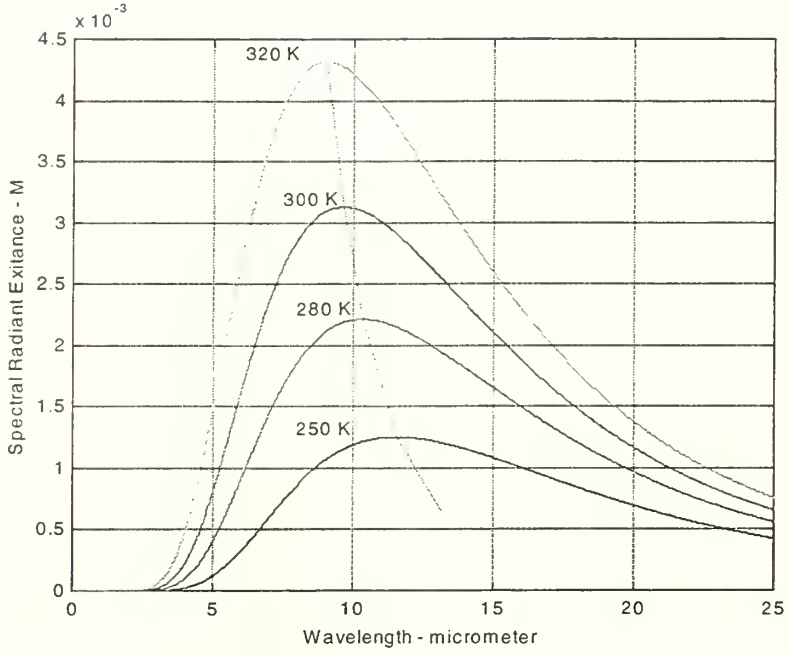

Figure 2.2 Spectral Radiant Exitance of Blackbodies at Various Temperatures. Dotted Curve Represents the Displacement Law. From Ref.[23].

2. Planck's Law

The equation that represents a blackbody's spectral exitance as a function of its temperature is known as Planck's Radiation Law and has the following form:

$$M_{\lambda,b} = \frac{2\pi hc^2}{\lambda^5\left(e^{hc/\lambda kT} - 1\right)} \times 10^{-6} \qquad (2.6)$$

where:

$M_{\lambda,b}$ = the blackbody spectral radiant exitance at wavelength λ (Watt/m^2 μm)

c = The vacuum velocity of light (2.9979250×10^8 m/s)

h = Planck's constant (6.626196×10^{-34} Joule/s)

k = Boltzmann's constant (1.380622×10^{-23} Joule/K)

T = Absolute temperature of the blackbody (K)

λ = Wavelength (m)

In infrared theory the radiant exitance is directly proportional to the emissivity. The "emissivity", ε, of a surface is the ratio of radiant exitance emitted from a surface to that emitted from a blackbody (perfect emitter) at the same temperature. The radiant exitance of a non blackbody then can be defined as

$$M_\lambda = \varepsilon_\lambda M_{\lambda,b} \qquad (2.7)$$

where ε_λ is the spectral emissivity which is always less than 1 for non-black bodies. [Ref. 2] A material which has an emissivity that is independent of wavelength is called a gray body. Table 2.2 shows emissivities of some common materials.

gray body. Table 2.2 shows emissivities of some common materials.

Material	ε
Aluminum Foil	0.09
Copper,polished	0.05
Copper,oxidized	0.78
Carbon	0.95
Paint,oil	0.94
Concrete	0.92
Sand	0.90

Table 2.2 Emissivities (ε) of Common Materials. From Ref.[4].

3. Wien Displacement and Stefan-Boltzmann Laws

Figure 2.2 shows blackbody curves in terms of the radiant exitance as a function of wavelength for a number of different temperatures, each one of higher temperature completely above the others. The wavelength of the peaks, i.e. the wavelengths where the maximum radiation occurs for a given temperature, can be found from the equation known as the Wien Displacement Law,

$$\lambda_{max} = \frac{2898}{T} \qquad (2.8)$$

where:
λ_{max} = wavelength where the peak of radiation occurs (μm).

The peak wavelength in micrometers is approximately 3000 divided by the temperature in Kelvin.

The Planck curve can be integrated to obtain the expression for total radiant exitance at all wavelengths.

$$W_b = \sigma T^4 \qquad (2.9)$$

where:

W_b = Total radiant exitance of a blackbody

σ = The Stefan-Boltzmann constant (5.6691 X 10^{-8} Watts/m^2K^4)

T = The temperature in K

For use with non-black body sources this law is modified by the inclusion of an "effective emissivity", ε, giving the form

$$W_b = \varepsilon \sigma T^4 \qquad (2.10)$$

This equation is known as the Stefan-Boltzmann Law.

D. ATMOSPHERIC PROPAGATION OF INFRARED RADIATION

The earth's atmosphere consists of different molecules and suspended particles. When infrared radiation passes through the atmosphere these molecules and suspended particles both absorb and scatter radiation. The degree and type of the attenuation depend on the properties of the

atmosphere and the distance between the source of the radiation and the receiver.

The gases and particles suspended in the path may themselves radiate. This path radiance and its fluctuations may "blur" the scene and reduce the contrast. Scattering agents in the path may also deflect or scatter radiation from other sources in such a way that the source radiance appears to be increased. [Ref. 7]

The two main causes of atmospheric attenuation of infrared radiation, however, are absorption by molecules in the atmosphere and scattering due to particles suspended in the path. Beer's law quantifies the total attenuation at any wavelength by the atmosphere as:

$$I_z = I_o e^{-\mu z} \tag{2.11}$$

where

- I_o is the initial radiant intensity
- I_z is the radiant intensity of radiation after propagation distance z in the atmosphere
- μ is the extinction coefficient of atmosphere, which is defined as the sum of absorption and scattering coefficients
- z is propagation distance

1. Absorption

Absorption of radiation within the atmosphere can occur in electronic, vibrational or rotational transitions. Transitions between electronic states in an atom generally take place in the visible or ultraviolet region of the spectrum. Infrared molecular absorption is due to transitions between vibrational and/or rotational energy states of a gas molecule. [Ref. 5]

Since the atmosphere contains many different particles and behaves in a dynamic way it is not very easy to predict the extinction coefficient and transmittance. An accurate atmospheric transmission calculation requires that all molecular, aerosol, and precipitation effects be taken into account. When exact results are required a detailed model must be used. In infrared technology computer models such as the LOWTRAN, MODTRAN, FASCODE and the SEARAD Radiance Models are used to compute the extinction coefficient and transmittance.

In this project the latest version of MODTRAN4 and the SEARAD Radiance Model are used for transmittance, path radiance, and background radiance calculations. An example of transmittance values obtained for a 1-km path length is shown in Figure 2.3.

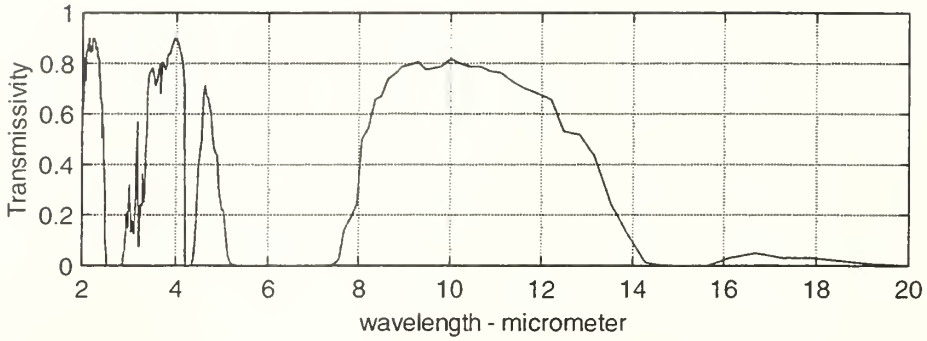

Figure 2.3 Typical Atmospheric Transmission for a 1-km Length and Midlatitude Summer Conditions. After Ref.[24].

2. Scattering

Scattering is a process that changes the direction of motion of individual photons, causing divergence of the energy and decrease in the forward radiance.

a. Rayleigh Scattering

The decrease in forward spectral radiance, due to scattering, depends on the wavelength of the incident radiation and the diameter of the particles. When the particles are small compared with the wavelength of the radiation, the process is known as Rayleigh scattering. In this case the radiance loss due to scattering decreases rapidly with increase in wavelength.

In the infrared spectrum, scattering is greatest in the near infrared region adjoining the visible spectrum, and decreases rapidly for longer wavelengths. [Ref. 6]

b. Mie Scattering

For larger particle sizes greater than about one tenth of the wavelength, the Rayleigh approximation is no longer valid, and another scattering theory, Mie theory, applies. [Ref. 2] These classes of particles generally cause haze, rain, and fog conditions. Since smoke and light mist particles are small compared to the infrared wavelengths, infrared radiation can propagate further through smoke and mist than visible radiation. However, fog, and rain particles are larger and as a result they scatter infrared and visible radiation to a similar degree.

In the atmosphere, transmission of infrared radiation is attenuated by both absorption and scattering, which occur together. Absorption may be much greater than scattering, or vice versa, depending upon the nature of the atmosphere, the particle size, and the wavelength. Furthermore, the combined sum of the percentages of absorption, scattering, and transmission always totals 100.

E. INFRARED POLARIZATION PHYSICS

Polarization has recently received increased interest in discrimination of targets from background, since it provides more information than pure intensity imaging. When the intensity contrast between target and background is not distinguishable, the polarization contrast may offer new dimensions in discrimination. [Ref. 17] In this section the polarization physics is summarized while the effects of polarization phenomena in thermal imaging sensors' performance and target and background thermal signatures are studied in detail in Chapter III.

For a plane wave propagating in the z-direction, the electric field components in the plane perpendicular to the direction of propagation may be represented by:

$$E_x(z,t) = E_{ox}\cos(wt + \delta_x) \tag{2.12}$$

$$E_y(z,t) = E_{oy}\cos(wt + \delta_y) \tag{2.13}$$

Where E_x = x-component amplitude

E_y = y-component amplitude

δ_x = phase constant of x component

δ_y = phase constant of y-component

The polarization of electromagnetic radiation is defined by the behavior of the electric vector over time

intervals that are long compared to the response time of the detector to be used.

When the end point of the electric vector at each point in the plane of incidence moves periodically around an ellipse with increasing time, the radiation is called "elliptically polarized". The ellipse reduces in special cases to a circle (circularly polarized) or a straight line (linearly polarized). [Ref. 12]

It is known that the polarization behavior could be completely represented in terms of four measurable quantities known as the Stokes polarization parameters. The Stokes polarization parameters for a plane wave are: [Ref. 2]

$$I = E^2_{ox} + E^2_{oy} \tag{2.14}$$

$$M = E^2_{ox} - E^2_{oy} \tag{2.15}$$

$$C = 2E_{ox}E_{oy}\cos\delta \tag{2.16}$$

$$S = 2E_{ox}E_{oy}\sin\delta \tag{2.17}$$

where

I= the total intensity of the light

M= the degree of polarization in the horizontal or vertical direction

E_{ox}= the component of the wave electric field normal to the plane of propagation

E_{oy}= the component of the wave electric field parallel to the plane of propagation

C= the degree of polarization in the ±45° direction

S= the degree of polarization of right or left circular polarization contained within the beam

δ= the phase difference between the s and p components of the electric field

Unpolarized light has M=C=S=0. To describe completely the polarization of light, all four of Stokes parameters must be used.

An important quantity that collectively describes the parameters is the degree of polarization POL. It can be calculated by:

$$POL = \frac{\langle N_v \rangle - \langle N_h \rangle}{\langle N_v \rangle + \langle N_h \rangle} \qquad (2.18)$$

where:

$\langle N_v \rangle$ = mean apparent vertically polarized radiance.

$\langle N_h \rangle$ = mean apparent horizontally polarized radiance.

The observed degree of polarization depends on several parameters such as the refractive index of the surface, the viewing angle, the surface temperature, the radiating environment, surface roughness and so on.

Polarization of light can also be generated by reflection and refraction. The polarization of the wave can change while passing from one medium to another. This phenomenon including the reflection and refraction characteristics of light is governed by the Fresnel Equations and by Snell's Law. For nonmagnetic media the Fresnel equations can be written

$$r_{\text{perpendicular}} = -\frac{\sin(\theta_i - \theta_t)}{\sin(\theta_i + \theta_t)} \tag{2.19}$$

$$r_{\text{parallel}} = -\frac{\tan(\theta_i - \theta_t)}{\tan(\theta_i + \theta_t)} \tag{2.20}$$

$$t_{\text{perpendicular}} = \frac{2 \cdot \sin(\theta_t) \cdot \cos(\theta_i)}{\sin(\theta_i + \theta_t)} \tag{2.21}$$

$$t_{\text{parallel}} = \frac{2 \cdot \sin(\theta_t) \cdot \cos(\theta_i)}{\sin(\theta_i + \theta_t) \cdot \cos(\theta_i - \theta_t)} \tag{2.22}$$

where:

θ_i = incident angle.

θ_t = angle of transmission.

r = reflection coefficient.

t = transmission coefficient.

"Perpendicular" and "parallel" refer to the component fields perpendicular and parallel to the plane of incidence.

For plane waves incident at a boundary between two media of different complex refractive indices n_1 and n_2, the angle of reflection equals the angle of incidence. The angle of transmission (refraction) θ_t as a function of the incidence angle θ_i is given by Snell`s law:

$$n_1 \sin(\theta_i) = n_2 \sin(\theta_t) \qquad (2.23)$$

III. BACKGROUND - TARGET RADIANCE AND POLARIZATION EFFECTS

A. BACKGROUND RADIANCE

1. General

In an environment where there are some optical targets present, the surrounding elements that emit, reflect or scatter random radiation in the same spectral region as the target can be defined as "background". There are numerous background infrared radiation sources occurring in nature that can be divided into three groups; terrestrial, celestial and atmospheric sources. Terrestrial background refers to radiance seen by infrared systems working within the atmosphere of the earth. This type of background includes the radiation that several natural sources occurring on the surface of the earth are emitting or reflecting (oceans, clouds, vegetation, etc.). It also includes sunlight scattered by particles in the atmosphere and atmospheric molecular emission (sky radiance). Celestial refers to that background seen by a system working in space and consists of radiation from the stars and the sun, reflectance from planets, and space debris. Dust particles, water droplets, and molecules of the

various gases occurring in the earth's atmosphere behave like background sources of radiation with respect to an optical target. They scatter, reflect, absorb and re-emit primary radiation illuminating them from both celestial and terrestrial sources.

Background radiation is strongly affected by environmental conditions and the nature of the materials. Changes in emissivity and reflectance of the various background surfaces under varied conditions are considered primary parameters that effect the background radiation in terms of magnitude and polarization characteristics.

Since the target is always surrounded by some sort of background it is obvious that radiation reaching the detector from this background is confused with the radiation emitted or reflected from the target. [Ref. 5]

Background radiance measurements are generally made with thermal imagers and radiometers under various meteorological conditions. Technical properties of imagers and radiometers sometimes make the comparison of these devices very difficult in terms of thermal resolution. The geographical locations of measurements also may change.

All of the above make the background phenomena complicated and the modeling of a universal background radiance function very difficult.

Of particular interest in this project are the background radiances of the sea surface and the sky. In the rest of the Chapter, the main characteristics and spectral radiance properties of these backgrounds, especially for the spectral region 8μm to 14μm in which we are most interested, are reviewed.

2. Sea Background

The sea surface infrared radiance L_{sea} is the sum of the radiance caused by its inherent blackbody thermal emission L_{sst} from below the surface and the radiance due to reflected incident sky and solar radiation from the surface. This can be written in the following form.

$$L_{sea} = \varepsilon L_{sst} + \rho L_{sky} + \rho' L_{sun} \qquad (3.1)$$

where

ε = the sea surface emissivity

ρ = the sea surface reflectivity

ρ′ = reflectivity integrated over the angle subtended by the sun.

All of these are averaged over the wave slope distribution.

Equation 3.1 must then be corrected for atmospheric transmittance and path radiance over the range "R" so that the apparent radiance received L_{app} can be written:

$$L_{app}(R,\lambda,\theta,\phi,\varepsilon,\rho,t) = L_{sea}(T,\lambda,\theta,\phi,\varepsilon,\rho) * \tau(R,\lambda,\theta,\phi,t) + L_{atm}(R,\lambda,\theta,\phi,t) \quad (3.2)$$

where

R = range to the sensor

θ = azimuthal angle

ϕ = elevation angle

λ = wavelength

t = time

L_{sea} = total surface or zero range background radiance

L_{atm} = radiance emitted along the path to the sensor

τ = transmittance through the atmospheric path to the sensor.

[Ref. 1]

Major factors that determine the sea background character can be summarized as; Infrared optical properties of sea water, geometry of the sea surface and wave slope distribution, and finally the sea water temperature distribution and properties of the bottom material.

Each radiance component except path radiance is a function of the spectral emissivity or reflectivity ($\varepsilon_\lambda, \rho_\lambda$) of sea water and the orientation of the sea wave facet relative to the reflected sources and the observer. Since $\varepsilon_\lambda(\theta)+\rho_\lambda(\theta)=1$, both reflectivity and emissivity will depend on the polarization of the incident or emitted radiation.

The sea radiance may be modeled as a blackbody at the sea surface temperature. The reflected radiance component is integrated over the sky zenith and azimuth angles. [Ref.16] Direct reflected solar radiation is significant only in very restricted orientations close to the solar direction and dominates at short wavelengths.

To compute the radiance from an ocean surface, a FORTRAN computer code, the SEARAD Radiance Model developed at NCCOSC can be used. The SEARAD Radiance Code [Ref. 10] is a modification of MODTRAN valid for a spectral range extending from the visible to the far infrared. The latest SEARAD code takes into account the polarization characteristics of sea surface emission and reflected sky radiance components in calculations. Several variously modified versions exist such as a user-friendly, multi-range version that runs in MATLAB and a self-contained DOS-compatible version that runs in the DOS environment. The

SEARAD Radiance model computes four contributions (thermal emission, path radiance, reflected sky radiance, and reflected solar radiance) to sea radiance. It is based on the Cox-Munk (Cox and Munk, 1954,1956) [Ref. 26] statistical model for wind-driven capillary wave facets. The assumption for the model is that the strength of interaction between an optical ray and a capillary wave facet is proportional to the facet area projected normal to the ray.

SEARAD also allows computation of the atmospheric transmittance as in normal MODTRAN. It is used in this project many times for sea background radiance calculations and for part of the Apparent Temperature Difference calculations. Sample SEARAD input and output data files are presented in Appendix A.

3. Sky Background

a. General

The sky background radiance in the infrared is caused by radiation emitted from the molecules in the atmosphere and by sunlight scattered from the molecules, particles, and water droplets in the atmosphere. The scattering factor is especially influenced by the cloud distribution. It is important in the short wavelength

range, close to the visible, and is present only in daytime. The thermal emission happens at wavelengths longer than 4 μm and is present day and night.

An idealized representation of the sky spectral radiation is shown in Figure 3.1 [Ref. 4]

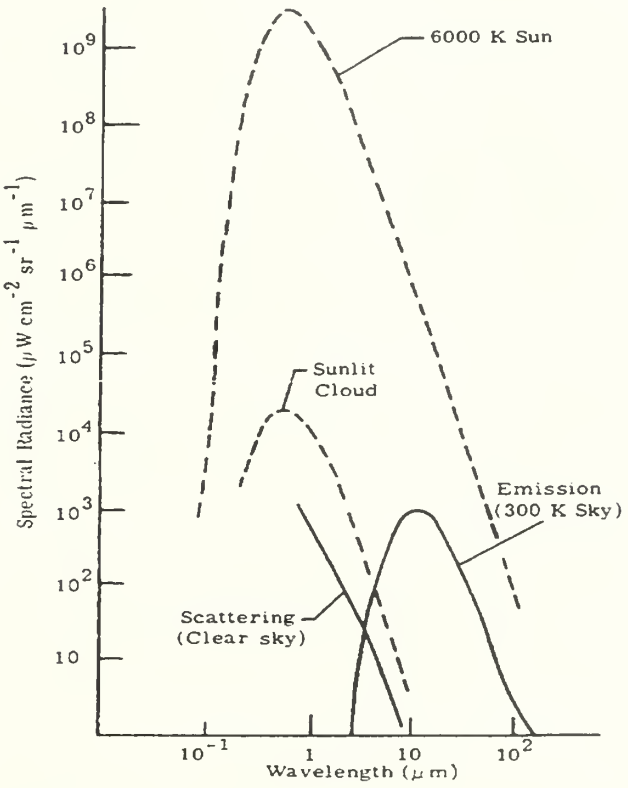

Figure 3.1 Contribution From Scattering and Atmospheric Emission To Background Radiation. From Ref.[4].

b. Spectral Radiance of Clear Sky

Spectral radiant intensity and spectral distribution of the clear sky in the infrared region depend on angle of elevation, water vapor and carbon dioxide contents of the atmosphere, the temperature of the atmosphere, and the altitude above the earth's surface. They are also affected by clouds and haze.

The spectral distribution of energy radiated from clear day and night skies is shown, not to scale, in Figure 3.2 which illustrate the primary differences between the day and night sky background radiation normal to the earth's surface. [Ref. 4]

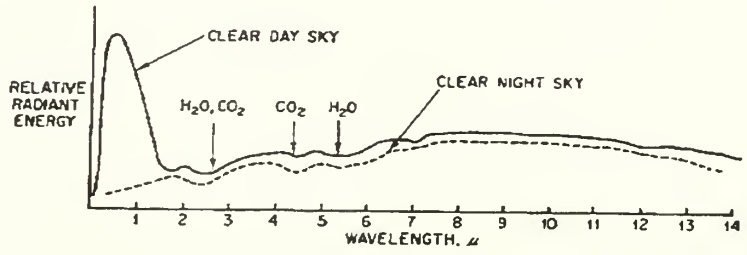

Figure 3.2 The Spectral Energy Distribution of Background Radiation from Clear Day and Night Skies. From Ref.[4].

The elevation angle determines the length of the atmospheric path and hence the emissivity, while the temperature determines the blackbody emission

characteristics. The elevation angle dependence of the spectral radiance is shown in Figure 3.3.

The effect of the ambient temperature is very strong for this kind of radiation, as shown in Figure 3.4. This figure shows the zenith sky spectral radiance for two different ambient temperatures.

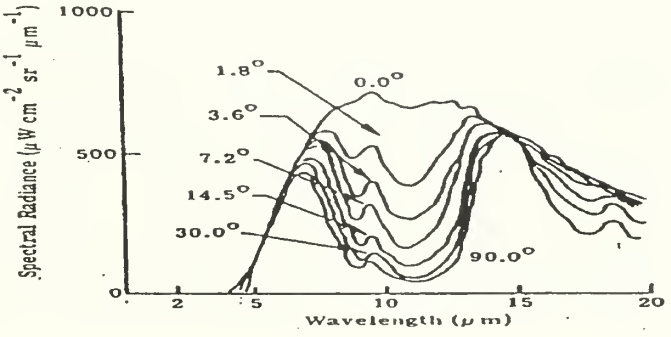

Figure 3.3 The Elevation Angle Dependence of Sky Spectral Radiance. From Ref.[4].

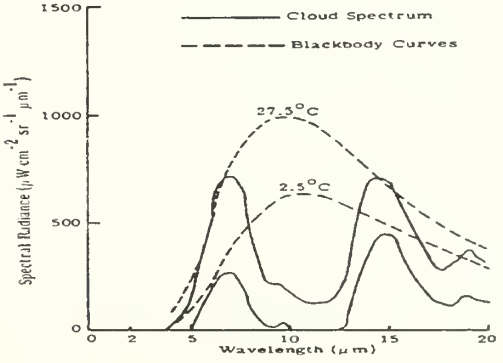

Figure 3.4 Sky Spectral Radiance Variation with Ambient Temperature. From Ref.[4].

c. Spectral Radiance of an Overcast Sky and Clouds

The infrared radiation from clouds, which results as clouds emit heat and scatter sunlight, is an important consideration in computations and produces considerable variation in sky background.

Overcast skies have been found to be very good blackbody radiators (ε=1), having a temperature at low altitudes within one or two °C from the ambient surface temperature. Infrared radiation incident on a cloud water droplet is highly absorbed and partially reflected and transmitted. However due to multiple scattering from all neighboring droplets in the cloud the transmittance of the cloud goes essentially to zero, and thus the emissivity approaches unity. We can say that clouds in the infrared region are good absorbers and consequently good emitters, causing overcast skies to behave as good blackbody radiators.

4. Land Background

The radiant energy emitted and reflected by the ground is determined by the emissivity, reflectivity, and temperature of the ground and the modification of this radiation by the intervening atmosphere.

The same general principles that govern the sky background determine the amount and variation of land background radiation. The radiation from the terrain is the sum of the reflected sky and solar radiation plus a percentage of the radiation emitted by a blackbody at the ground temperature. When the observed terrain is sufficiently distant, the radiation is modified by the atmosphere at the wavelengths where it absorbs.

Below 4 μm most of the radiation is from scattered or diffusely reflected sunlight. This radiation varies greatly with the sun's position, the amount of cloud cover, and the nature of the terrain.

Above 4 μm, measurements of the radiance of a terrain show that it closely follows the appropriate blackbody curve for the temperature of the ground. A few minor deviations from the blackbody curve may occur in regions where there is a strong atmospheric absorption band. The diurnal variation of the radiance from various types of terrain follows the temperature changes of the emitter. Differences in the radiances of trees, rocks, grasses, cities, and other types of terrain are easily observed. These result from differences both in their emissivities and in their temperatures under natural conditions. The

radiance of the terrain is higher in sunlit areas than in areas which do not receive sunlight because of clouds. [Ref. 8]

Figure 3.5 shows the surface radiance and temperature of a land background at two different times.

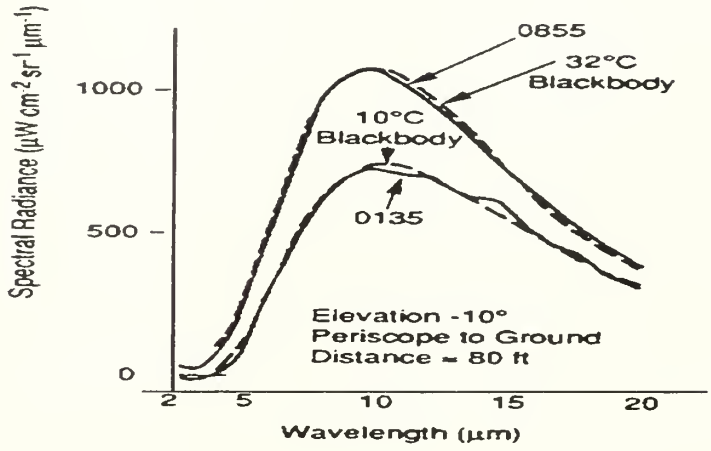

Figure 3.5 The Surface Radiance and Temperature of a Land Background Compared at Morning (0855) versus Pre-dawn (0135). From Ref.[9].

Since computation of radiation from backgrounds is one of the important steps in overall performance analysis of thermal imaging systems, the advanced models must be used to make these computations. In the sea background case the SEARAD Radiance Model is considered adequate for many applications.

In principle there are three different methods available to model land surface backgrounds. These are; a

pure statistical approach, models based on physical laws, and a combination of both methods. Models contain parameters such as soil type, soil moisture content, vegetation cover and type. The physical properties of the medium (soil water diffusivity, hydraulic conductivity, thermal diffusivity and thermal convectivity) are both temperature and moisture dependent and should be considered in the models. One thing common to all the different models is the fact that they only give mean conditions. No information on variances and the bandwidth of values found in reality can be obtained. To get this information new methods have to be developed. [Ref. 9]

B. TARGET RADIANCE

An infrared imaging system can detect a target when the target has a radiation signature that can be distinguished from all the background radiation within the field of view. If the target is an intense source such as a jet-engine or rocket exhaust, this can be achieved more easily. On the other hand if the target emits nearly the same radiance as the background, such as a man or tank on the ground, than it requires more work.

Infrared signatures of objects are functions of surface temperature, emissivity, reflectance, and the surrounding environment. At zero range the radiance consists of an emitted component and several reflected components.

The emitted portion of the signature is blackbody radiation, reduced by the directional emissivity of the target surface. The reflected radiance comes from other portions of the target and the surrounding environment(e.g. atmosphere, sun, moon, and other sources), all acting through the reflectance of the target coating. [Ref. 13]. The overall contributions to the signature from a target are shown in Figure 3.6.

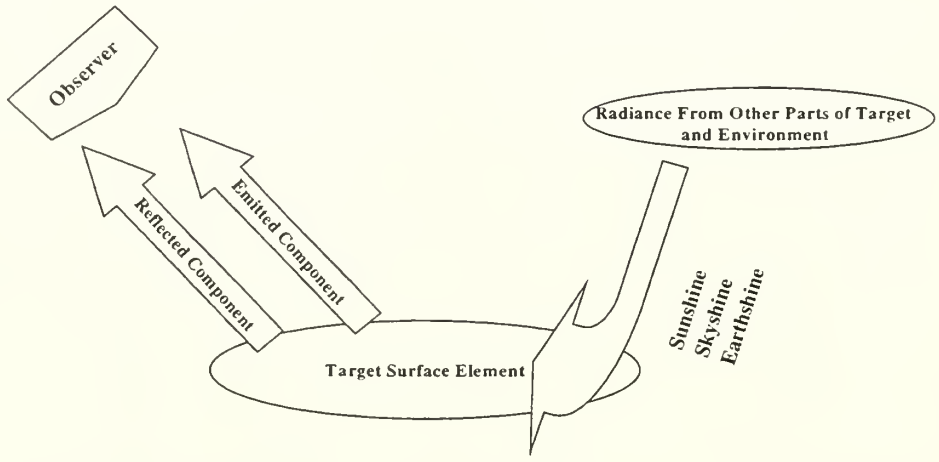

Figure 3.6 Infrared Signature Composition of a Target.

In this section, equations for predicting the radiance at a target observation point, using the fundamentals of

radiometry, will be discussed. In theory, using these expressions one can calculate the radiance from any given point on a target.

1. Emitted Radiance

The emitted component of target radiance is similar to blackbody radiation. The radiance for any portion of the surface is given by Equation 3.3.

$$L_{emit}(\theta_r, \phi_r) = \frac{1}{\pi} \int_{\lambda_1}^{\lambda_2} \varepsilon(\lambda, \theta_r, \phi_r) M_{bb}(\lambda, T) d\lambda \qquad (3.3)$$

The term $\varepsilon(\lambda, \phi_r, \theta_r)$ is the spectral directional emissivity at the target intercept point, and $M_{bb}(\lambda, T)$ is the spectral radiant emittance at target temperature T, whose value is given by the Planck function. The angles $\theta_{r,i}$ and $\phi_{r,i}$ refer to zenith and azimuth angles in reflected and incident directions respectively. The integration limits λ_1 and λ_2 define the waveband of interest.

If the emissivity does not vary with wavelength Equation 3.3 becomes

$$L_{emit}(\theta_r, \phi_r) = \frac{\varepsilon(\theta_r, \phi_r)}{\pi} \int_{\lambda_1}^{\lambda_2} M_{bb}(\lambda, T) d\lambda \qquad (3.4)$$

2. Reflected Radiance

The reflected radiance due to any source of incident flux may be computed as shown for any desired point on the target:

$$L_{ref}(\theta_r, \phi_r) = \int_{\lambda_1}^{\lambda_2} \int_{2\pi} f(\lambda, \theta_r, \phi_r, \theta_i, \phi_i) L(\lambda, \theta_i, \phi_i) \cos\theta d\Omega_i d\lambda \qquad (3.5)$$

where $f(\lambda, \phi_r, \theta_r, \phi_i, \theta_i)$ is the spectral bi-directional reflectance distribution function (BRDF), and $L(\lambda, \phi_i, \theta_i)$ is a specific component(e.g., target, atmosphere, sun, etc.) of the input radiance. The integration is performed over a hemisphere defined by the surface element under consideration, and over the wavelength limits defining the waveband of interest. [Ref. 13]

Natural sources of radiation affect target signatures by way of reflected solar radiation and earthshine and to a much lesser extent by lunar sources. As explained previously the reflected solar radiation is an important factor in sea background signature calculations as well as target signature calculations. Therefore, in this project reflected solar contributions are involved in the target signature computation model and in the background radiation computation model. In this consideration the time of the day when the measurements are made becomes important.

Reflected earthshine is a minor component of the total contrast signature for nadir viewing. However, as the view extends toward the horizon and the aspect becomes more side-on, the component increases. Since in this project the background is sea background, this component is included in the "reflected radiance from sea surface" part of the total radiance.

The total radiance from the target is then computed as:

$$L_{tot}(\theta_r,\phi_r) = L_{emit}(\theta_r,\phi_r) + L_{ref}{}^{atm}(\theta_r,\phi_r) + L_{ref}{}^{sun}(\theta_r,\phi_r) + L_{ref}{}^{trg}(\theta_r,\phi_r) + .. \quad (3.6)$$

where four terms refer to the emitted, reflected atmospheric, reflected direct solar, and reflected target radiances.

The radiant intensity is found by integrating the target radiance over the projected target area. [Ref. 13]

$$I(\theta_r,\phi_r) = \int_{target} L_{tot}(\theta_r,\phi_r)\cos\theta_r dA \quad (3.7)$$

3. Target Types

In terms of the radiances, targets can be considered in three different groups: ground targets, airborne targets and ship targets.

Ground targets show differences in emitted radiation due to their surface emissivities and temperatures. While some targets are heated with respect to the background by internal sources such as the power train in a tank, some of them are heated by natural sources. An automobile or tank is hotter than its surroundings for several hours after use. Personnel are usually warmer than their surroundings because of the biological processes that release heat within their bodies. Objects that do not release heat internally can also sometimes be detected by natural temperature differences between the object and the surroundings.

Airborne targets such as airplanes and rockets can be detected by the emission from the heated skin and from the hot motor parts and also by the radiation from the plume of hot gases from the motor. [Ref. 8]

A ship signature is made up of two main components: Internally generated, and externally generated. The primary internal IR source results from the main machinery onboard any vessel, in particular drive engines and electrical generators. The primary external sources of radiation are; the sun, sky radiance, and sea radiance. [Ref. 14]

In the case of a ground vehicle or ship, the interaction term may include reflections of the object off its environment as well as the reverse. For these cases, such reflections can be an important part of the object's total signature. [Ref. 11]

The target radiance is further affected by propagation through the atmosphere. To determine exactly the radiance originating from a target and propagating to the sensor, one must consider the atmospheric transmission as a function of wavelength. This phenomenon is studied in detail in Chapter II.

4. Geometry Effect

In the general case, targets are complex surfaces and can be treated by dividing the surface into flat facets of constant total bidirectional reflectance and then summing over all facets comprising the surface. The "faceted modeling" technique is a very popular method for describing the geometry of targets for use in infrared signature computations. Many infrared simulation models in current use, including the one which is used in this project, use faceted representations of targets. Figure 3.7 illustrates two sample targets that are approximated in this way. Each

facet is assigned thermal and optical properties and thickness for calculations later.

The measured value of radiance is affected by the location of the observer relative to the target. In some cases the radiance changes significantly as the aspect viewed changes.

Because of the many parameters involved in computation of radiance from a target, it becomes very difficult to establish a simple, single, rule of thumb that provides an accurate radiance value for all wavelengths or aspects.

There are many complex Infrared Signature Simulation Software Codes in the electro-optic technology literature to predict the infrared radiance as well as the zero range and apparent temperatures of various targets for different circumstances. These complex models are mostly based on realistic assumptions about the optical properties and thermal conditions of the target surface. They take into account quantitatively the potentially significant target radiation resulting from reflected earth, sea, skyshine, and sunshine, and the transmissivity of the atmosphere between the target and the observer. Aspect-dependent signature components, such as variation in target cross-sectional area and weather conditions are also included in

these models. Since each of these factors, in particular circumstances, can significantly impact the infrared signature of an object, using these models becomes crucial for obtaining the most accurate radiance magnitudes. Some of these models including short descriptions are listed in Appendix B from Ref. 13.

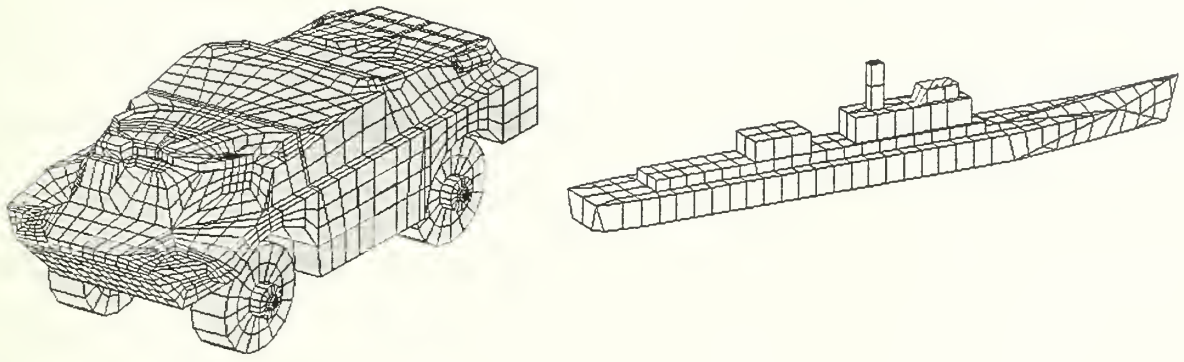

Figure 3.7 Typical Samples of Faceted Target Models Used in Signature Prediction Programs. After Ref.[25].

The computation of radiance from a specific target in the most accurate way available constitutes one of the main features of this thesis. In the following Chapters, the MuSES (Multi-Service Electro-Optic Signature) model is used

for this purpose. In Chapter IV detailed parameters and the output of this model are explained.

C. POLARIZATION EFFECTS ON RADIANCE & TARGET DISCRIMINATION

The presence of interfering background radiation during the detection process is a very common problem to most infrared sensors. This problem degrades the sensors' target detection capability and limits the performance. The use of polarized infrared energy and certain selective polarization properties of the target and background help to distinguish a target in complex natural backgrounds by improving the target radiance to background radiance ratio. The improvement is based on the selective rejecting of some part of the polarized radiation from backgrounds or target with a filter at the entrance of the sensor.

While researchers have recognized the potential usefulness of polarized image data for target detection and recognition, wide-spread use of polarization in the infrared has not occurred. This is probably because polarization-sensitive imaging methods have been slow to develop, and require detailed studies.

Polarization sensitive thermal imaging sensors have many potential military and commercial applications. In

particular, stealth ships and aircraft, because of their large planar faceted surfaces are expected to emit highly polarized thermal radiation which reveals the shape of the object. Therefore polarization characteristics of ships are being studied for use in detecting ships against ocean and sky backgrounds. [Ref. 15]

Polarization occurs in the emitted and reflected infrared radiation of targets and backgrounds. Man-made objects tend to be glossier and more regularly shaped than backgrounds and have unnaturally smooth surfaces, leading to radiation with greater polarization. Although natural backgrounds such as grass, trees, dirt, and sand emit and reflect radiation that is less polarized, the large sea surface near grazing incidence shows more polarization than the more detailed faceted man-made ship signature. Regarding the main theme of this thesis some important polarization sources are summarized below.

1. Sea Emission and Reflection

Background infrared radiation from the sea consists of two components; the partially vertically polarized emissions from the sea surface and the partially horizontally polarized reflected radiation from the sky, sun, moon, etc. Each radiance component is a function of

the spectral emissivity of seawater and the orientation of the sea wave facet relative to the reflected sources and the observer.

Sea surface polarization characteristics have complex mathematical models. Reference 20 presents detailed descriptions of some models frequently used for analysis of the polarization characteristics of the sea surface. Previous experiments and analyses [Ref. 1 and Ref. 16] have shown that the electric vector of sea surface radiance appears horizontally polarized within the sun glint regions and vertically polarized otherwise. Figure 3.8 shows the predicted degree of polarization for MWIR and LWIR in and near the sun glint region as a function of solar zenith angle for an observer looking in the vertical plane of the sun. The negative values of polarization outside of the sun glint regions indicate vertical polarization. In these previous experiments measured LWIR surface radiance shows a degree of polarization with vertical orientation around 7 to 30%.

In this project the degree of polarization of a sea background radiance for the specified geometry and conditions is predicted by the polarized version of the SEARAD Radiance Model.

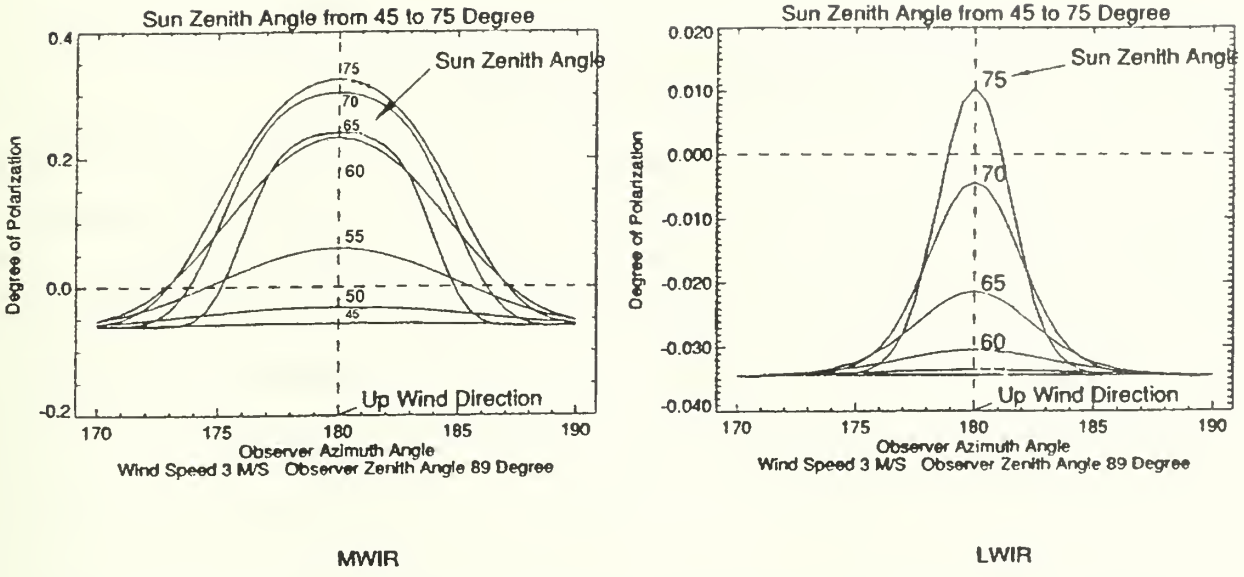

Figure 3.8 Theoretical Degree of Polarization as Function of Azimuth Angle and Solar Zenith Angle, for MWIR and LWIR. From Ref.[1].

2. Sky Emission and Reflection

Atmospheric path radiance will not contribute to a change in apparent target to background radiance contrast ratio seen with a polarized sensor. The only absorption mechanism for path radiance will be the transmissivity of the polarized filter. In this project, atmospheric path radiance is included into the total target and total background radiance values separately, and in each case treated as having 0% degree of polarization.

Due to the high concentration of water in the atmosphere, the sky is generally an excellent absorber. Since it is an excellent absorber, it is a poor reflector.

3. Target Emission and Reflection

As sea surface radiance shows a net vertical polarization characteristic, primary contrast improvement can be obtained by placing a horizontal filter in a sensor. In cases where the polarization due to emission from the target has a perpendicular direction compared to the background polarization, the use of a polarized filter will cause an additional contrast improvement. In previous work [Ref.1] it was concluded that polarization features were not prominent in the images of ship targets, in either the MWIR or LWIR bands, with no observations greater than ±5% in degree of polarization. A parallel conclusion is stated in Ref. 19 also, where it is pointed out that the degree of polarization from target surfaces in the IR is typically 5 to 8 percent under appropriate viewing conditions. Although 5 to 8 percent degree of polarization seems to be a small value, in suitable conditions it can create a significant temperature difference and consequently a significant signal for detection.

Painted surfaces such as found on all types of vehicles and ships display emission polarization particularly at angles close to the Brewster angle. Figure 3.9 shows 21 measurements taken on various paint samples ranging from very smooth texture through sand-paint mixtures. The amount of polarization depends on the index of refraction of the paint and any degradation due to the surface roughness.

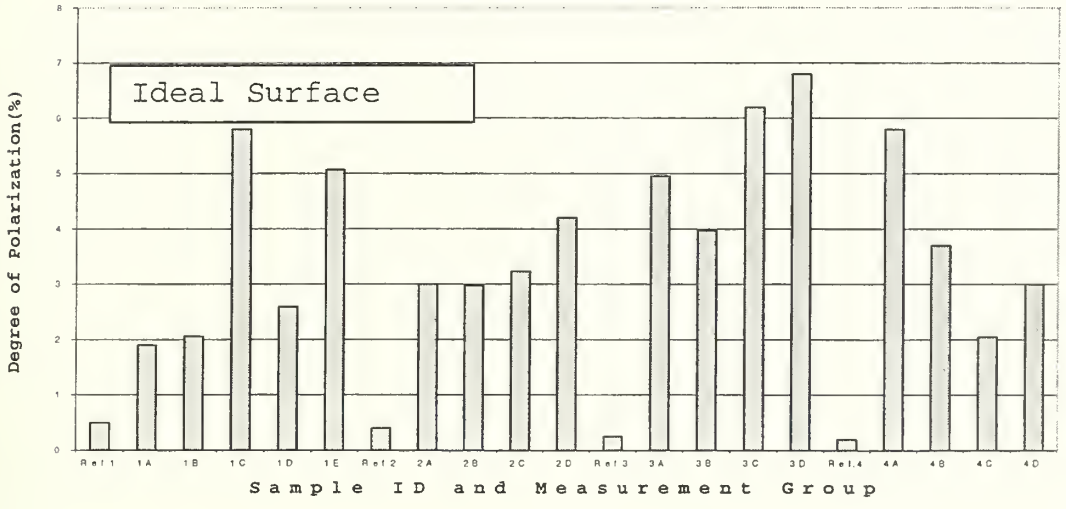

Figure 3.9 Measured Polarized Signature Components in the 7.5-12μm band for Selected Paint Samples. After Ref.[12].

The index of refraction of the surface material of the target determines the magnitude of the polarized components of total radiance and the net polarization will vary

according to the balance between thermal emission and reflection in the total radiance.

In this project the performance of a polarized second generation sensor was studied for a target degree of polarization limited to 0 to 8 percent in both directions.

IV. MODEL DEFINITION AND TARGET SIGNATURE COMPUTATION

A. MODELING APPROACH

1. Background

Maximum range analysis for thermal imaging systems with and without polarizer was studied in previous projects, by Yu (Ref. 27, 1997), Lagaras (Ref.18, 1999), and by Guimaraes (Ref. 23, 1999). While Yu used a scenario selected from the database of the EOMET95 measurements series in Monterey Bay off Moss Landing, the analyses carried out by Lagaras and Guimaraes were based on the EOPACE data acquired in April 1996 in San Diego Bay. In Ref. 27, maximum ranges were calculated without polarization filtering. In Ref. 18, the calculations were performed for an unpolarized target considering the polarization filter effect, since no target polarization was observed in the MAPTIP or EOPACE data. The effect of a polarization filter on the Minimum Resolvable Temperature Difference of a sensor is studied in Ref. 23. In all of the above target-to-background models the common inadequacy is lack of a valid target signature computation model. In the models used, by Guimaraes and Lagaras the ship targets are assumed to be unpolarized and the sea background degree of

polarization is averaged within the required bandwidth. In Ref.18 it is observed that when a horizontally polarized filter is used, at some distance the apparent temperature difference passes through zero and goes negative, whereas it is expected that at greater ranges the apparent temperatures of the target and background should approach each other asymptotically, so that the apparent temperature difference should approach zero. This inconstancy in apparent temperature difference found in Ref. 18 is interpreted as probably resulting from the use of different incompatible procedures for target and background apparent temperature calculations. In this project an algorithm is developed for apparent temperature difference calculation to overcome the anomaly.

In this thesis a model that contains a commercial advanced target signature prediction program, MuSES (Multi-Service Electro-optic Signature)[Ref. 25], is developed to predict the maximum range of a sensor for specific tasks. The model includes a ship target and sea background, each having a degree of polarization. The scenario and the model are defined in the following sections.

2. Scenario

For the model a single scenario is designed. The target

in the scenario is a modified version of a ship target contained in the MuSES program. The ship target in the program is a faceted model of a 210 foot ship (dimensions: 64.8LX7.14WX7.93H (m)) which is similar to the Cyclone class ships (170 foot). The geometry and ship dimensions are detailed in Appendix C.

The background in the scenario is a typical sea background with an average polarization value -13% in the specified bandwidth. The overall analysis is performed in the 8-12μm region.

The sensor simulated has the generic characteristics of a Second Generation FLIR sensor. The characteristics are given in Appendix F. For the scenario it is assumed that the hypothetical sensor is mounted on an aircraft which approaches the target at 300m elevation. Figure 4.1 shows a schematic representation of the scenario.

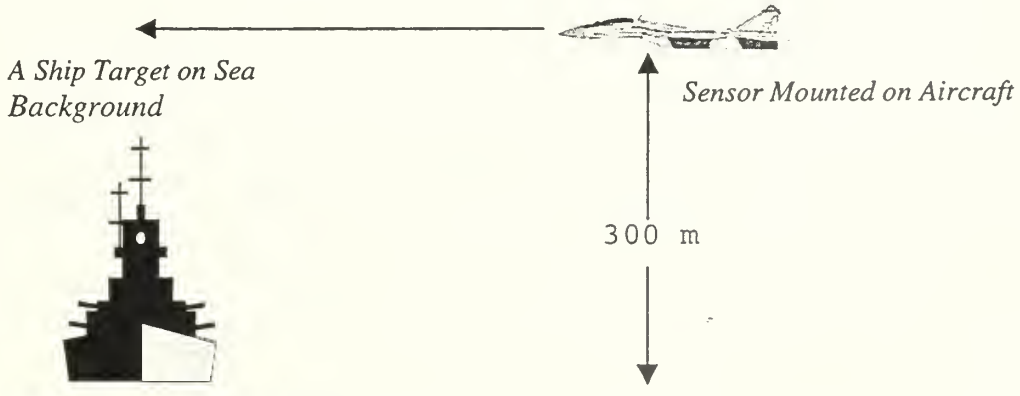

Figure 4.1 Schematic Representation of the Scenario.

Sea radiance and atmospheric propagation are modeled with the SEARAD propagation code. For the atmospheric data required as input to SEARAD and to the target model in MuSES one of the weather data files available in the MuSES program database is used. The Natural Environment (weather) option in the program uses models or measurements of the weather conditions and the solar position to calculate the cooling or heating that occurs from the influence of weather. Currently there are four different weather files available in the program. For the target signature calculations in this project the file dated Jul 20,1984 is used. The parameters are as follows:

Global Positioning:

Latitude (deg.): 47.2, Longitude (deg.): 88.5, Time Zone (hrs.): 4, Elevation (m): 332

Date of the Measurements: 07/19/1984

Available Solution Times: From 07/19/1984 06:20 AM to 07/20/1984 08:59 AM

Selected Solution Time: 07/19/1984 18:00 PM

This weather file is selected as being compatible with a standard MODTRAN atmosphere (Midlatitude Summer).

3. Model Definition

The model developed in this project contains a defined scenario and a series of calculations that are carried out in this and in following Chapters. It can be summarized in following four steps:

- Target, Background, and Path Radiance Calculations
- Minimum Resolvable Temperature Difference (MRTD) Prediction
- Apparent Temperature Difference (ATD) Calculation
- Maximum Range Predictions

The steps, more detailed, are shown in Figure 4.2. As opposed to the previous models, in this model an advanced target signature prediction program is used and both target and sea background polarization effects are included. Target and background computations are considered to be compatible. The program description and computations are presented in the following section.

B. TARGET SIGNATURE COMPUTATION

The performance of many infrared seekers and other sensor systems operating in the far infrared spectral region of 8μm -12 μm is critically dependent on the magnitude of thermal signatures (i.e., thermal contrasts,

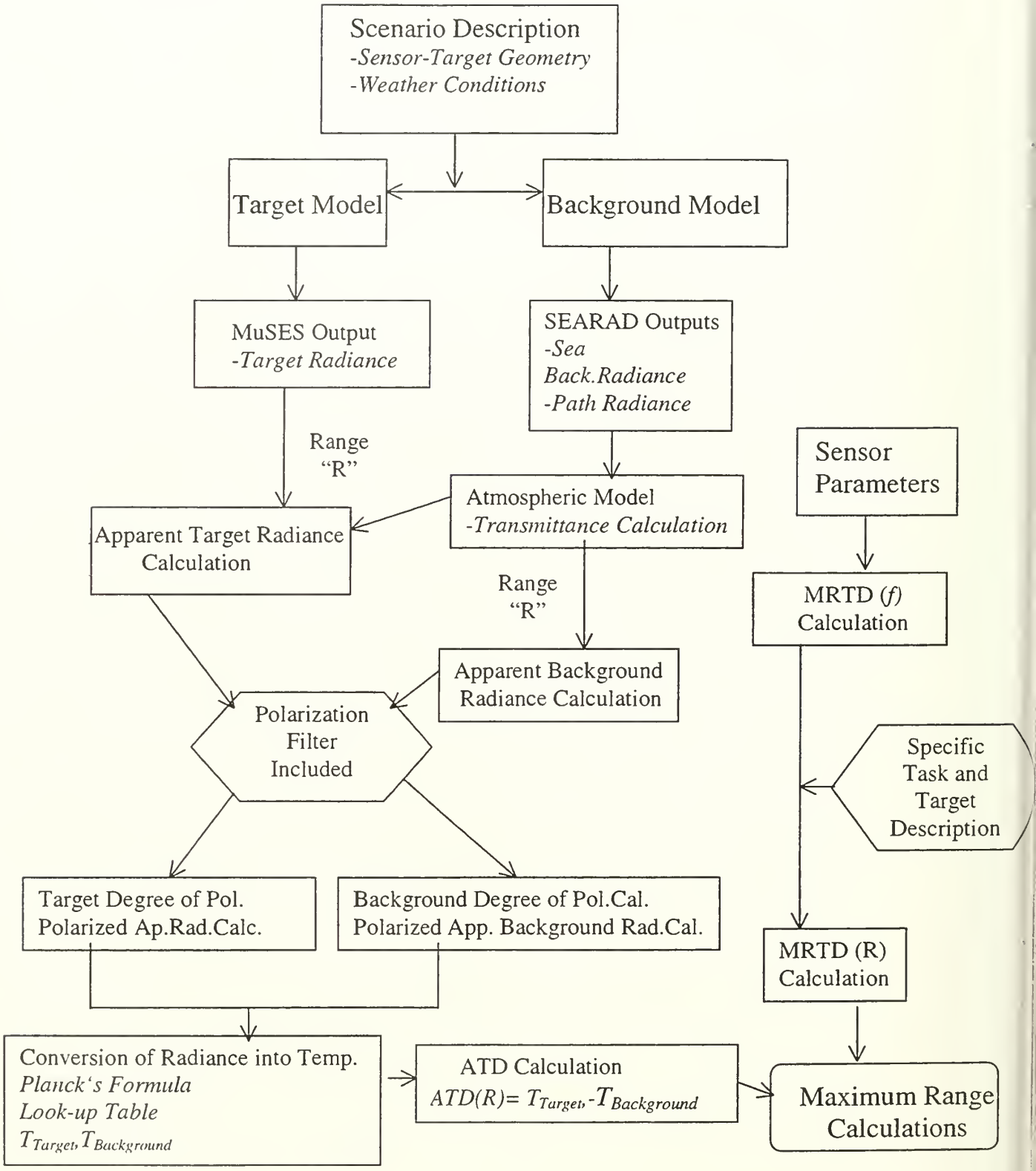

Figure 4.2 Flow Chart of The Model Used in This Project.

or equivalently, differences in thermal radiance values between various scene components).[Ref. 11]

To detect a target in a background, a contrast in radiance alone is not enough, but is, however essential. Since signature description is a primary part of infrared systems analysis, signature calculation models play an important role in performance prediction of infrared systems.

These models should include and reproduce the effects of the most important radiative signature processes. Because infrared systems typically predict contrast between a target and its background, and because natural sources of target infrared radiation are frequently important, environmental as well as target radiative phenomena must be included in predictive analysis tools.

To achieve reasonably accurate estimates of target signatures it is most important to understand the complex phenomenology that determines the levels of radiation. The phenomenological processes are particularly dependent on the scenario considered.[Ref. 11]

In the rest of this Chapter the MuSES (Multi-Service Electro-optic Signature) infrared signature prediction

program is used in order to obtain accurate radiance predictions of ship targets.

C. MUSES INFRARED SIGNATURE PREDICTION PROGRAM

MuSES [Ref. 25] is a new commercial "next generation" infrared signature prediction program developed by ThermoAnalytics Inc. which lets the user do complete thermal modeling and infrared signature prediction within an integrated easy-to-use interface. This software is the replacement for PRISM (The Physically Reasonable Infrared Signature Model), the previous standard US Army infrared prediction code and the TCMII model which are both used for ground vehicles and other targets of interest. With MuSES one can create one's own target model or use one of the standard models in the program. It has also a capability of editing and manipulating the existing model geometry e.g., to scale, translate, rotate, copy and delete. This model includes the detailed environmental radiation effects into the radiance and temperature computations. Modifying the characteristics of target and background, such as emissivity, conductivity, density and specific heat, various scenarios can be analyzed.

D. COMPUTATIONS WITH MUSES

In this project a ship thermal model is used which is modified from the original MuSES sea vehicle thermal model. The target dimensions, the other important characteristics of the target, and the geometry of the calculation are presented in Appendix C. The target model is used with the weather file (included in MuSES) which is shown in Appendix D. In the model scenario chosen the target is heading in the direction of north so the simulated measurement made in the late afternoon was not affected by sun glint. The result of these calculations as well as the time varying temperature and radiance measurements are presented in Appendix E. These results are then used in overall performance analysis of the thermal imaging sensor in Chapter V.

THIS PAGE INTENTIONALLY LEFT BLANK

V. MRTD-ATD COMPUTATIONS AND ANALYSIS

A. MINIMUM RESOLVABLE/DETECTABLE TEMPERATURE DIFFERENCE

The overall performance of a thermal imaging system is governed by both its thermal sensitivity and its spatial resolution, and is generally defined in terms of its Minimum Resolvable Temperature Difference (MRTD) and Minimum Detectable Temperature Difference (MDTD).

MRTD has become a standardized test methodology for thermal imaging systems. It measures the temperature difference at which an observer is just able to discern a four bar (7:1 aspect ratio) chart against a background thermal scene. MRTD gives the detectable temperature difference as a function of the spatial frequency of the bars.

The parameter MRTD was originally defined for a scanning FLIR, and in the measurement procedure the bars of the four-bar pattern were oriented perpendicular to the scan direction of the FLIR. The observer is allowed to adjust the gain and level settings of the FLIR as well as his or her position relative to the system display during the measurement in order to minimize the temperature difference required to just resolve the target.

MDTD is the temperature difference between a square (or circular) target and a uniform background when viewed through a FLIR, which is required by a observer to just detect the target. [Ref. 21]

There are various approaches used to calculate MRTD and MDTD values in the infrared community. One of these formulas,and maybe the most common one, is given in Ref.22:

$$MRTD(f) = \frac{20 \cdot SNR_T \cdot \left(FOV_x \cdot FOV_y\right)^{1/2} f \cdot \rho_x^{1/2}}{\tau_o \cdot D \cdot D^* \cdot (\pi \cdot n \cdot \eta_{sc})^{1/2} \cdot (\alpha\beta)^{1/2} \cdot MTF_{system} \cdot (L \cdot T_e)^{1/2} \cdot \frac{\partial N}{\partial T}} \qquad (5.1)$$

where:

SNR_T = perceived signal-to-noise ratio set according to the desired probability of performing the given task

f = spatial frequency (cycles/mrad)

D = aperture diameter (m)

D* = detectivity (cm $Hz^{½}$ W^{-1})

n = number of detectors

η_{sc} = scan efficiency

τ_o = transmission of the optics

α = in-scan detector angular subtense (mrad)

β = cross-scan detector angular subtense (mrad)

MTF_{system} = the system modulation transfer function

L = the length-to-width ratio for the bar chart (7)

T_e = eye integration time (0.2s)

$\frac{\partial N}{\partial T}$ = derivative of Planck's Law (watt cm^{-2} K^{-1} sr^{-1})

FOV_x = in-scan field of view (mrad)

FOV_y = cross-scan field of view (mrad)

ρ_x = noise filter factor

B. MRTD COMPUTATION

In this project a hypothetical second generation FLIR sensor developed in Ref.14 is used for performance modeling. The parameters of the sensor are presented in Appendix F and Figure 5.1 shows the plot of MRTD values of the sensor versus spatial frequency.

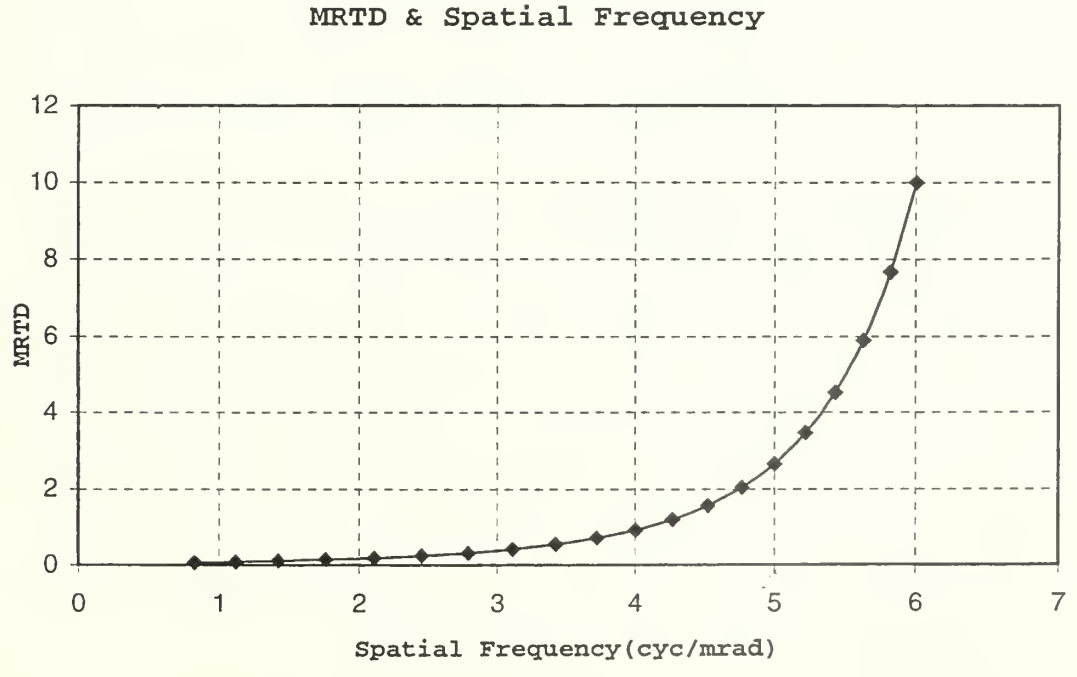

Figure 5.1 MRTD Plot of a Generic GenerationII FLIR Sensor.

The inclusion of a polarized filter into the system may alter the effect of some parameters in MRTD computation. Guimaraes (Ref. 23) has reported an experimental evaluation of this topic and concluded that the polarizer transmissivity (τ_p), polarizer Modulation Transfer Function (MTF_p), and the partial derivative of Planck's Equation with respect to the temperature are the parameters which have the greatest impact in the reformulation of MRTD for the polarized case. The MRTD values of the sensor which is used in this project, were computed using the 3D Noise concept. [Ref. 24] Therefore the functional relation between the MRTD values and the sensor parameters is not well defined. To identify the variation of the MRTD values due to the polarization effect, the algorithm of the calculation has to be known. Bearing in mind that next generation FLIR sensor performance models may not use the 3D noise concept, and that the impact of changing the other parameters in Equation 5.1 will not effect the overall conclusion, only τ_p, the polarizer transmissivity value, was taken into account in the "polarization filter included MRTD calculation".

At this point, in agreement with the conclusions of Guimaraes (Ref.23) the MRTD values were divided by 0.85, which is manufacturer's value for the filter used in the work. It must be recognized that the process used here and in Ref.23 i.e., dividing MRTD values by a transmissivity, is not a completely appropriate solution to the polarization-included MRTD calculation issue, but that it is an approximation that needs further discussion. While the transmittance can be applied to radiant flux or irradiance, it should not be applied directly to the temperature difference term. Appendix G shows the MRTD values of the sensor with and without the polarization filter. In the rest of the project the MRTD values and MRTD curves refer to the case in which the polarizer is added to the system.

C. DETECTION CRITERIA AND PROJECTED AREA OF THE TARGET

In order to compare the sensor's maximum range performance with and without the polarization filter, we need to express MRTD values in terms of range. So far all the MRTD calculations have been made as a function of spatial frequency. In performance test studies if the specific task is given and target dimensions are known, the spatial frequency can be converted into distance with the

help of some established criteria, (e.g. Johnson Criteria) which relate the resolution of bar charts to levels of visual discrimination.

The first experimental determination of these criteria was conducted by John Johnson in 1957. Later Moser and O'Neil made separate studies relating especially to ship targets. Although the approaches show slight differences, all the criteria address the number of resolution elements per critical dimension required by a typical experienced operator for the specified task. The Johnson criterion provides a relation between the target angular subtense (TAS) and the spatial frequency scale on the MRTD graph. The number of cycles that appear across the critical target dimension, which can just be resolved by the sensor at range R, can be found by the relation

$$N = f.TAS \qquad (5.2)$$

where TAS= Critical Target Dimension (D_c)/Range and f is the spatial frequency. Figure 5.2 shows the relation between parameters and Table 5.1 shows the current discrimination criteria with 50% probability for the one and two-dimensional MRTDs. The same approach here to find the MRTD as a function of range has been used in some of the previous works related to the subject.

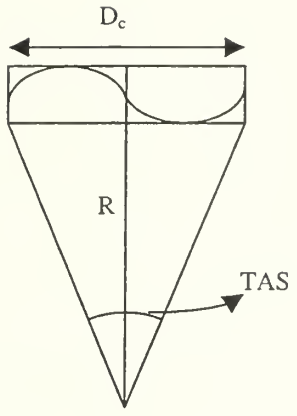

For 2 resels =1 cycle on Critical Dimension

Spatial Frequency, f = 1/TAS where TAS= D_c/R

For N cycles on Critical Dimension f= N Dc/R (cycles/mrad)

Figure 5.2 Conversion of Spatial Frequency into Range. After Ref.[23].

Discrimination level	*Meaning*	*One-D cycles across critical dimension*	*Two-D cycles across critical dimension, N_{50}*
Detection	An object is present	1	0.75
Recognition	Class to which an object belongs (e.g., human, tank, truck)	4	3
Identification	Object is discerned with enough clarity to specify type (M1A, T-62, T-72 Tank)	8	6

Table 5.1 Resolution Cycles on Target Required for Specified Levels of Recognition for Johnson Criteria. From Ref.[24].

The second step in converting spatial frequency into distance is to calculate the "critical dimension", D_c. This dimension is the average target dimension being observed for detection or recognition and simply defined as the square root of the target-projected area.

In this project a ship model created in the MuSES environment is used as a target. Its dimensions and the orientation of the target when the radiance measurements were made are displayed in Appendix C.

The same orientation is used for the calculation of projected area. As expected the aspect angle plays a major role in the calculation. The projected area of the target as a function of its dimensions and the azimuth and elevation angle is found by:

$$A_T = lh \cos\theta \cos\phi + wh \cos\theta \sin\phi + lw \sin\theta \qquad (5.3)$$

where:

l= ship length

w=ship width

h=ship height

θ= elevation angle

ϕ= azimuth angle

Using Equation 5.3, for the scenario conditions, projected area of target is found to be 610.77m^2 and the critical dimension, D_c, is found to be 24.71m. From these parameters and using Equation 5.2, the MRTD values of the sensor were computed as a function of range, using the values N=0.75 for detection, N=3 for recognition and N=6 for identification. The tabulated values are presented in Appendix G. Figure 5.3 shows the MRTD for detection, recognition, and identification respectively.

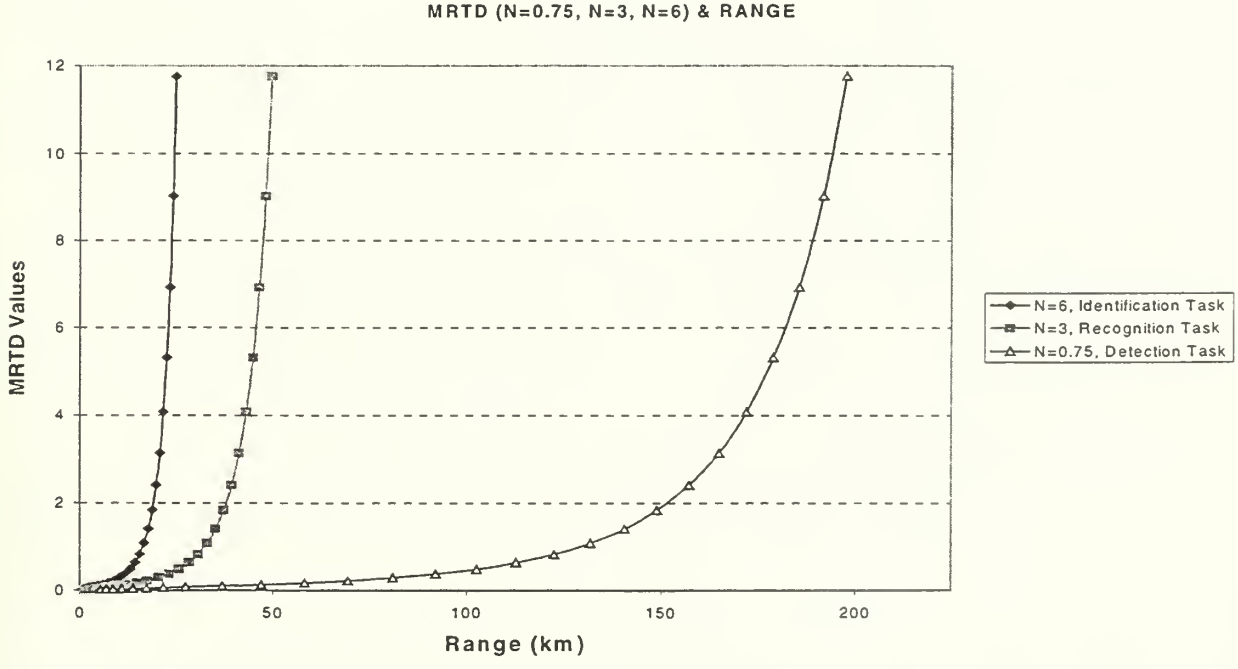

Figure 5.3 Minimum Resolvable Temperature As a Function Of Range, For Detection (N=0.75), Recognition (N=3), and Identification (N=6). "N" is Number of Resolved Cycles on The Critical Dimension.

These results were used in the following sections to find the maximum detection, recognition and identification range of the polarized sensor for the given weather conditions.

D. APPARENT TEMPERATURE DIFFERENCE COMPUTATION

Apparent differential temperatures are equivalent blackbody differential temperatures that represent a target-to-background contrast with degradation due to atmospheric effects. Apparent differential temperature or more commonly "apparent delta T" depends on a number of parameters including source emission characteristics and atmospheric transmission characteristics. There are many different techniques for calculating apparent delta T.

In this project the "radiance computation method" is used for calculation of apparent delta T. The method can be summarized by the following seven steps:

- Calculate the total radiance from the target using the MuSES signature computation model at zero range for the specific weather conditions and target orientation. The weather file and the result file for this computation are presented in Appendix D and E respectively. The target radiance calculations

were made as explained in the last section of Chapter IV.

- Calculate the background radiance, including emission and reflection components, from the sea background, using the SEARAD Radiation Model for different zenith angles that correspond to different ranges.
- Correct the "zero range total target radiance" component of ATD for atmospheric attenuation for a set of different ranges that are appropriate to the data set. At this point the wavelength interval is divided into four sub-bands, then the atmospheric transmittance values were computed corresponding to each sub-band and the inband radiance values were multiplied by those transmittance values. By doing so we have reduced the error that comes from averaging transmittance values in broadband.
- Correct the background and target radiances for path radiance, for the same set of ranges and the transmission coefficients, computed by using SEARAD propagation code. The results are presented in Appendix I.

- Calculate corrected total apparent target radiance by adding the path radiance and target radiance values together. This step can be expressed in an equation as:

$$L_{App.Target(total)} = L_{Target} * \tau\ (Range) + L_{Path\ Radiance} \quad (5.4)$$

- Convert these radiances, i.e "total ship radiance plus path radiance" and "background radiance" values were converted into temperature values by using Planck's formula (Equation 2.6).

$$L_{App.Target}(Range) \longrightarrow T_{App.Target}(Range)$$

$$L_{App\cdot Background}(Range) \longrightarrow T_{App\cdot Background}(Range)$$

For this conversion a short MATLAB code radconv.m and a look-up table, which was created with the result of this code, were used. The code and the look-up table are presented in Appendix H.

- Subtract the temperature values found from conversion of the full range background radiance from the temperature values found from conversion of total ship plus path radiance, to find the apparent temperature difference(ATD) for the specific range.

A schematic representation of the ATD calculation process is given in Figure 5.4.

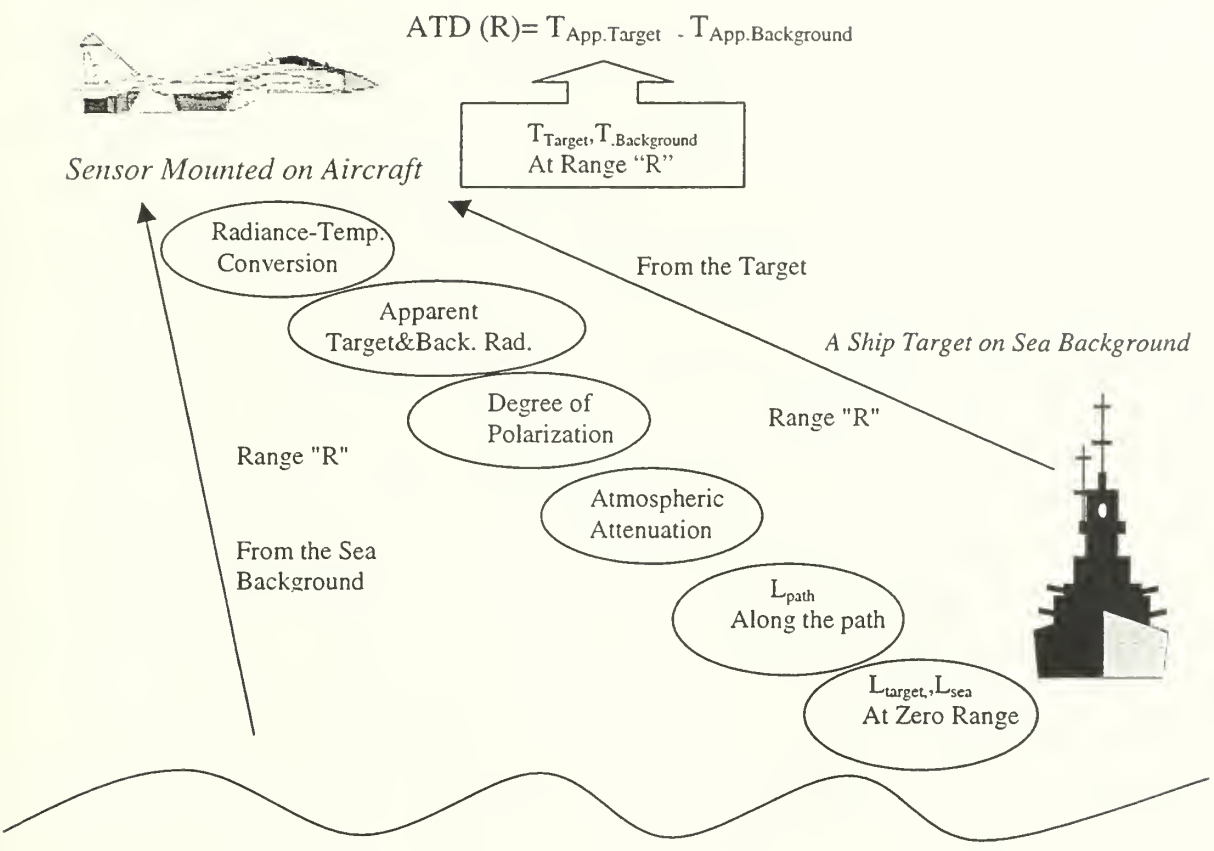

Figure 5.4 A Schematic Representation of ATD Calculation.

Appendix I shows the computed background radiance, target radiance values and ATD values for the corresponding range values. The ATD values were then plotted versus the range values as seen in Figure 5.5. From the plot it is observed that the curve fluctuates in the short range region (1-5 km). This behavior is further discussed in Chapter VI, Conclusions and Recommendations.

In Appendix K the radiance difference values and corresponding temperature difference values are tabulated.

By using a simple Microsoft Excel regression model a relation which is almost linear and independent of the range was found. This result simply states that both radiance difference and temperature difference behave in the same manner. The different aspects of the study are considered under discussion Chapter VI.

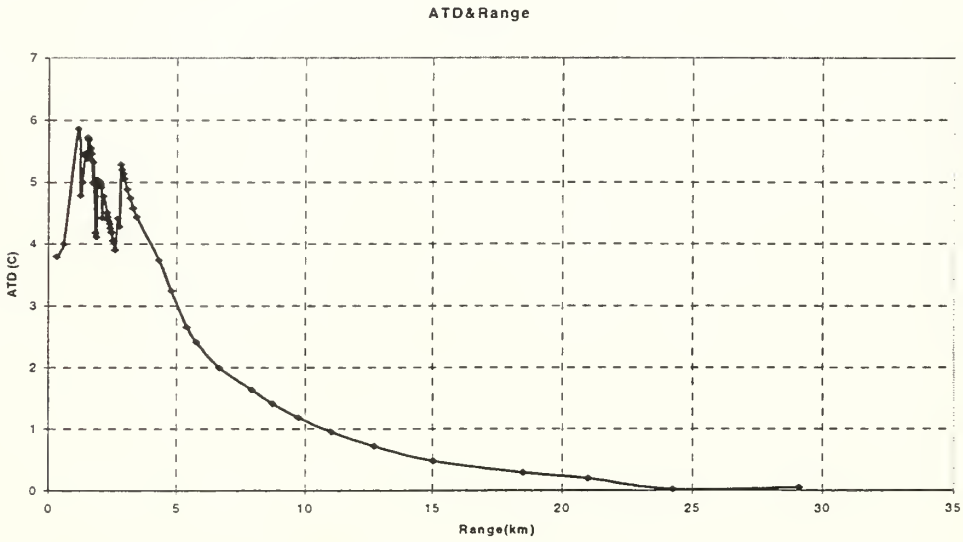

Figure 5.5 Apparent Temperature Difference versus Range for Unpolarized Ship Target and Unpolarized Sea Background Case where Sensor Altitude is 300m.

E. THE EFFECT OF DEGREE OF POLARIZATION

The observed degree of polarization of the radiance can be defined as:

$$POL = \frac{\langle N_v \rangle - \langle N_h \rangle}{\langle N_v \rangle + \langle N_h \rangle} \qquad (5.5)$$

where:

$\langle N_v \rangle$ = mean apparent vertically polarized radiance.

$\langle N_h \rangle$ = mean apparent horizontally polarized radiance.

According to this definition a degree of polarization greater than zero implies a net vertical polarization while the degree of polarization value less than zero implies horizontal polarization.

In general the total radiance from any object has a vertical and horizontal component frequently expressed as a function of the total. While the addition of these normalized components is always unity, the difference between them is defined as the degree of polarization. These two expressions are shown in Equations 5.6 and 5.7.

$$\frac{\langle N_v \rangle}{\langle N_v \rangle + \langle N_h \rangle} - \frac{\langle N_h \rangle}{\langle N_v \rangle + \langle N_h \rangle} = \mathrm{POL} \tag{5.6}$$

$$\frac{\langle N_v \rangle}{\langle N_v \rangle + \langle N_h \rangle} + \frac{\langle N_h \rangle}{\langle N_v \rangle + \langle N_h \rangle} = 1 \tag{5.7}$$

Using these two equations we can express the fractional vertical and horizontal polarization radiance in terms of the degree of polarization as:

$$\frac{\langle N_v \rangle}{\langle N_v \rangle + \langle N_h \rangle} = \frac{(1 + \mathrm{POL})}{2} \tag{5.8}$$

$$\frac{\langle N_h \rangle}{\langle N_v \rangle + \langle N_h \rangle} = \frac{(1 - \mathrm{POL})}{2} \tag{5.9}$$

It can be shown from the above equations that with a zero degree of polarization, i.e., in an unpolarized case, half of the total radiance shows vertical polarization and the other half shows horizontal polarization. This notation is found in previous publications.

Defining the effect of the degree of polarization on radiance components in this way, we can now compute the polarized target radiance and polarized background radiance that enter the sensor when a polarizer is added to the sensor. As mentioned before, in performance analysis knowledge of the polarization characteristics of backgrounds and targets is very important. The contrast difference between target and the background can be improved by using an appropriate polarizing filter. In some previous works (e.g., Ref. 20), it has been showed that the radiation from the sea surface shows vertical polarization in the LWIR. Knowing this fact we can use a horizontally polarized filter to eliminate some of the background radiation and obtain better contrast difference depending on the degree of polarization from a target.

In this project the first goal is to find the effect of degree of polarization on the apparent temperature difference and investigate whether this degree of

polarization makes any improvement in the maximum ranges of a sensor when a polarized filter is added. In order to achieve this goal, the computations were made for the cases where sea background shows vertical polarization with values between 12% - 14%. The exact polarization values were computed from the SEARAD Radiance Model and included into the calculations. In order to find the effect of target polarization in range performance the cases, in which the target has a polarization with values between 0%-8%, both vertically and horizontally, were studied. As an example, when a perfect horizontally polarizing filter is used and the target has a 2% horizontal degree of polarization, 51% of the target radiance would pass the filter while, for an average 15% vertical degree of polarization of sea surface 57.5% of the background radiance would be eliminated.

Appendix J shows the radiance values from target and from background when the horizontal polarizing filter is added and the corresponding ATD values for this configuration. Figure 5.6 shows the ATD curves for polarized cases versus range for target polarization from 0 to 8% (horizontal).

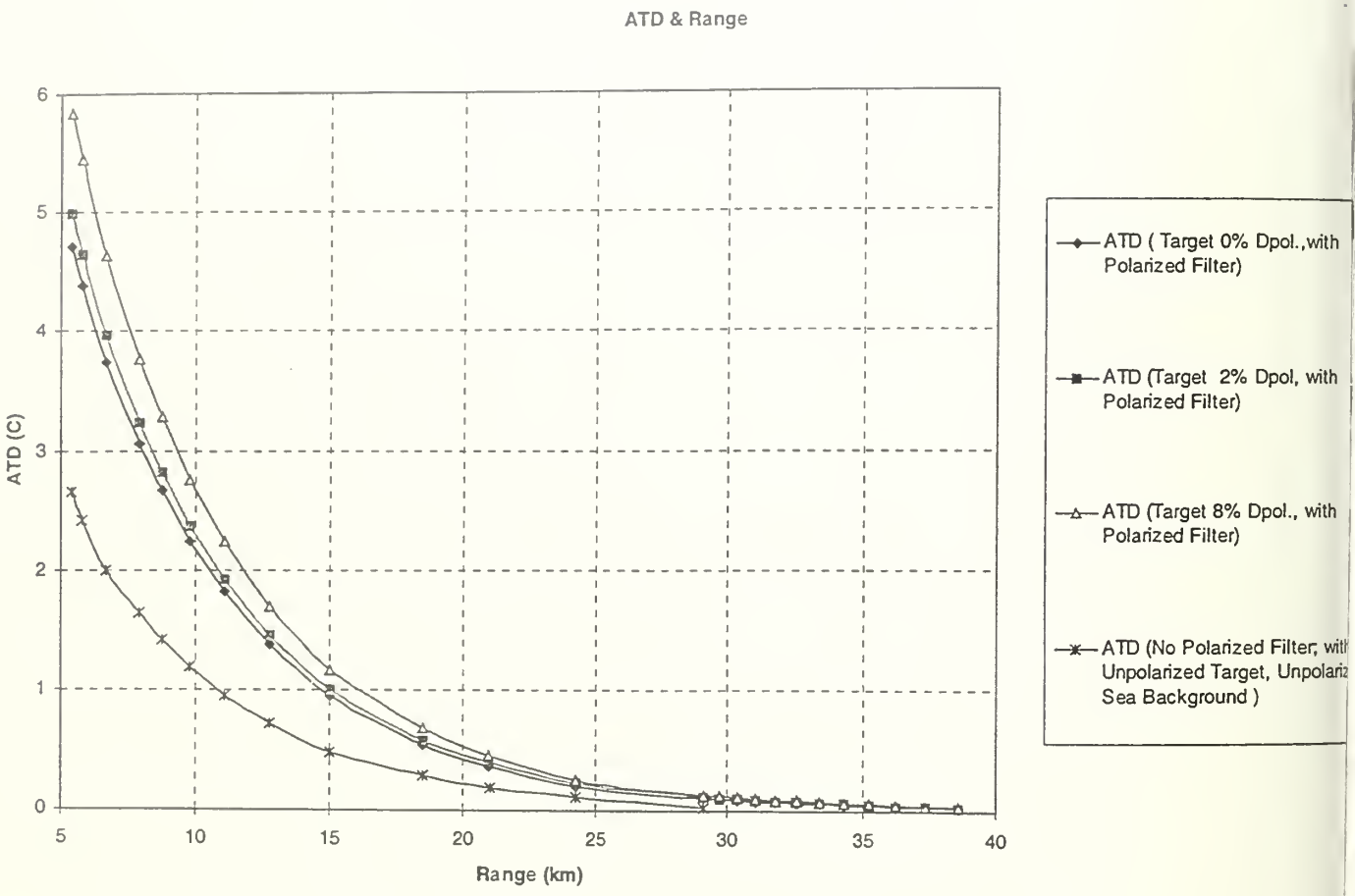

Figure 5.6 Apparent Temperature Difference Values For Polarized and Unpolarized Cases versus Range; Target Polarization as Parameter.

F. RANGE CALCULATIONS

The maximum range of a sensor for detection, recognition or identification can be estimated using the Apparent Temperature Difference (ATD) and the MRTD-MDTD curves. The condition for detection at maximum range is that the ATD will match the required MRTD or MDTD at the same range.

As a last step, the ATD and the MRTD curves for different tasks are plotted on the same scale as a function of range for the selected target with a critical dimension of 24.71m. In each case the intersection of corresponding ATD and MRTD curves gives the maximum range required for that specific task. Figures 5.7 to 5.12 show the different cases.

G. DISCUSSION OF THE DATA

Figure 5.6 shows the expected decrease in ATD with range, all curves approaching zero in the long range limit,as opposed to Ref.18. As expected, increase in horizontal polarization of target leads to increase of the ATD, while removing the filter (transmitting the polarized sea radiance) leads to a decrease. These results are consistent with previous experiences in Refs. 18, 23, and 27.

Figures 5.7 to 5.12 are shown in pairs showing the detection, recognition, and identification ranges for each degree of polarization 0, 2% and 8% of the target. In each case the background polarization is vertical and dependent on range, computed using the SEARAD Radiance Model. Each pair consists of a wide range plot on which is shown the intersection point of the ATD curves for no polarization filter and for horizontal filter with the same target polarization values. As expected in each case the critical range is increased. The second plot of each pair shows an expanded plot of ATD versus MRTD to display the limiting ranges more precisely. On this scale the no-filter case for the detection task cannot be included.

In Table 5.2 the summary of the results, obtained using the model is given for the specific scenario conditions. The scenario consists of a ship target with a critical dimension of 24.71m. The ship target model defined in the MuSES program is similar to the Cyclone class ships (170 feet) which serve as patrol coastal boats-PC. In the scenario the sea background has average 13% vertical polarization while the target has 0%, 2%, and 8% horizontal polarization. The sensor used in the model is a generic second generation FLIR sensor mounted on an aircraft that

approaches the target at 300m elevation. All the calculations and predictions in the model are made within the 8-12μm band.

Range (km) / Specific Task:	No Polarization Filter	Polarization Filter Included		
		Target Degree of Polarization (Horizontal)		
		0%	2%	8%
Detection (N=0.75)	23	30.70	31.20	32.15
Recognition (N=3)	19.15	21.60	21.80	22.25
Identification (N=6)	13.8	15.60	15.75	16.10

Table 5.2 Summary of Maximum Range Prediction Results Obtained From Application of The Model for The Described Scenario.

The model was applied for only one set of meteorological conditions and only one target. Thus there is basically only one data point for each criterion, i.e., detection, recognition, and identification.

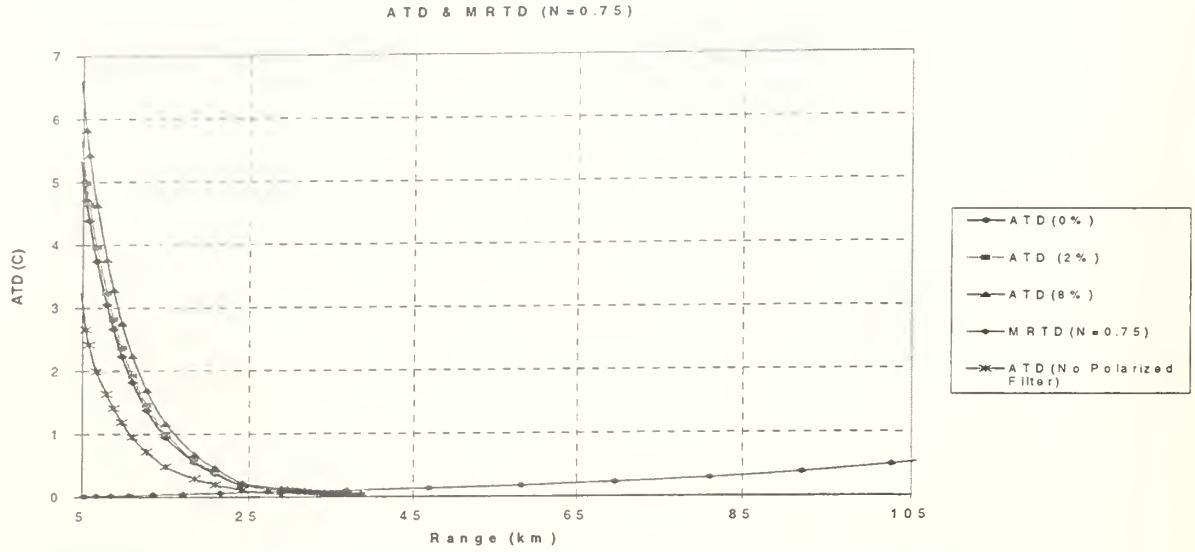

Figure 5.7 ATD & MRTD vs Range for Detection Task (Cycles Across Critical Dimension (N)=0.75) With A Target Polarization 0,+2%,+8% and Background Polarization Between -12.7% -14.6%.

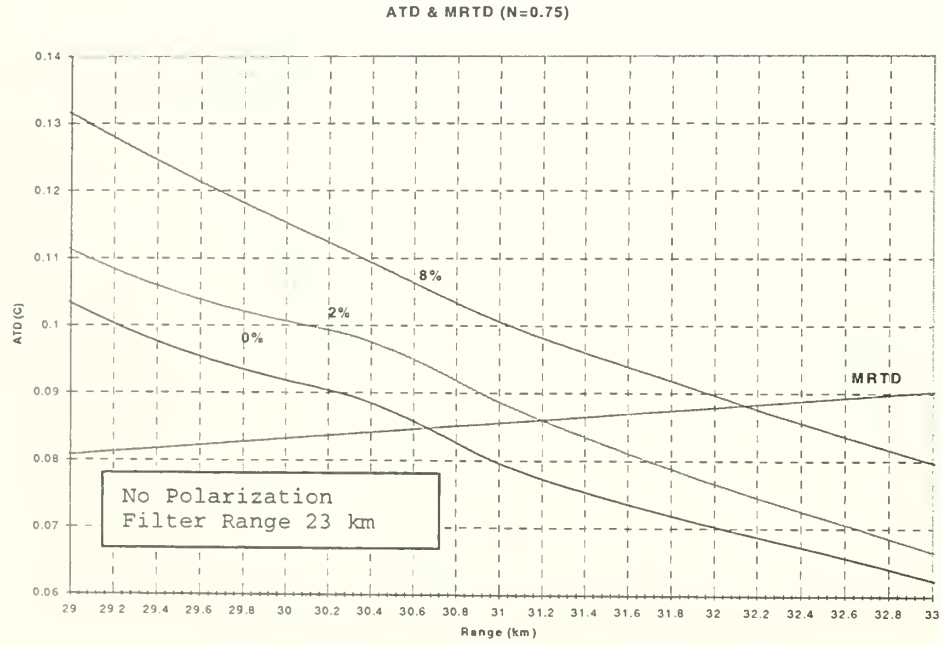

Figure 5.8 ATD & MRTD vs Range for Detection Task (Cycles Across Critical Dimension (N)=0.75) With A Target Polarization 0,+2%,+8% and Background Polarization Between -12.7% -14.6%. Expanded Detail.

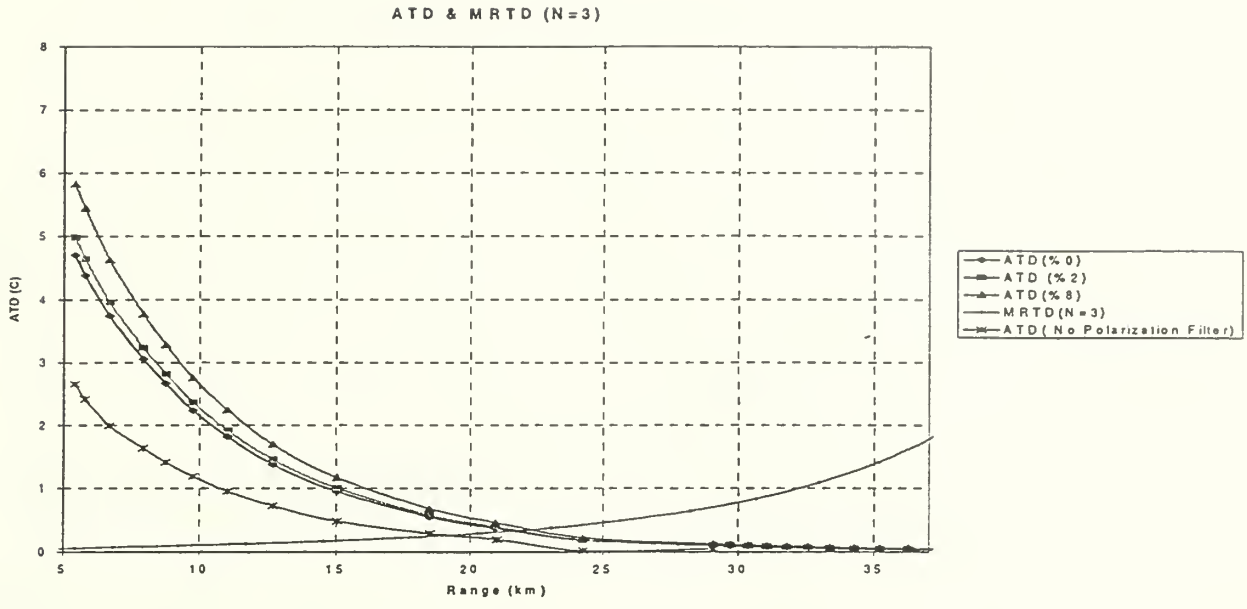

Figure 5.9 ATD & MRTD vs Range for Recognition Task (Cycles Across Critical Dimension (N)=3) With A Target Polarization 0,+2%,+8% and Background Polarization Between -12.7% -14.6%.

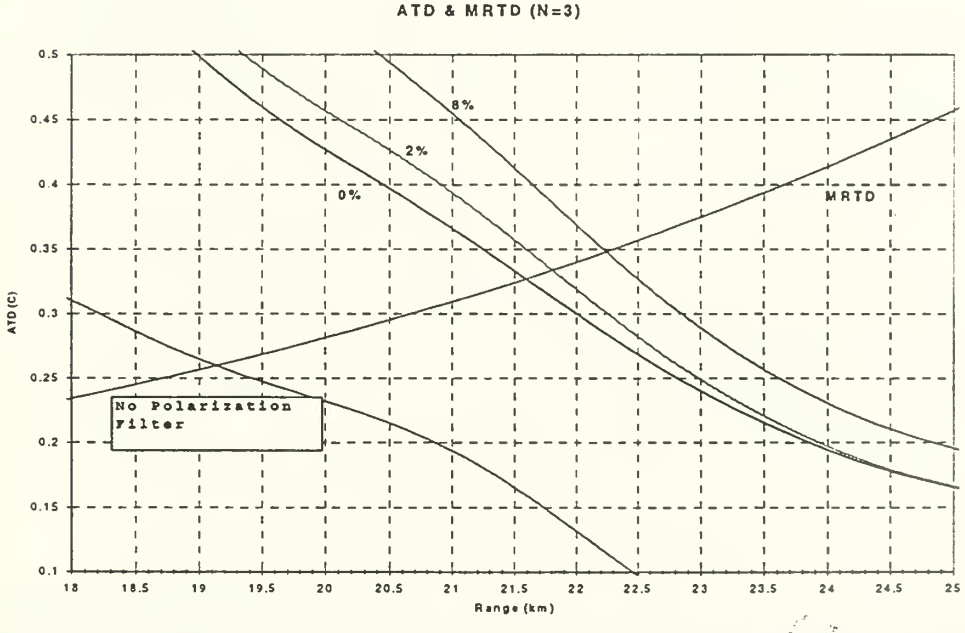

Figure 5.10 ATD & MRTD vs Range for Recognition Task (Cycles Across Critical Dimension (N)=3) With A Target Polarization 0,+2%,+8% and Background Polarization Between -12.7% -14.6%.Expanded Detail.

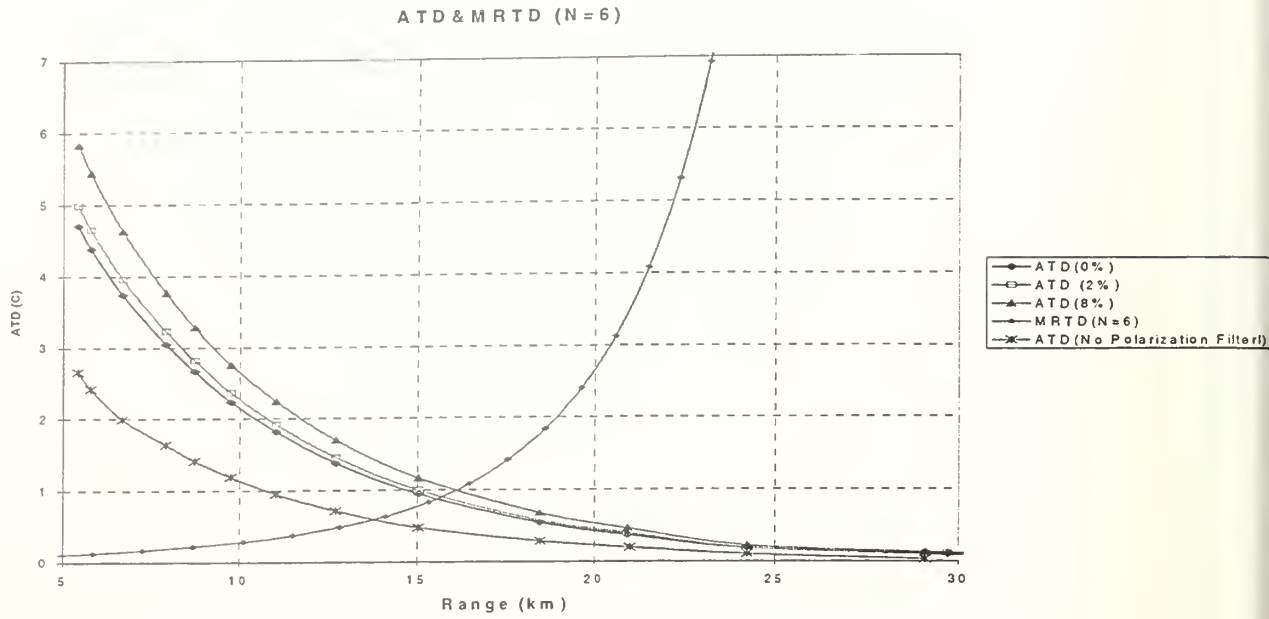

Figure 5.11 ATD & MRTD vs Range for Identification Task (Cycles Across Critical Dimension (N)=6) With A Target Polarization 0,+2%,+8% and Background Polarization Between -12.7% -14.6%..

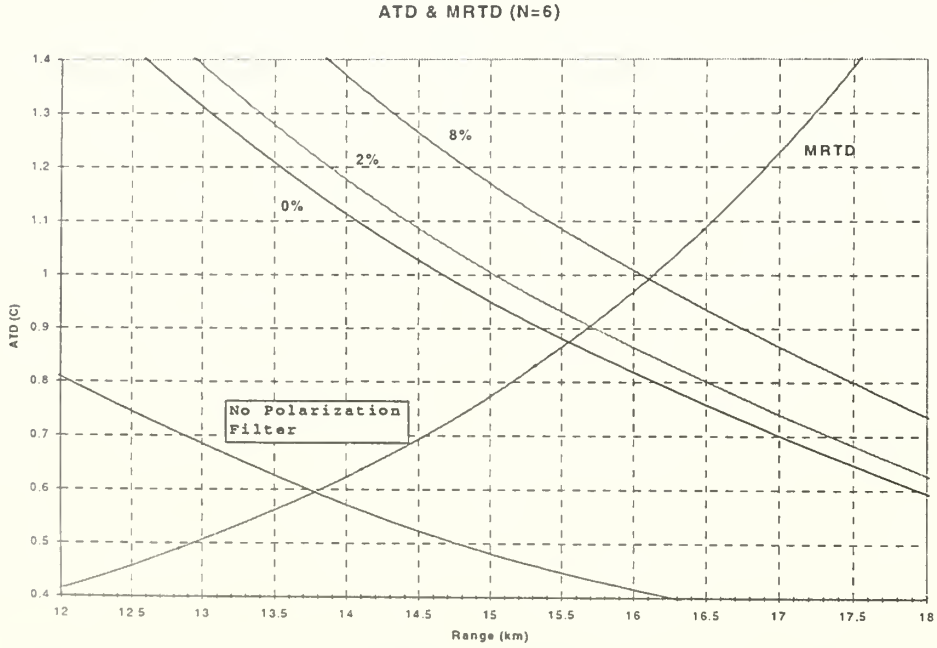

Figure 5.12 ATD & MRTD vs Range for Identification Task (Cycles Across Critical Dimension (N)=6) With A Target Polarization 0,+2%,+8% and Background Polarization Between -12.7%-14.6%. Expanded Detail.

VI. CONCLUSIONS AND RECOMMENDATIONS

The main objectives of this project were to determine the effect of degree of polarization on maximum range performance analysis using an advanced signature prediction model, and also to verify previous project results and models which have studied target-background contrast improvement using horizontal polarizers on sensors.

After obtaining the ATD plot for the given conditions and the MRTD plot of the second-generation sensor, it becomes easy to determine the effect of target degree of polarization on range improvements. As defined before the intersection of the ATD with the MRTD shows the maximum range at which the task can be performed.

The main conclusions of this work and recommendations are listed below:

- Figure 5.7, 5.9 and 5.11 show that there is certainly an improvement in maximum range of the sensor for all tasks when a horizontal filter is included provided that the target does not have a negative degree of polarization. The summary of the improvement amounts as percentage of range with polarizer is shown in Figure 6.1. The figure

indicates that when the target has 0% degree of polarization, for a detection task the improvement with respect to an unpolarized target is 770m (33.4%) for the recognition task 245m (12.79%), and for the identification task 180m (13.04%).

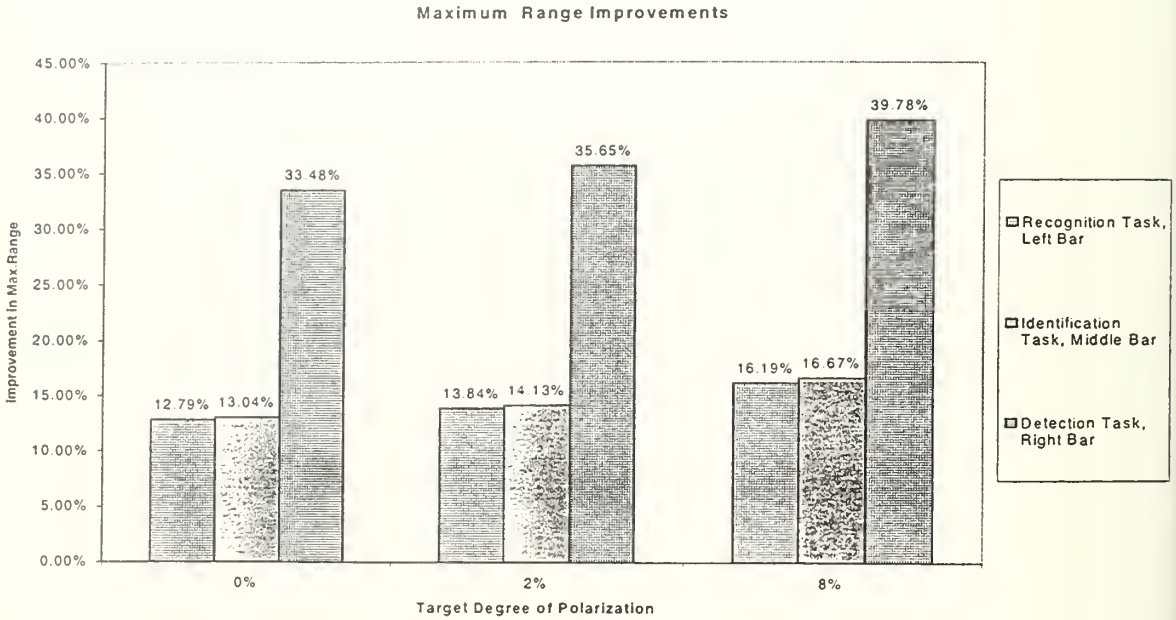

Figure 6.1 Maximum Range Improvement Values For Specific Tasks.

- The model used in this study involved only one target-sensor scenario under one meteorological condition, so no variations with conditions can be concluded. To evaluate the effectiveness of polarization filtering extensive analysis is needed.

- The analysis is based on the assumption that the target has a non-negative degree of polarization. More study and a polarized target model are needed to understand the target polarization characteristics and the techniques for improving polarization values of man made targets.
- In the analysis, SEARAD Radiance Model transmittance values are used for determination of apparent radiance values at the specified wavelengths. It is known that SEARAD calculates the average transmittance value over the selected bandwidth, and this averaging might cause a suppression of strong emission or absorption sub-bands within the specified wavelength range. To minimize this source of possible error, the 8-12μm region over which the whole analysis is done was divided into four sub-bands and the corresponding spectral transmittance values computed. In the analysis the spectral transmittance values were multiplied by the spectral radiance values of the source to obtain apparent radiance values. The results showed that the difference between the apparent radiance values within 8-12μm found by using spectral values and

average transmittance values is not very significant for the scenario in the model. The average difference was found to be less than 1 Watts/m^2sr, spectral values 0.442% greater than average values. The difference becomes less significant with increasing range. Although this approach appears to have small effect on the overall calculations, it may be an important factor in regions other than 8-12μm.

- In the whole analysis some points require special care such as path radiance characteristics. It should be remembered that path radiance is a component of both the sea background radiance and target radiance, and has a 0 degree of polarization. Since at great ranges the radiance incident on the sensor will be mostly from the path radiance, the difference between target apparent temperature and the background apparent temperature should approach zero. In Figure 5.6 the apparent temperatures of target and background approach each other asymptotically. This result can be seen only if the effect of the polarized filter on each radiance element is studied separately. In this analysis the

above procedure is applied and the expected results are obtained. In previous attempts to model this phenomenon, the calculated ATD did not behave logically-i.e., tend to zero at long range. This is believed to be due to the different approaches used to determine $T_{Target}(R)$ and $T_{Background}(R)$. Use of MuSES and better modeling here give more acceptable behavior for ATD and as a result for maximum range calculations. This point is one the most important conclusions of this project. A better modeling of ATD calculations comparing the transmittance calculation method with Beer's Law modeling, and integration of degree of polarization into the calculations may also contribute to further studies.

- Another point that should be noted is the "fluctuation" of the apparent temperature difference in the ranges up to 5km (Figure 5.5). This phenomena is seen both in unpolarized and in polarized signatures and has been seen and interpreted in some previous studies. Although no explanation has been advanced based on physical events, a possible reason for this "fluctuation" is the variation in the spectral radiance of the sky at different angles of

elevation and at different ranges. The parameters of ATD are path radiance and the signatures from target and background. Target signature, and the sea surface emission component of background signature follow an exponentially decaying form with increasing range, while path radiance follows an exponentially increasing course (in the form of $(1-e^{-x})$). As seen in Figure 6.2 sky reflection shows an unsteady character in short ranges.

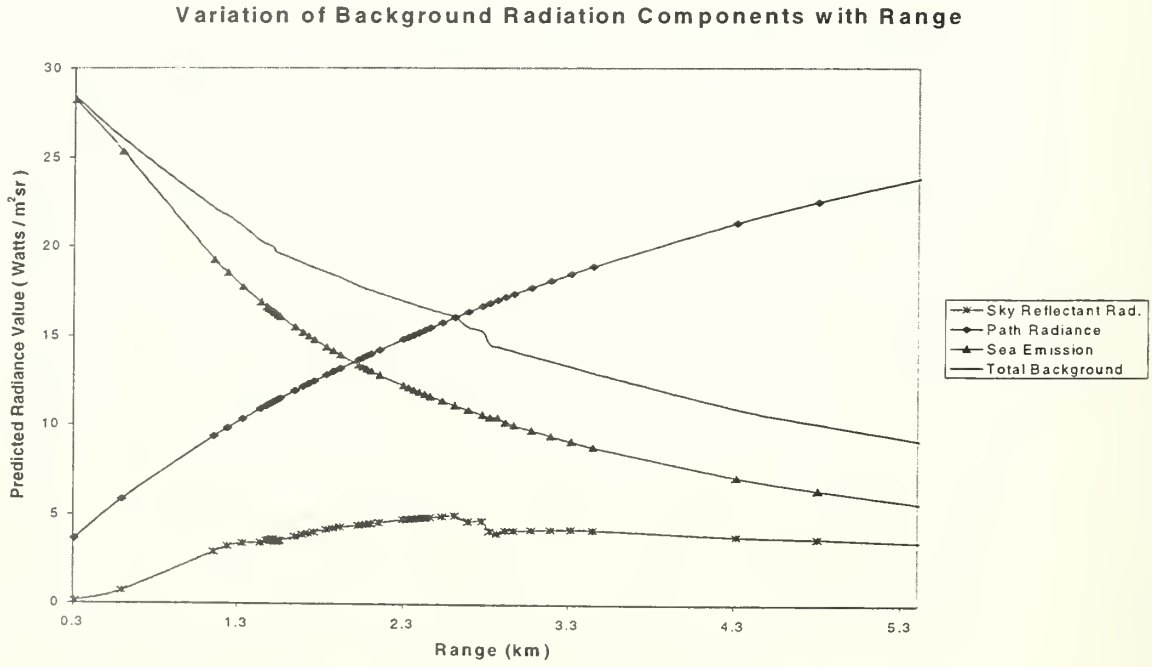

Figure 6.2 Variation of Background Radiance Components and Total Background Radiance with Slant Range.

- The issue of conversion of source temperature to and from in-band radiance is also one of the points that requires further study. In this project conversion is done by direct use of Planck's formula. One surprising consequence was seen when the apparent temperature differences were compared with corresponding radiance differences (Delta W). Having nearly a hundred data pairs, a linear Microsoft Excel regression model was applied and an almost linear relation found between ATD and Delta W. The result simply denotes that the ATD can be approximated for a given range by multiplying the apparent radiance difference between the target and the background by a constant (in this particular scenario) 0.3516237 i.e.,

$$ATD(R) = 0.3516237 * \text{Delta W} \qquad (6.1)$$

The approach is more promising at the ranges greater than 1 km. The results are presented in Appendix K.

It should be expressed clearly that this study is a successor of extensive studies previously performed in performance measurement modeling. Although this study developed an improved maximum range calculation model compared to the models in previous studies [Ref. 18, 23,

27], it is not yet complete due to the lack of a polarized target model. As a suggestion for future work, it would be appropriate to modify the whole analysis by including a polarized target model and a complete polarized MRTD model. The results of this work, with the results of others in the same area, may be useful to demonstrate the effect of target polarization on performance of a sensor in theory.

APPENDIX A

SEARAD RADIATION CODE

```
This is an example of the  SEARAD Radiance Code input file.
The atmospheric model and weather data are obtained from the weather file.

F  2    3    1    1    0    0    0    0    0    0    0    0    0  288.15   0.00
   2    0    0    0    0    0    0.000     5.000     6.000      .000      .000
   00.300      .000    90.680    0.000      .000      0.00    0    90.000    T
      833      1250        10         2
    0
```

This is an example of the SEARAD output file for above input file.

```
                    ***** SEARAD, A MODIFICATION OF LOWTRAN7 *****

DATE: 11/27/2000                                          TIME: 11:24:34.38

THERMAL RADIANCE MODE

MULTIPLE SCATTERING USED

SLANT PATH TO SPACE

          H1       =        .300 KM
          HMIN     =        .000 KM
          ANGLE    =      90.680 DEG

FREQUENCY RANGE

          IV1      =         830 CM-1  (  12.05 MICROMETERS)
          IV2      =        1250 CM-1  (   8.00 MICROMETERS)
          IDV      =          10 CM-1
          IFWHM    =           2 CM-1
          IFILTER  =           0

SUMMARY OF THE GEOMETRY CALCULATION

          H1       =        .300 KM
          H2       =        .000 KM
          ANGLE    =      90.680 DEG
          RANGE    =      30.360 KM
          BETA     =        .273 DEG
          PHI      =      89.547 DEG
          HMIN     =        .000 KM
          BENDING  =        .046 DEG
          LEN      =           0
```

SEA AT 288.15 K REPLACES BLACK BODY BOUNDARY

UPWIND = 90.000 DEG EAST OF LINE OF SIGHT

ZERO RANGE UNPOLARIZED VALUES

SEA EMISSION	=	18.01540 W M-2 SR-1	(AV. EMISS. .5637)
SKY REFLECTION	=	11.41543 W M-2 SR-1	
SUN GLINT	=	.00000 W M-2 SR-1	
TOTAL RADIANCE	=	29.43082 W M-2 SR-1	
BLACK BODY TEMP.	=	10.6 C	

FULL RANGE UNPOLARIZED VALUES

SEA EMISSION	=	.01017 W M-2 SR-1	
SKY REFLECTION	=	.00622 W M-2 SR-1	
SUN GLINT	=	.00000 W M-2 SR-1	
PATH TO FOOTPRINT	=	33.55154 W M-2 SR-1	(AV. TRANS. .0006)
TOTAL RADIANCE	=	33.56792 W M-2 SR-1	
BLACK BODY TEMP.	=	18.0 C	

ZERO RANGE POLARIZED VALUES

	HORIZONTAL (W M-2 SR-1)	VERTICAL (W M-2 SR-1)	(H-V)/(H+V) (%)
SEA EMISSION	7.93007	10.08533	-12.0
SKY REFLECTION	6.52375	4.89168	14.3
SUN GLINT	.00000	.00000	.0
TOTAL RADIANCE	14.45381	14.97701	-1.8
BLACK BODY TEMP. (C)	-24.0	-22.5	

FULL RANGE POLARIZED VALUES

SEA EMISSION	.00446	.00571	-12.3
SKY REFLECTION	.00356	.00265	14.6
SUN GLINT	.00000	.00000	.0
PATH TO FOOTPRINT	16.77577	16.77577	.0
TOTAL RADIANCE	16.78379	16.78413	.0
BLACK BODY TEMP. (C)	-17.5	-17.5	

THIS PAGE INTENTIONALLY LEFT BLANK

APPENDIX B

IR SIGNATURE SIMULATION SOFTWARES

This Appendix contains information on IR signature simulation, materials and background modeling, and performance prediction programs. Some of the programs are commercial and have been widely used. Descriptions of the programs are taken from Ref. 13. Contact points and more information about the programs can be found in the same reference.

AEMAT :Avlab Electro-optical Model for Aerial Targeting

This model also known as EMAT (Electro-optical Model for Aerial Targeting). It has some surface target analysis capability and includes targets, atmospheres, backgrounds, and sensor models in all wavebands. Incorporates SPIRITS by Aerodyne Research. Owner of the model is Horizons Technology, Inc.

CHARM: High Altitude Radiation Model

This model is a plume flow and radiation model for non-air breathing vehicles at altitudes above 40km, the model SIRRM is the plume radiation model applicable for both air breathing and non-air breathing vehicles. Owner of the model is Photon Research Associates.

CREEP : Coating Reflectance Engineering Evaluation Code

First principle method for computation of BRDF of paint coatings. Performs both surface and volume computations. For

subsurface material, the code uses computed Mie scattering phase functions with multiple scattering computational techniques to determine the equivalent BRDF. Owner of the model is ERIM.

EMAT: Electro-optical Model for Aerial Targeting

GTSIG (also known as TCMII): Georgia Tech Thermal Contrast Model. Thermal model development with GTSIG starts with a geometrical model and allows user to incorporate thermal conditions such as thermal loading, hardbody heat sources, and so forth. It models both targets and backgrounds. GTSIG is also known as TCMII, which is the same program that is owned by Georgia Tech Research Institute.

IASPM : Infrared Atmospherics and Signatures prediction Model

IRMA: Infrared Modeling and Analysis

It models passive IR, CO2 laser radar, and passive millimeter wave systems. Output is high resolution imagery. Models ground mobile and high value fixed targets and backgrounds. Owner of the model is Nichols Research Corporation.

PCNirATAM: NATO infrared Air Target Model

This is a complete package to compute the infrared signature of an air vehicle and the associated atmosphere. The package includes executable code for data input, screen and hardcopy plotting, image processing, and target signature calculations. Owner of the model is Ontar Corp.

PRISM: Physically Reasonable Infrared Signature Model

This model predicts the surface temperature and radiance of vehicles, soil, and vegetative background from measured or modeled environment conditions. Radiometric calculations do not include atmospheric or sensor effects. The results are sometimes referred to as zero distance source values. Owner of the model is Keweenaw Research Center, Michigan Tech. University.

SIRIM : Simulated Infrared Image Model

This model is used to generate simulated thermal imagery of targets embedded in synthetic or collected backgrounds. SIRIM combines CSG (combinatorial solid geometry) model, an automatic mesh generator, a thermal diffusion model, and the radiance calculation into one integrated thermal signature prediction code. Owner of the model is ERIM.

SIRRM: Standardized Infrared Radiation Model

SOSIS: Ship and Ocean Surface Image Simulation

SPF: Standard Plume Flow Model

SPIRITS: Spectral and In- Band Radiometric Imaging of Targets and Scenes Model. SPIRITS is a first-principles target signature model developed originally for aircraft, but now applicable to tactical missiles and low altitude strategic missiles. It combines a variety of models to produce a flexible and high performing target/signature modeling capability. It incorporates

LOWTRAN or MODTRAN for atmospherics. Owner of the model is Aerodyne Research, Inc.

SSGM: Strategic Scene Generation Model

APPENDIX C

TARGET DIMENSIONS, ORIENTATION and GEOMETRY of COMPUTATIONS

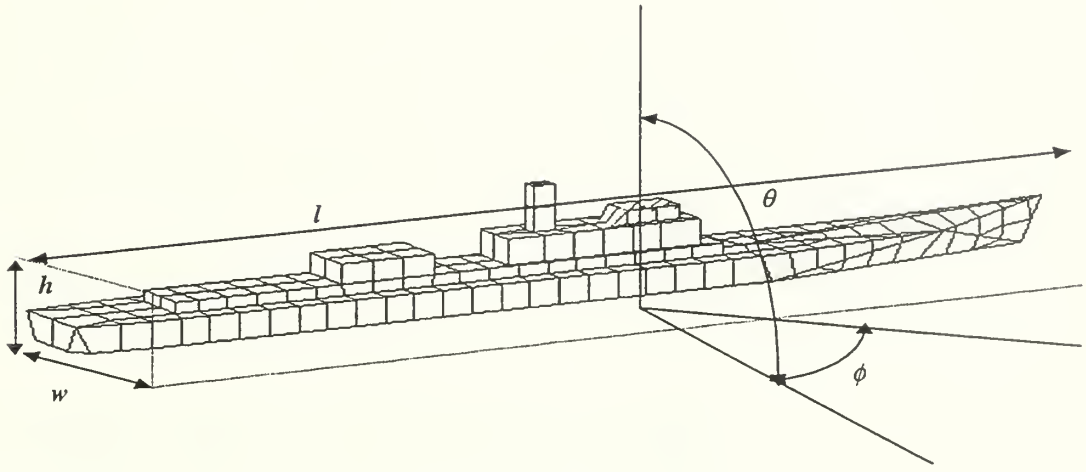

ϕ = Elevation Angle (~0 degree)

θ = Azimuth Angle (~70 degrees)

l = Length (64.832 meters)

h = Height (7.934 meters)

w = Width (7.143 meters)

THIS PAGE INTENTIONALLY LEFT BLANK

APPENDIX D

SAMPLE WEATHER FILE FOR COMPUTATIONS

The Natural environment(weather) option in MuSES uses models or measurements of the weather conditions and the solar position to calculate the cooling or heating that occurs from the influence of weather.Currently there are four different weather files present in the program. The parameters are as follows:

Global Positioning:

Latitude (deg.):47.2 Longitude (deg.): 88.5

Time Zone (hrs.):4 Elevation (m): 332

Date of The Measurements: 07/19/1984.

Available Solution Times: From 07/19/1984 06:20 AM to 07/20/1984 08:59 AM

Selected Solution Time: 07/19/1984 18:00 PM. Late afternoon before dusk. This weather file is selected and made compatible with a standard MODTRAN atmosphere (Midlatitude Summer) by modifying some of the default surface parameters.

Time	Air Temp (C^o)	Solar Rad. (W/m^2str)	Wind Speed (m/sec)	Humidity (%)	Cloud Heigth (km)	Wind Direct. (Deg.)
6:10 AM	18.8	0	1.299	78.833	5	155.808
6:15 AM	18.9	2	0.828	78.25	6	150.912
6:20 AM	18.7	4	0.903	77.667	6	151.92
6:25 AM	18.6	6	1.532	77.083	6	180.216
6:30 AM	18.7	10	1.055	76.5	7	169.704
6:35 AM	18.4	20	1.63	75.917	7	162.72
6:40 AM	18.4	24	1.016	75.333	7	171.936
6:45 AM	18.4	34	1.39	74.75	8	159.408
6:50 AM	18.5	50	1.131	74.167	8	149.184
6:55 AM	19.7	116	2.397	73.583	8	137.088
7:00 AM	18.8	94	1.633	73	7	163.512
7:05 AM	18.5	34	0.467	72.583	7	182.232
7:10 AM	18.4	26	1.758	72.167	7	147.456
7:15 AM	18	14	2.811	71.75	6	161.28
7:20 AM	17.8	16	1.647	71.333	6	142.056
7:25 AM	17.8	14	0.659	70.917	6	170.928
7:30 AM	17.9	12	3.116	70.5	5	157.248
7:35 AM	17.8	10	1.309	70.083	5	214.848
7:40 AM	18	10	1.679	69.667	4	148.464
7:45 AM	18.2	28	2.012	69.25	4	166.32
7:50 AM	18.5	70	2.727	68.833	4	152.496
7:55 AM	18.8	160	2.131	68.417	4	168.48
8:00 AM	19.5	282	2.072	68	4	156.528
8:05 AM	20	306	2.419	67.917	3	153.792

8:10 AM	19.7	260	1.402	67.833	3	144.432
8:15 AM	20	294	1.209	67.75	3	176.544
8:20 AM	19.9	308	2.516	67.667	3	172.368
8:25 AM	19.9	310	1.515	67.583	3	182.232
8:30 AM	19.8	292	1.483	67.5	3	147.528
8:35 AM	19.9	286	2.031	67.417	3	151.776
8:40 AM	20.2	354	1.293	67.333	2	237.168
8:45 AM	20.3	352	1.631	67.25	2	173.448
8:50 AM	20.1	368	1.807	67.167	2	159.48
8:55 AM	20.1	384	1.446	67.083	2	140.472
9:00 AM	20.3	400	1.967	67	2	148.464
9:05 AM	20.1	398	1.504	66.917	2	164.16
9:10 AM	20.1	414	1.03	66.833	2	160.416
9:15 AM	20.1	430	2.862	66.75	2	189.936
9:20 AM	20.1	440	1.435	66.667	2	159.048
9:25 AM	20.1	450	1.752	66.583	1	132.552
9:30 AM	20.4	462	2.231	66.5	1	125.352
9:35 AM	20.3	480	0.707	66.417	1	172.008
9:40 AM	20.4	510	2.117	66.333	1	160.344
9:45 AM	20.3	520	1.52	66.25	1	163.368
9:50 AM	20.4	526	2.134	66.167	1	169.992
9:55 AM	20.2	542	1.522	66.083	1	169.272
10:00 AM	20.3	554	3.271	66	1	167.328
10:05 AM	20.8	564	1.01	66.083	1	159.984
10:10 AM	20.6	578	1.016	66.167	1	124.344
10:15 AM	20.8	590	1.779	66.25	1	170.208
10:20 AM	20.4	600	2.04	66.333	1	154.944
10:25 AM	20.6	606	1.791	66.417	0	168.264
10:30 AM	20.4	624	3.125	66.5	0	169.92
10:35 AM	20.6	632	1.561	66.583	0	175.824
10:40 AM	20.6	644	2.837	66.667	0	174.888
10:45 AM	21.2	650	0.753	66.75	0	186.84
10:50 AM	20.7	658	0.916	66.833	0	192.816
10:55 AM	21.2	672	1.224	66.917	0	163.44
11:00 AM	20.4	690	1.726	67	0	158.688
11:05 AM	21.1	700	1.956	66.917	0	171.936
11:10 AM	21.1	708	1.387	66.833	0	198.792
11:15 AM	21.6	710	0.884	66.75	0	192.672
11:20 AM	21.4	722	1.577	66.667	0	159.552
11:25 AM	21.8	734	1.431	66.583	0	211.824
11:30 AM	21.2	740	2.232	66.5	0	170.352
11:35 AM	20.7	748	2.599	66.417	0	188.856
11:40 AM	21.4	762	0.714	66.333	0	203.76
11:45 AM	21.3	770	2.549	66.25	0	186.912
11:50 AM	21.5	772	0.992	66.167	0	155.232
11:55 AM	21.1	782	1.933	66.083	0	207.144
12:00 PM	21.5	790	1.344	66	0	201.384
12:05 PM	21	798	2.328	65.75	0	176.976
12:10 PM	21.7	802	1.727	65.5	0	189.216

12:15 PM	21.2	810	2.532	65.25	0	176.472
12:20 PM	21.3	820	1.106	65	0	152.496
12:25 PM	22.4	824	1.661	64.75	0	210.888
12:30 PM	21.5	830	2.452	64.5	0	190.584
12:35 PM	21.6	834	1.366	64.25	0	188.28
12:40 PM	21.9	840	1.851	64	0	219.6
12:45 PM	22.1	844	1.342	63.75	0	192.96
12:50 PM	21.8	848	2.102	63.5	0	153.576
12:55 PM	22.2	850	3.257	63.25	0	157.536
1:00 PM	22.2	850	1.933	63	0	161.136
1:05 PM	21.9	856	1.944	63.167	0	148.248
1:10 PM	21.8	862	2.694	63.333	0	184.176
1:15 PM	21.7	868	1.807	63.5	0	167.544
1:20 PM	21.8	872	1.839	63.667	0	172.584
1:25 PM	22.2	874	1.284	63.833	0	163.656
1:30 PM	21.9	876	2.331	64	0	189.936
1:35 PM	22.3	880	1.232	64.167	0	168.408
1:40 PM	22.4	880	1.541	64.333	0	163.728
1:45 PM	23.1	880	1.55	64.5	0	198.936
1:50 PM	22.8	880	1.375	64.667	0	170.928
1:55 PM	22.5	880	2.155	64.833	0	167.544
2:00 PM	22.7	880	1.243	65	0	171.072
2:05 PM	23.1	880	1.073	65.833	0	186.192
2:10 PM	22.8	880	1.734	66.667	0	153.792
2:15 PM	23.3	880	3.066	67.5	0	198.288
2:20 PM	22.9	880	2.306	68.333	0	147.168
2:25 PM	22.9	878	1.891	69.167	0	143.136
2:30 PM	23.9	874	0.649	70	0	139.464
2:35 PM	23.8	866	1.251	70.833	0	151.92
2:40 PM	23.6	860	1.179	71.667	0	201.744
2:45 PM	23.5	860	1.489	72.5	0	166.104
2:50 PM	23.4	860	1.439	73.333	0	189.072
2:55 PM	23	852	2.124	74.167	0	191.52
3:00 PM	23.3	850	1.72	75	0	196.344
3:05 PM	23.6	850	1.198	73.833	0	157.032
3:10 PM	23.8	842	1.814	72.667	0	227.088
3:15 PM	22.9	838	3.068	71.5	0	163.8
3:20 PM	23.3	832	0.935	70.333	0	188.784
3:25 PM	23.3	828	2.096	69.167	0	144.936
3:30 PM	23.7	820	0.808	68	0	166.032
3:35 PM	23.2	814	1.257	66.833	0	175.896
3:40 PM	23.3	808	1.646	65.667	0	162.648
3:45 PM	23.8	802	1.209	64.5	0	199.008
12:00 AM	23.7	798	0.746	63.333	0	190.584
3:55 PM	23.9	788	3.028	62.167	0	190.368
4:00 PM	23.7	780	2.494	61	0	164.88
4:05 PM	24	772	1.487	59	0	186.984
4:10 PM	23.8	766	1.95	57	0	176.328

4:15 PM	24.1	758	2.375	55	0	176.472
4:20 PM	24.2	750	0.931	53	0	156.672
4:25 PM	24.2	744	1.568	51	0	187.56
4:30 PM	24.3	738	1.75	49	0	218.592
4:35 PM	24.7	714	1.078	47	0	154.944
4:40 PM	24.4	708	1.027	45	0	158.256
4:45 PM	24.4	700	1.411	43	0	151.488
4:50 PM	24.6	692	0.788	41	0	192.24
4:55 PM	24.8	684	1.224	39	0	220.176
5:00 PM	25	674	1.247	37	0	156.744
5:05 PM	24.4	662	1.431	37.083	0	193.032
5:10 PM	24	650	2.481	37.167	0	183.456
5:15 PM	24	640	1.322	37.25	0	163.08
5:20 PM	24.6	626	2.553	37.333	0	164.232
5:25 PM	24.3	618	1.084	37.417	0	177.48
5:30 PM	24.4	604	0.714	37.5	0	173.592
5:35 PM	24.2	594	1.37	37.583	0	215.928
5:40 PM	24.7	582	0.757	37.667	0	139.176
5:45 PM	24.7	568	0.693	37.75	0	184.608
5:50 PM	24.8	552	1.349	37.833	0	180.36
5:55 PM	24.6	542	1.225	37.917	0	194.112
6:00 PM	24.4	530	0.968	38	0	196.344
6:05 PM	24.2	516	1.418	38.417	0	194.256
6:10 PM	25.1	502	0.554	38.833	0	179.784
6:15 PM	24.3	488	0.86	39.25	0	176.976
6:20 PM	24.3	474	0.981	39.667	0	168.84
6:25 PM	24.7	460	0.941	40.083	0	204.768
6:30 PM	24.4	444	0.824	40.5	0	201.168
6:35 PM	24.1	434	1.095	40.917	0	223.2
6:40 PM	23.9	418	0.87	41.333	0	185.76
6:45 PM	23.8	400	0.973	41.75	0	201.528
6:50 PM	23.7	386	1.339	42.167	0	178.632
6:55 PM	23.9	374	1.111	42.583	0	190.152
7:00 PM	23.9	358	1.211	43	0	209.448
7:05 PM	23.9	344	1.674	43	0	164.952
7:10 PM	23.9	328	0.624	43	0	178.2
7:15 PM	23.7	316	1.223	43	0	212.472
7:20 PM	23.3	300	0.753	43	0	199.44
7:25 PM	23.6	286	0.791	43	0	181.08
7:30 PM	23.4	272	0.482	43	0	183.96
7:35 PM	23.3	260	0.622	43	0	140.904
7:40 PM	23.7	240	0.626	43	0	181.224
7:45 PM	23.4	230	0.505	43	0	167.544
7:50 PM	23.4	216	0.303	43	0	204.912
7:55 PM	23	202	0.783	43	0	186.768
8:00 PM	22.4	184	0.2	43	0	198.648
8:05 PM	22	176	0.337	44.167	0	216.36
8:10 PM	21.9	168	0.2	45.333	0	141.912
8:15 PM	21.8	154	0.202	46.5	0	186.768

12:24 AM	13.7	0	0.2	67.578	1	166.968
12:29 AM	14.3	0	0.2	67.837	1	172.584
12:34 AM	14.4	4	0.704	68.096	1	175.752
12:39 AM	14.6	0	0.2	68.356	1	180.648
12:44 AM	14.6	0	0.336	68.615	1	176.976
12:49 AM	14.7	0	0.227	68.874	1	184.248
12:54 AM	14.6	0	0.302	69.133	1	180.144
12:59 AM	14.8	0	0.218	69.393	0	183.6
1:04 AM	14.5	0	0.252	69.652	0	177.192
1:09 AM	14.5	0	0.205	69.911	0	170.208
1:14 AM	14.2	2	0.2	70.17	0	187.488
1:19 AM	14.6	2	0.421	70.43	0	191.664
1:24 AM	14.5	0	0.29	70.689	0	225.792
1:29 AM	14.4	0	0.369	70.948	0	214.848
1:34 AM	13.9	0	0.199	71.207	0	187.704
1:39 AM	14.6	0	0.266	71.467	0	188.208
1:44 AM	14.6	0	0.291	71.726	0	182.808
1:49 AM	14.6	0	0.531	71.985	0	182.88
1:54 AM	14.8	0	0.887	72.244	0	190.08
1:59 AM	14.8	0	0.415	72.504	0	206.424
2:04 AM	14.9	0	0.498	72.763	0	187.2
2:09 AM	14.8	0	0.304	73.022	0	206.784
2:14 AM	14.8	4	0.514	73.281	0	195.336
2:19 AM	14.6	0	0.855	73.541	0	193.248
2:24 AM	14.2	0	0.344	73.8	0	193.896
2:29 AM	13.8	0	0.747	74.059	0	159.768
2:34 AM	13.3	2	0.213	74.319	0	167.76
2:39 AM	13.3	0	0.2	74.578	0	178.128
2:44 AM	13.2	2	0.529	74.837	0	168.768
2:49 AM	13.3	0	0.938	75.096	0	173.16
2:54 AM	13.6	4	0.423	75.356	0	165.024
2:59 AM	13.8	0	0.572	75.615	0	175.752
3:04 AM	13.9	0	0.599	75.874	0	188.64
3:09 AM	13.3	0	0.28	76.133	0	201.168
3:14 AM	13.3	0	0.352	76.393	0	179.136
3:19 AM	13.3	0	0.64	76.652	0	179.784
3:24 AM	13	4	1.227	76.911	0	162.072
3:29 AM	13.3	0	0.761	77.17	0	175.248
3:34 AM	13.3	0	0.627	77.43	0	187.272
3:39 AM	13.2	0	0.689	77.689	0	169.632
3:44 AM	13.3	0	1.235	77.948	0	191.304
3:49 AM	13.9	0	0.551	78.207	0	193.392
3:54 AM	13.9	0	1.011	78.467	0	194.688
3:59 AM	14.1	0	0.877	78.726	0	207.648
4:04 AM	13.8	0	1.102	78.985	0	191.88
4:09 AM	13.2	2	0.341	79.244	0	182.304
4:14 AM	12.6	0	0.397	79.504	0	192.168
4:19 AM	12.6	0	0.595	79.763	0	194.04
4:24 AM	12.4	0	0.432	80.022	0	180.144

4:29 AM	12.3	0	0.911	80.281	0	181.728
4:34 AM	12.2	0	0.573	80.541	0	170.928
4:39 AM	12.1	4	0.283	80.8	0	190.728
4:44 AM	12.1	0	0.259	81.059	0	191.016
4:49 AM	12.4	0	0.323	81.318	0	189.36
4:54 AM	12.3	0	0.904	81.578	0	183.384
4:59 AM	11.7	0	0.98	81.837	0	187.56
5:04 AM	11.7	0	0.464	82.096	0	183.816
5:09 AM	12	0	0.601	82.356	0	184.464
5:14 AM	12.4	0	0.474	82.615	0	179.352
5:19 AM	12.3	0	0.64	82.874	0	190.8
5:24 AM	11.8	0	0.254	83.133	0	179.856
5:29 AM	11.9	0	0.553	83.393	0	180.576
5:34 AM	12.1	0	0.984	83.652	0	169.632
5:39 AM	12	0	1.041	83.911	0	168.984
5:44 AM	11.9	4	0.271	84.17	0	174.024
5:49 AM	11.9	2	0.938	84.43	0	166.752
5:54 AM	12.2	4	0.423	84.689	0	163.656
5:59 AM	12.3	2	0.812	84.948	0	164.016
6:04 AM	12.3	0	0.556	85.207	0	165.384
6:09 AM	12.3	10	0.699	85.467	0	166.392
6:14 AM	12.2	10	0.492	85.726	0	169.272
6:19 AM	12.3	10	0.698	85.985	0	162.792
6:24 AM	12.3	10	0.627	86.244	0	167.112
6:29 AM	12.2	12	0.581	86.504	0	168.048
6:34 AM	12.2	18	0.207	86.763	0	182.16
6:39 AM	12.1	20	0.57	87.022	0	174.816
6:44 AM	12.8	26	0.245	87.281	0	166.824
6:49 AM	13	48	0.696	87.541	0	181.728
6:54 AM	13.2	60	0.254	87.8	0	176.616
6:59 AM	13.6	68	0.875	88.059	0	177.264
7:04 AM	13.9	82	0.345	88.318	0	166.608
7:09 AM	14.3	96	0.877	88.578	0	165.6
7:14 AM	14.3	106	0.6	88.837	0	169.272
7:19 AM	14.7	120	0.81	89.096	0	162.504
7:24 AM	15	132	0.305	89.356	0	171.216
7:29 AM	15.1	142	1.043	89.615	0	165.096
7:34 AM	15.6	154	0.539	89.874	0	157.392
7:39 AM	15.8	168	0.57	90.133	0	166.896
7:44 AM	15.9	178	1.42	90.393	0	172.152
7:49 AM	16.3	192	0.948	90.652	0	180.144
7:54 AM	16.7	206	1.574	90.911	0	169.992
7:59 AM	16.9	220	0.471	91.17	0	172.368
8:04 AM	17.2	230	0.997	91.43	0	170.784
8:09 AM	17.4	240	0.935	91.689	1	180.072
8:14 AM	17.6	262	0.85	91.948	1	181.224
8:19 AM	17.7	280	1.625	92.207	1	173.664
8:24 AM	17.9	286	0.243	92.467	1	170.928
8:29 AM	18.2	308	0.51	92.726	1	169.704

8:34 AM	18.4	324	0.924	92.985	1	202.752
8:39 AM	18.7	336	1.342	93.244	2	189.792
8:44 AM	19.2	350	0.519	93.504	2	190.368
8:49 AM	19.1	366	1.182	93.763	2	191.664
8:54 AM	19.2	376	1.207	94.022	2	205.704
8:59 AM	19.3	390	1.113	94.281	2	162.072

THIS PAGE INTENTIONALLY LEFT BLANK

APPENDIX E

TARGET RADIANCE COMPUTATION RESULTS

MuSES ascii Results File
Exported from model: c:\Program Files\MuSES\Work\Examples\tez1
Tue Jun 13 00:22:47 2000
Units in the file: SI Units

Radiance Band: 8 to 9 micron

Time Step 10, Time = Jul 19, 1984 18:00:00, Lat.47.2°, Long.,88.5°, Time Zone 4 hr

Element (Number&Location in the Model)	Radiance (W/m^2-sr)	Area(m^2)	Eff.Intensity (W/sr)
1 103 (front)	7.958443	1.2388	9.8589
2 102 (front)	7.992607	4.1946	33.5258
3 101 (front)	7.967958	3.798	30.2623
4 211 (front)	8.007335	1.512	12.1071
5 96 (front)	8.012812	1.729	13.8542
6 99 (front)	7.965985	1.373	10.9373
7 100 (front)	7.993531	3.537	28.2731
8 314 (front)	7.561034	2.776	20.9894
9 313 (front)	7.579693	4.1102	31.1541
10 98 (front)	7.996742	2.459	19.6640
11 95 (front)	8.006999	4.3818	35.0851
12 94 (front)	8.00824	4.4529	35.6599
13 97 (front)	8.033536	0.3109	2.4976
14 312 (front)	7.587668	3.928	29.8044
15 318 (front)	7.598871	5.806	44.1190
16 93 (front)	8.010954	6.6406	53.1975
17 89 (front)	8.161586	0.8872	7.2410
18 88 (front)	8.163546	1.583	12.9229
19 92 (front)	8.01196	4.2047	33.6879
20 91 (front)	8.014287	3.1853	25.5279
21 87 (front)	8.156629	2.3744	19.3671
22 86 (front)	8.15473	3.167	25.8260
23 90 (front)	8.031284	1.3385	10.7499
24 204 (front)	8.020765	1.7346	13.9128
25 85 (front)	8.157871	3.558	29.0257
26 84 (front)	8.178525	4.2141	34.4651
27 205 (front)	8.039721	0.4487	3.6074
28 83 (front)	8.194448	4.8426	39.6824
29 82 (front)	8.199583	2.2895	18.7729
30 81 (front)	8.201283	4.8426	39.7155
31 117 (front)	9.210635	2.0937	19.2843
32 116 (front)	9.238527	2.0938	19.3436
33 80 (front)	8.20176	4.8427	39.7187
34 79 (front)	8.201813	4.8426	39.7181
35 115 (front)	9.244595	2.0938	19.3563

36	114 (front)	9.241716	2.0938	19.3503
37	78 (front)	8.201728	4.8426	39.7177
38	77 (front)	8.201805	4.8426	39.7181
39	113 (front)	9.239729	2.0938	19.3461
40	112 (front)	9.214361	2.0938	19.2930
41	75 (front)	8.201061	4.8426	39.7145
42	76 (front)	8.201627	4.8426	39.7172
43	111 (front)	9.141351	2.0949	19.1502
44	110 (front)	9.116871	2.0937	19.0880
45	74 (front)	8.200602	4.8426	39.7122
46	73 (front)	8.200427	4.8426	39.7114
47	109 (front)	9.137383	1.9801	18.0929
48	221 (front)	9.203058	2.2074	20.3148
49	72 (front)	8.201587	4.8426	39.7170
50	71 (front)	8.201874	4.8426	39.7184
51	222 (front)	9.234715	2.0937	19.3347
52	108 (front)	9.193591	2.1922	20.1542
53	70 (front)	8.2017	4.8426	39.7176
54	69 (front)	8.200892	4.8426	39.7136
55	107 (front)	9.137054	1.9953	18.2312
56	106 (front)	9.087182	2.0937	19.0258
57	68 (front)	8.200092	4.8426	39.7098
58	67 (front)	8.199725	4.8426	39.7080
59	105 (front)	9.069571	2.0937	18.9890
60	104 (front)	9.063439	2.0937	18.9761
61	66 (front)	8.199563	4.8426	39.7072
62	65 (front)	8.199446	4.8426	39.7066
63	225 (front)	9.05103	2.0937	18.9501
64	226 (front)	8.982138	1.563	14.0391
65	64 (front)	8.19859	4.8426	39.7025
66	63 (front)	8.206901	4.8426	39.7427
67	62 (front)	8.232753	4.873	40.1182
68	234 (front)	8.064871	1.8129	14.6208
69	61 (front)	8.230124	5.9936	49.3281
70	123 (front)	8.651789	6.2584	54.1464
71	122 (front)	8.676771	4.7116	40.8815
72	121 (front)	8.680046	4.7116	40.8969
73	120 (front)	8.677021	4.7116	40.8827
74	119 (front)	8.677439	4.7116	40.8846
75	118 (front)	8.663925	5.9623	51.6569
76	224 (front)	8.62009	4.1013	35.3536
77	223 (front)	8.629618	3.6995	31.9253
78	126 (front)	8.621908	4.0475	34.8972
79	25 (front)	8.67183	3.1649	27.4455
80	125 (front)	8.556823	2.9062	24.8678
81	124 (front)	8.830137	2.5541	22.5531
82	11 (front)	8.73445	2.0339	17.7650
83	30(front)	9.08509	5.7346	52.0994
TOTAL			287.2313	2401.0082

MuSES ascii Results File
Exported from model: c:\Program Files\MuSES\Work\Examples\tez1
Tue Jun 13 00:22:47 2000
Units in the file: SI Units
Radiance Band: 9 to 10 micron
Time Step 10, Time = Jul 19, 1984 18:00:00

Element (Number&Location in the Model)		Radiance (W/m^2-sr)	Area(m^2)	Eff.Intensity (W/sr)
1	103 (front)	8.395911	1.2388	10.4009
2	102 (front)	8.428118	4.1946	35.3526
3	101 (front)	8.404932	3.798	31.9219
4	211 (front)	8.454721	1.512	12.7835
5	96 (front)	8.459952	1.729	14.6273
6	99 (front)	8.403075	1.373	11.5374
7	100 (front)	8.428987	3.537	29.8133
8	314 (front)	7.980424	2.776	22.1537
9	313 (front)	7.998057	4.1102	32.8736
10	98 (front)	8.432007	2.459	20.7343
11	95 (front)	8.454469	4.3818	37.0458
12	94 (front)	8.455703	4.4529	37.6524
13	97 (front)	8.466532	0.3109	2.6322
14	312 (front)	8.005523	3.928	31.4457
15	312 (front)	8.016232	5.806	46.5422
16	312 (front)	8.4582	6.6406	56.1675
17	312 (front)	8.582376	0.8872	7.6143
18	312 (front)	8.584213	1.583	13.5888
19	312 (front)	8.459149	4.2047	35.5682
20	312 (front)	8.461345	3.1853	26.9519
21	312 (front)	8.57773	2.3744	20.3670
22	312 (front)	8.575952	3.167	27.1600
23	312 (front)	8.477506	1.3385	11.3471
24	312 (front)	8.467646	1.7346	14.6880
25	312 (front)	8.578896	3.558	30.5237
26	312 (front)	8.598026	4.2141	36.2329
27	312 (front)	8.485527	0.4487	3.8075
28	312 (front)	8.613157	4.8426	41.7101
29	312 (front)	8.617968	2.2895	19.7308
30	312 (front)	8.61956	4.8426	41.7411
31	312 (front)	9.562263	2.0937	20.0205
32	312 (front)	9.588289	2.0938	20.0760
33	312 (front)	8.620008	4.8427	41.7441
34	312 (front)	8.620056	4.8426	41.7435
35	312 (front)	9.593952	2.0938	20.0878
36	312 (front)	9.591261	2.0938	20.0822
37	312 (front)	8.619977	4.8426	41.7431
38	312 (front)	8.620049	4.8426	41.7434

39	312 (front)	9.589403	2.0938	20.0783
40	312 (front)	9.565712	2.0938	20.0287
41	312 (front)	8.619352	4.8426	41.7401
42	312 (front)	8.619883	4.8426	41.7426
43	312 (front)	9.497645	2.0949	19.8966
44	312 (front)	9.474776	2.0937	19.8373
45	312 (front)	8.618921	4.8426	41.7380
46	312 (front)	8.618758	4.8426	41.7372
47	312 (front)	9.494009	1.9801	18.7991
48	312 (front)	9.555324	2.2074	21.0924
49	312 (front)	8.619844	4.8426	41.7425
50	312 (front)	8.620113	4.8426	41.7438
51	312 (front)	9.584821	2.0937	20.0677
52	312 (front)	9.546453	2.1922	20.9277
53	312 (front)	8.6199	4.8426	41.7427
54	312 (front)	8.619194	4.8426	41.7393
55	312 (front)	9.493543	1.9953	18.9425
56	312 (front)	9.446975	2.0937	19.7791
57	312 (front)	8.618444	4.8426	41.7357
58	312 (front)	8.6181	4.8426	41.7340
59	312 (front)	9.430511	2.0937	19.7447
60	312 (front)	9.424775	2.0937	19.7327
61	312 (front)	8.617949	4.8426	41.7333
62	312 (front)	8.617839	4.8426	41.7327
63	312 (front)	9.413185	2.0937	19.7084
64	312 (front)	9.348808	1.563	14.6122
65	312 (front)	8.617038	4.8426	41.7289
66	312 (front)	8.624819	4.8426	41.7665
67	312 (front)	8.649023	4.873	42.1467
68	312 (front)	8.501824	1.8129	15.4130
69	312 (front)	8.646563	5.9936	51.8240
70	312 (front)	9.041137	6.2584	56.5831
71	312 (front)	9.064513	4.7116	42.7084
72	312 (front)	9.067591	4.7116	42.7229
73	312 (front)	9.064775	4.7116	42.7096
74	312 (front)	9.065146	4.7116	42.7113
75	312 (front)	9.052497	5.9623	53.9737
76	312 (front)	9.009426	4.1013	36.9504
77	312 (front)	9.018324	3.6995	33.3633
78	312 (front)	9.011096	4.0475	36.4724
79	312 (front)	9.059747	3.1649	28.6732
80	312 (front)	8.951976	2.9062	26.0162
81	312 (front)	9.207458	2.5541	23.5168
82	312 (front)	9.118356	2.0339	18.5458
83	312 (front)	9.4452	5.7346	54.1644
TOTAL			287.2313	2518.0562

MuSES ascii Results File
Exported from model: c:\Program Files\MuSES\Work\Examples\tez1
Tue Jun 13 00:22:47 2000
Units in the file: SI Units
Radiance Band: 10 to 11 micron
Time Step 10, Time = Jul 19, 1984 18:00:00

Element (Number&Location in the Model)	Radiance (W/m^2-sr)	Area(m^2)	Eff.Intensity (W/sr)
1 103 (front)	8.356647	1.2388	10.3522
2 102 (front)	8.385643	4.1946	35.1744
3 101 (front)	8.364804	3.798	31.7695
4 211 (front)	8.418959	1.512	12.7295
5 96 (front) 8	8.423718	1.729	14.5646
6 99 (front) 7	8.363135	1.373	11.4826
7 100 (front)	8.386425	3.537	29.6628
8 314 (front)	7.95239	2.776	22.0758
9 313 (front)	7.968305	4.1102	32.7513
10 98 (front)	8.389138	2.459	20.6289
11 95 (front)	8.418777	4.3818	36.8894
12 94 (front)	8.419935	4.4529	37.4931
13 97 (front)	8.420107	0.3109	2.6178
14 312 (front)	7.97499	3.928	31.3258
15 318 (front)	7.984747	5.806	46.3594
16 93 (front)	8.42214	6.6406	55.9281
17 89 (front)	8.520856	0.8872	7.5597
18 88 (front)	8.522503	1.583	13.4911
19 92 (front)	8.422995	4.2047	35.4162
20 91 (front)	8.424973	3.1853	26.8361
21 87 (front)	8.516693	2.3744	20.2220
22 86 (front)	8.515099	3.167	26.9673
23 90 (front)	8.439624	1.3385	11.2964
24 204 (front)	8.430789	1.7346	14.6240
25 85 (front)	8.517737	3.558	30.3061
26 84 (front)	8.534717	4.2141	35.9662
27 205 (front)	8.446896	0.4487	3.7901
28 83 (front)	8.54843	4.8426	41.3966
29 82 (front)	8.55274	2.2895	19.5815
30 81 (front)	8.554167	4.8426	41.4244
31 117 (front)	9.397755	2.0937	19.6761
32 116 (front)	9.421009	2.0938	19.7257
33 80 (front)	8.554566	4.8427	41.4272
34 79 (front)	8.55461	4.8426	41.4266
35 115 (front)	9.42607	2.0938	19.7363
36 114 (front)	9.423661	2.0938	19.7313
37 78 (front)	8.55454	4.8426	41.4262
38 77 (front)	8.554604	4.8426	41.4265

39	113 (front)	9.421999	2.0938	19.7278
40	112 (front)	9.400816	2.0938	19.6834
41	75 (front)	8.55398	4.8426	41.4235
42	76 (front)	8.554455	4.8426	41.4258
43	111 (front)	9.340044	2.0949	19.5665
44	110 (front)	9.319592	2.0937	19.5124
45	74 (front)	8.553594	4.8426	41.4216
46	73 (front)	8.553448	4.8426	41.4209
47	109 (front)	9.336844	1.9801	18.4879
48	221 (front)	9.391642	2.2074	20.7311
49	72 (front)	8.55442	4.8426	41.4256
50	71 (front)	8.554662	4.8426	41.4268
51	222 (front)	9.417978	2.0937	19.7184
52	108 (front)	9.383682	2.1922	20.5709
53	70 (front)	8.554516	4.8426	41.4261
54	69 (front)	8.553838	4.8426	41.4228
55	107 (front)	9.336308	1.9953	18.6287
56	106 (front)	9.294678	2.0937	19.4603
57	68 (front)	8.553166	4.8426	41.4196
58	67 (front)	8.552858	4.8426	41.4181
59	105 (front)	9.279945	2.0937	19.4294
60	104 (front)	9.274809	2.0937	19.4187
61	66 (front)	8.552723	4.8426	41.4174
62	65 (front)	8.552625	4.8426	41.4169
63	225 (front)	9.264443	2.0937	19.3970
64	226 (front)	9.206858	1.563	14.3903
65	64 (front)	8.551907	4.8426	41.4135
66	63 (front)	8.558875	4.8426	41.4472
67	62 (front)	8.580549	4.873	41.8130
68	234 (front)	8.456082	1.8129	15.3300
69	61 (front)	8.578346	5.9936	51.4152
70	123 (front)	8.931857	6.2584	55.8991
71	122 (front)	8.95279	4.7116	42.1820
72	121 (front)	8.955557	4.7116	42.1950
73	120 (front)	8.953047	4.7116	42.1832
74	119 (front)	8.953365	4.7116	42.1847
75	118 (front)	8.942036	5.9623	53.3151
76	224 (front)	8.901906	4.1013	36.5094
77	223 (front)	8.909859	3.6995	32.9620
78	126 (front)	8.903377	4.0475	36.0364
79	25 (front)	8.948543	3.1649	28.3212
80	125 (front)	8.851626	2.9062	25.7246
81	124 (front)	9.080413	2.5541	23.1923
82	11 (front)	9.000957	2.0339	18.3070
83	30(front)	9.2932	5.7346	53.2928
TOTAL			287.2313	2494.7707

MuSES ascii Results File
Exported from model: c:\Program Files\MuSES\Work\Examples\tez1
Tue Jun 13 00:22:47 2000
Units in the file: SI Units
Radiance Band: 11 to 12 micron
Time Step 10, Time = Jul 19, 1984 18:00:00

Element (Number&Location in the Model)	Radiance (W/m^2-sr)	Area(m^2)	Eff.Intensity (W/sr)
1 103 (front)	8.003191	1.2388	9.9144
2 102 (front)	8.028575	4.1946	33.6767
3 101 (front)	8.010359	3.798	30.4233
4 211 (front)	8.064414	1.512	12.1934
5 96 (front) 8	8.068616	1.729	13.9506
6 99 (front) 7	8.0089	1.373	10.9962
7 100 (front)	8.029258	3.537	28.3995
8 314 (front)	7.62776	2.776	21.1747
9 313 (front)	7.641724	4.1102	31.4090
10 98 (front)	8.03163	2.459	19.7498
11 95 (front)	8.064289	4.3818	35.3361
12 94 (front)	8.065336	4.4529	35.9141
13 97 (front)	8.058656	0.3109	2.5054
14 312 (front)	7.647551	3.928	30.0396
15 318 (front)	7.656176	5.806	44.4518
16 93 (front)	8.067234	6.6406	53.5713
17 89 (front)	8.144329	0.8872	7.2256
18 88 (front)	8.145765	1.583	12.8947
19 92 (front)	8.067982	4.2047	33.9234
20 91 (front)	8.069715	3.1853	25.7045
21 87 (front)	8.140698	2.3744	19.3293
22 86 (front)	8.139308	3.167	25.7772
23 90 (front)	8.082613	1.3385	10.8186
24 204 (front)	8.074909	1.7346	14.0067
25 85 (front)	8.141609	3.558	28.9678
26 84 (front)	8.1563	4.2141	34.3715
27 205 (front)	8.089013	0.4487	3.6295
28 83 (front)	8.16837	4.8426	39.5561
29 82 (front)	8.172127	2.2895	18.7101
30 81 (front)	8.17337	4.8426	39.5804
31 117 (front)	8.909106	2.0937	18.6530
32 116 (front)	8.929345	2.0938	18.6963
33 80 (front)	8.173718	4.8427	39.5829
34 79 (front)	8.173758	4.8426	39.5822
35 115 (front)	8.933751	2.0938	18.7055
36 114 (front)	8.931651	2.0938	18.7011
37 78 (front)	8.173696	4.8426	39.5819
38 77 (front)	8.173752	4.8426	39.5822

39	113 (front)	8.930202	2.0938	18.6981
40	112 (front)	8.911756	2.0938	18.6594
41	75 (front)	8.173208	4.8426	39.5796
42	76 (front)	8.173621	4.8426	39.5816
43	111 (front)	8.8589	2.0949	18.5585
44	110 (front)	8.841086	2.0937	18.5106
45	74 (front)	8.1728	4.8426	39.5776
46	73 (front)	8.172744	4.8426	39.5773
47	109 (front)	8.85615	1.9801	17.5361
48	221 (front)	8.903842	2.2074	19.6543
49	72 (front)	8.173592	4.8426	39.5814
50	71 (front)	8.173801	4.8426	39.5824
51	222 (front)	8.926758	2.0937	18.6900
52	108 (front)	8.896885	2.1922	19.5038
53	70 (front)	8.173675	4.8426	39.5818
54	69 (front)	8.173083	4.8426	39.5790
55	107 (front)	8.855595	1.9953	17.6696
56	106 (front)	8.81935	2.0937	18.4651
57	68 (front)	8.172499	4.8426	39.5761
58	67 (front)	8.17223	4.8426	39.5748
59	105 (front)	8.806512	2.0937	18.4382
60	104 (front)	8.802034	2.0937	18.4288
61	66 (front)	8.172112	4.8426	39.5743
62	65 (front)	8.172026	4.8426	39.5739
63	225 (front)	8.793005	2.0937	18.4099
64	226 (front)	8.742841	1.563	13.6651
65	64 (front)	8.1714	4.8426	39.5708
66	63 (front)	8.177474	4.8426	39.6002
67	62 (front)	8.196365	4.873	39.9409
68	234 (front)	8.093132	1.8129	14.6720
69	61 (front)	8.194445	5.9936	49.1142
70	123 (front)	8.502962	6.2584	53.2149
71	122 (front)	8.521213	4.7116	40.1485
72	121 (front)	8.523636	4.7116	40.1600
73	120 (front)	8.521456	4.7116	40.1497
74	119 (front)	8.521722	4.7116	40.1509
75	118 (front)	8.511845	5.9623	50.7502
76	224 (front)	8.475698	4.1013	34.7614
77	223 (front)	8.482619	3.6995	31.3814
78	126 (front)	8.476961	4.0475	34.3105
79	25 (front)	8.517634	3.1649	26.9575
80	125 (front)	8.432584	2.9062	24.5068
81	124 (front)	8.632243	2.5541	22.0476
82	11 (front)	8.563214	2.0339	17.4167
83	30(front)	8.8182	5.7346	50.5688
TOTAL			287.2313	2380.5369

2. VARIATION IN RADIATION FROM SHIP TARGET SURFACE USED IN MuSES PROGRAM

The Radiance values on the scale show the reference value.

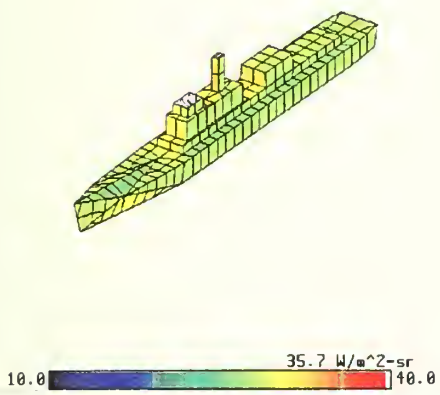

11:00 AM

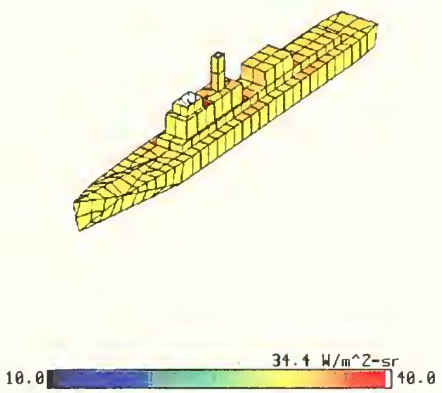

3:00 PM

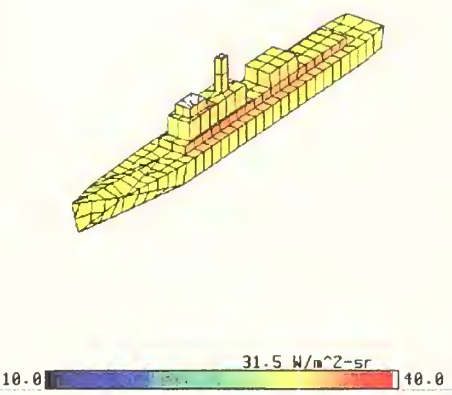

5:00 PM

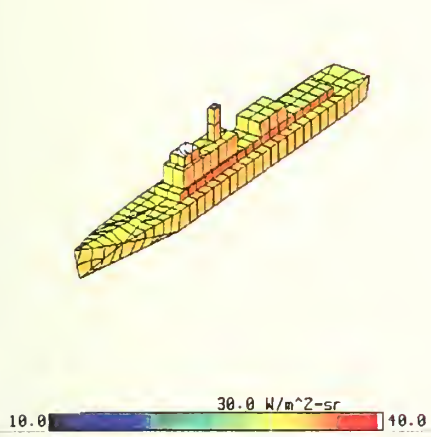

7:00 PM

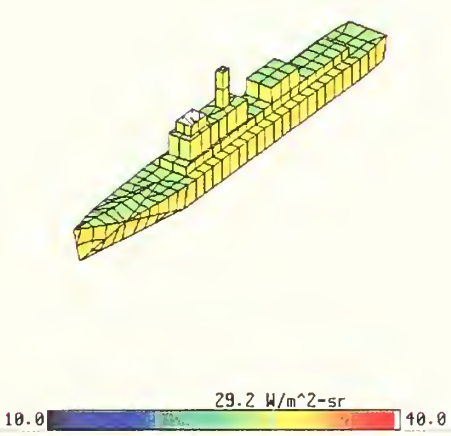

9:00 PM

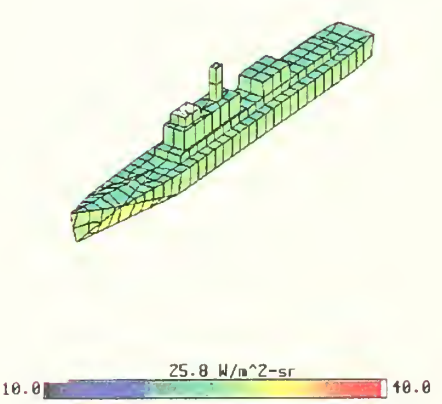

23:00 PM

THIS PAGE INTENTIONALLY LEFT BLANK

APPENDIX F

SECOND GENERATION FLIR SENSOR PARAMETERS

```
U.S. Army CECOM NVESD FLIR92        Thu May 18 23:24:55 2000

output file: SADAII.1   short listing

data file: SADAII
command line arguments:  -d SADAII -o SADAII -p MRT

begin data file listing . . .
gen2: sample data file for RISTA II 2nd generation FLIR with SADA II FPA
        >spectral
            spectral_cut_on                8.0       microns
            spectral_cut_off              12.0       microns
            diffraction_wavelength         0.0       microns
        >optics_1
            f_number                       0.0       --
            eff_focal_length              20.0       cm
            eff_aperture_diameter         10.0       cm
            optics_blur_spot               0.01      mrad
            average_optical_trans          0.7       --
        >optics_2
            HFOV:VFOV_aspect_ratio         0.0       --
            magnification                  0.0       --
            frame_rate                    30.0       Hz
            fields_per_frame               1.0       --
        >detector
            horz_dimension_(active)       25.4       microns
            vert_dimension_(active)       25.4       microns
            peak_D_star                    1.5e10    cm-sqrt(Hz)/W
            integration_time               0.007     microseconds
            1/f_knee_frequency             3.0       Hz
        >fpa_parallel
            #_detectors_in_TDI             4.0       --
            #_vert_detectors             480.0       --
            #_samples_per_HIFOV            2.0       --
            #_samples_per_VIFOV            2.0       --
            3dB_response_frequency      2032.0       Hz
            scan_efficiency                0.75      --
      >electronics
            high_pass_3db_cuton            1.0       Hz
            high_pass_filter_order         0.0       --
            low_pass_3db_cutoff       100000.0       Hz
            low_pass_filter_order          0.0       --
            boost_amplitude                0.0       --
            boost_frequency                0.0       Hz
          sample_and_hold               HORZ      NO_HORZ_VERT
        >display
            display_brightness            10.0       milli-Lamberts
            display_height                15.24      cm
            display_viewing_distance      30.0       cm
        >crt_display
            #_active_lines_on_CRT        480.0       --
```

```
            horz_crt_spot_sigma                 0.0         mrad
            vert_crt_spot_sigma                 0.0         mrad
          >eye
            threshold_SNR                       2.5         --
            eye_integration_time                0.1         sec
            MTF                                 EXP         EXP_or_NL
        >random_image_motion
            horz_rms_motion_amplitude           0.02        mrad
            vert_rms_motion_amplitude           0.02        mrad
        >sinusoidal_image_motion
            horz_rms_motion_amplitude           0.0         mrad
            vert_rms_motion_amplitude           0.0         mrad
        >3d_noise_default
           noise_level                    MOD                NO_LO_MOD_or_HI
        >spectral_detectivity
           #_points: 9          microns____detectivity
                                8.00       0.666
                                8.50       0.708
                                9.00       0.750
                                9.50       0.792
                                 10.00           0.833
                                 10.50           0.875
                                 11.00           0.917
                                 11.50           0.958
                                 12.00           1.00
          >end
end data file listing . . .

MESSAGES
  diagnostic(): Using default 3D noise components.
  diagnostic(): Using _MOD_ level 3D noise defaults.
  diagnostic(): Diffraction wavelength set to spectral band midpoint.
  diagnostic(): HFOV:VFOV aspect ratio defaulted to 1.33.
  diagnostic(): Fields-of-view calculated by model.
  diagnostic(): Electronics high pass filter defaulted to order 1.
  diagnostic(): Electronics low pass filter defaulted to order 1.


CALCULATED SYSTEM PARAMETERS
      field-of-view:      2.323h x  1.746v degrees
                          40.54h x  30.48v mrad
      magnification:                16.323
      optics blur spot:             48.800 microns (diffraction-limited)
                                     0.244 mrad

      detector IFOV:      0.127h x  0.127v mrad

      scan velocity:                1621.29 mrad/second
      dwell time:                 7.833e-005 seconds

TEMPERATURE DEPENDENCE
      parameter   NETD @ 300 K      NETD @   0 K      noise bandwidth
      ---------   ------------      ------------      ---------------
      white NETD  0.185 deg C 0.000 deg C 1.003e+004 Hz
      classical NETD    0.185 deg C 0.000 deg C 1.007e+004 Hz
      sigma_TVH NETD    0.103 deg C 0.000 deg C 3.134e+003 Hz
```

sigma_TV NETD	0.077 deg C	0.000 deg C	
sigma_V NETD	0.077 deg C	0.000 deg C	
Planck integral	1.978e-004	0.000e+000	W/(cm*cm*K)
. . . w/D-star	2.439e+006	0.000e+000	sqrt(Hz)/(cm*K)

TOTAL HORIZONTAL MTFs

cy/mr	H_SYS	H_PRE	H_TPF	H_SPF
0.000	1.000	1.000	1.000	1.000
0.394	0.875	0.945	0.954	0.971
0.787	0.697	0.880	0.847	0.936
1.181	0.527	0.808	0.728	0.897
1.575	0.388	0.731	0.623	0.853
1.969	0.282	0.651	0.537	0.806
2.362	0.202	0.570	0.468	0.757
2.756	0.143	0.491	0.414	0.706
3.150	0.100	0.416	0.369	0.653
3.543	0.069	0.345	0.333	0.601
3.937	0.046	0.280	0.303	0.549
4.331	0.031	0.222	0.277	0.498
4.724	0.020	0.171	0.256	0.449
5.118	0.012	0.127	0.237	0.401
5.512	0.007	0.091	0.221	0.356
5.906	0.004	0.063	0.207	0.314
6.299	0.002	0.040	0.194	0.275
6.693	0.001	0.024	0.183	0.239
7.087	0.000	0.012	0.173	0.206
7.480	0.000	0.004	0.164	0.176
7.874	0.000	0.000	0.156	0.149

TOTAL VERTICAL MTFs

cy/mr	H_SYS	H_PRE	H_SPF
0.000	1.000	1.000	1.000
0.394	0.918	0.945	0.972
0.787	0.827	0.880	0.940
1.181	0.731	0.808	0.905
1.575	0.634	0.731	0.867
1.969	0.538	0.651	0.827
2.362	0.448	0.570	0.785
2.756	0.365	0.491	0.742
3.150	0.290	0.416	0.698
3.543	0.225	0.345	0.654
3.937	0.171	0.280	0.610
4.331	0.125	0.222	0.566
4.724	0.089	0.171	0.523
5.118	0.061	0.127	0.481
5.512	0.040	0.091	0.440
5.906	0.025	0.063	0.401
6.299	0.015	0.040	0.363
6.693	0.008	0.024	0.328
7.087	0.004	0.012	0.295
7.480	0.001	0.004	0.263
7.874	0.000	0.000	0.235

PREFILTER VALUES AT NYQUIST

horz H_PRE(7.87) = 0.000 vert H_PRE(7.87) = 0.000

SAMPLING RATES

horizontal	15.75 samples/mr
vertical	15.75 samples/mr
effective	15.75 samples/mr

SENSOR LIMITING FREQUENCIES

	spatial	Nyquist
horizontal	7.87	7.87
vertical	7.87	7.87
effective	7.87	7.87

MRTD 3D NOISE CORRECTION (AVERAGE)

	300 K	0 K
horizontal	1.000	0.000
vertical	3.833	0.000

MRTD AT 300 K BACKGROUND TEMPERATURE

	cy/mr	horz		cy/mr	vert		cy/mr	2D
0.05	0.394	0.007	0.05	0.394	0.065		0.830	0.065
0.10	0.787	0.017	0.10	0.787	0.100		1.120	0.085
0.15	1.181	0.031	0.15	1.181	0.134		1.424	0.110
0.20	1.575	0.053	0.20	1.575	0.176		1.767	0.144
0.25	1.969	0.085	0.25	1.969	0.228		2.112	0.188
0.30	2.362	0.133	0.30	2.362	0.295		2.458	0.245
0.35	2.756	0.206	0.35	2.756	0.385		2.794	0.319
0.40	3.150	0.318	0.40	3.150	0.508		3.116	0.416
0.45	3.543	0.494	0.45	3.543	0.680		3.425	0.542
0.50	3.937	0.778	0.50	3.937	0.929		3.720	0.706
0.55	4.331	1.245	0.55	4.331	1.301		4.001	0.921
0.60	4.724	2.038	0.60	4.724	1.872		4.268	1.200
0.65	5.118	3.433	0.65	5.118	2.785		4.522	1.564
0.70	5.512	6.000	0.70	5.512	4.314		4.767	2.039
0.75	5.906	10.815	0.75	5.906	7.021		4.998	2.658
0.80	6.299	21.134	0.80	6.299	12.206		5.219	3.464
0.85	6.693	45.254	0.85	6.693	23.284		5.429	4.515
0.90	7.087	99.999	0.90	7.087	51.641		5.629	5.886
0.95	7.480	99.999	0.95	7.480	99.999		5.820	7.672
1.00	7.874	99.999	1.00	7.874	99.999		6.003	10.000

FLIR92. . . SADAII.1: end of listing

APPENDIX G

MRTD VALUES and CONVERSION TABLE

Spatial Frequecy (cyc/mrad)	Range Values For Different Tasks (km)			MRTD_2D	MRTD(With pol.filter)
	N=0.75	N=3	N=6		
0.161	5.30441	1.3261	0.663	0.009	0.011
0.204	6.72112	1.6803	0.84	0.012	0.014
0.258	8.50024	2.1251	1.063	0.016	0.019
0.325	10.7077	2.6769	1.338	0.021	0.025
0.411	13.5411	3.3853	1.693	0.028	0.033
0.52	17.1323	4.2831	2.142	0.037	0.044
0.656	21.613	5.4033	2.702	0.049	0.058
0.83	27.3457	6.8364	3.418	0.065	0.076
1.12	36.9003	9.2251	4.613	0.085	0.100
1.424	46.9161	11.729	5.865	0.11	0.129
1.767	58.2168	14.554	7.277	0.144	0.169
2.112	69.5834	17.396	8.698	0.188	0.221
2.458	80.9829	20.246	10.12	0.245	0.288
2.794	92.053	23.013	11.51	0.319	0.375
3.116	102.662	25.665	12.83	0.416	0.489
3.425	112.842	28.211	14.11	0.542	0.638
3.72	122.562	30.64	15.32	0.706	0.831
4.001	131.82	32.955	16.48	0.921	1.084
4.268	140.616	35.154	17.58	1.2	1.412
4.522	148.985	37.246	18.62	1.564	1.840
4.767	157.057	39.264	19.63	2.039	2.399
4.998	164.667	41.167	20.58	2.658	3.127
5.219	171.949	42.987	21.49	3.464	4.075
5.429	178.867	44.717	22.36	4.515	5.312
5.629	185.457	46.364	23.18	5.886	6.925
5.82	191.75	47.937	23.97	7.672	9.026
6.003	197.779	49.445	24.72	10	11.765

THIS PAGE INTENTIONALLY LEFT BLANK

APPENDIX H

CONVERSION OF INBAND RADIANCE INTO TEMPERATURE

1. MATLAB CODE FOR CONVERSION

```
%*******Program Calculates the Exitance of Given
Temperature(s)******
clc;
Tmin = input('Enter the initial temperature you want to
calculate=    ');

Tmax = input('Enter the final temperature you want to
calculate=    ');
Emit = input('Enter the emittance=  ');
h=6.626e-34;
c=2.998e8;
k=1.38e-23;
dt=0.001;
%change the bandwidth if you want

low=8e-6; %** lower limit of band**
up=12e-6; %** upper limit of band**
dx=0.001e-6;
m=0;
n=0;
for T=Tmin:dt:Tmax
   m=m+1;
   tot=0.0;
      for x=low:dx:up-dx
         xm=x+dx/2;
         %planck formula
         f1=(2*h*c^2)/(xm^5);
         f2=1/(exp((h*c)/(xm*k*T))-1);
         fx=f1*f2*Emit;
         tot=(tot+fx*dx);
      end;

      fprintf('Temp:%d Radiance:%e\n',T,tot)

   end;
```

2. LOOK UP TABLE FOR CONVERSION OF INBAND RADIANCE INTO TEMPERATURE

T (K°)	Rad.(W/m²st)	T (K°)	Rad.(W/m²st)	T (K°)	Rad.(W/m²st)	T (K°)	Rad.(W/m²st)
245.00	12.9028	245.48	13.0524	245.97	13.2064	246.46	13.3615
245.01	12.9059	245.49	13.0556	245.98	13.2095	246.47	13.3647
245.02	12.9090	245.5	13.0587	245.99	13.2127	246.48	13.3679
245.03	12.9122	245.51	13.0618	246	13.2158	246.49	13.3711
245.04	12.9153	245.52	13.0650	246.01	13.2190	246.50	13.3743
245.05	12.9184	245.53	13.0681	246.02	13.2222	246.51	13.3774
245.06	12.9215	245.54	13.0712	246.03	13.2253	246.52	13.3806
245.07	12.9246	245.55	13.0744	246.04	13.2285	246.53	13.3838
245.08	12.9277	245.56	13.0775	246.05	13.2316	246.54	13.3870
245.09	12.9308	245.57	13.0806	246.06	13.2348	246.55	13.3902
245.10	12.9339	245.58	13.0838	246.07	13.2379	246.56	13.3934
245.10	12.9339	245.59	13.0869	246.08	13.2411	246.57	13.3965
245.11	12.9370	245.6	13.0900	246.09	13.2443	246.58	13.3997
245.12	12.9401	245.61	13.0932	246.1	13.2474	246.59	13.4029
245.13	12.9432	245.62	13.0963	246.11	13.2506	246.60	13.4061
245.14	12.9464	245.63	13.0994	246.12	13.2537	246.61	13.4093
245.15	12.9495	245.64	13.1026	246.13	13.2569	246.62	13.4125
245.16	12.9526	245.65	13.1057	246.14	13.2601	246.63	13.4157
245.17	12.9557	245.66	13.1089	246.15	13.2632	246.64	13.4188
245.18	12.9588	245.67	13.1120	246.16	13.2664	246.65	13.4220
245.19	12.9619	245.68	13.1151	246.17	13.2696	246.66	13.4252
245.20	12.9650	245.69	13.1183	246.18	13.2727	246.67	13.4284
245.21	12.9681	245.7	13.1214	246.19	13.2759	246.68	13.4316
245.22	12.9713	245.71	13.1246	246.2	13.2791	246.69	13.4348
245.23	12.9744	245.72	13.1277	246.21	13.2822	246.70	13.4380
245.24	12.9775	245.73	13.1308	246.22	13.2854	246.71	13.4412
245.25	12.9806	245.74	13.1340	246.23	13.2886	246.72	13.4444
245.26	12.9837	245.75	13.1371	246.24	13.2917	246.73	13.4476
245.27	12.9869	245.76	13.1403	246.25	13.2949	246.74	13.4507
245.28	12.9900	245.77	13.1434	246.26	13.2981	246.75	13.4539
245.29	12.9931	245.78	13.1465	246.27	13.3012	246.76	13.4571
245.30	12.9962	245.79	13.1497	246.28	13.3044	246.77	13.4603
245.31	12.9993	245.8	13.1528	246.29	13.3076	246.78	13.4635
245.32	13.0024	245.81	13.1560	246.3	13.3107	246.79	13.4667
245.33	13.0056	245.82	13.1591	246.31	13.3139	246.80	13.4699
245.34	13.0087	245.83	13.1623	246.32	13.3171	246.81	13.4731
245.35	13.0118	245.84	13.1654	246.33	13.3203	246.82	13.4763
245.36	13.0149	245.85	13.1686	246.34	13.3234	246.83	13.4795
245.37	13.0181	245.86	13.1717	246.35	13.3266	246.84	13.4827
245.38	13.0212	245.87	13.1749	246.36	13.3298	246.85	13.4859
245.39	13.0243	245.88	13.1780	246.37	13.3329	246.86	13.4891
245.40	13.0274	245.89	13.1812	246.38	13.3361	246.87	13.4923
245.41	13.0306	245.9	13.1843	246.39	13.3393	246.88	13.4955

245.42	13.0337	245.91	13.1875	246.4	13.3425	246.89	13.4987
245.43	13.0368	245.92	13.1906	246.41	13.3456	246.90	13.5019
245.44	13.0399	245.93	13.1938	246.42	13.3488	246.91	13.5051
245.45	13.0431	245.94	13.1969	246.43	13.3520	246.92	13.5083
245.46	13.0462	245.95	13.2001	246.44	13.3552	246.93	13.5115
245.47	13.0493	245.96	13.2032	246.45	13.3584	246.94	13.5147
246.95	13.5179	247.46	13.6820	247.97	13.8474	248.48	14.0141
246.96	13.5211	247.47	13.6852	247.98	13.8506	248.49	14.0174
246.97	13.5243	247.48	13.6884	247.99	13.8539	248.5	14.0207
246.98	13.5275	247.49	13.6917	248.00	13.8572	248.51	14.0240
246.99	13.5307	247.5	13.6949	248.01	13.8604	248.52	14.0273
247	13.5339	247.51	13.6981	248.02	13.8637	248.53	14.0306
247.01	13.5371	247.52	13.7014	248.03	13.8669	248.54	14.0338
247.02	13.5404	247.53	13.7046	248.04	13.8702	248.55	14.0371
247.03	13.5436	247.54	13.7078	248.05	13.8735	248.56	14.0404
247.04	13.5468	247.55	13.7111	248.06	13.8767	248.57	14.0437
247.05	13.5500	247.56	13.7143	248.07	13.8800	248.58	14.0470
247.06	13.5532	247.57	13.7175	248.08	13.8832	248.59	14.0503
247.07	13.5564	247.58	13.7208	248.09	13.8865	248.6	14.0536
247.08	13.5596	247.59	13.7240	248.10	13.8898	248.61	14.0569
247.09	13.5628	247.6	13.7273	248.11	13.8930	248.62	14.0601
247.1	13.5660	247.61	13.7305	248.12	13.8963	248.63	14.0634
247.11	13.5692	247.62	13.7337	248.13	13.8996	248.64	14.0667
247.12	13.5725	247.63	13.7370	248.14	13.9028	248.65	14.0700
247.13	13.5757	247.64	13.7402	248.15	13.9061	248.66	14.0733
247.14	13.5789	247.65	13.7435	248.16	13.9094	248.67	14.0766
247.15	13.5821	247.66	13.7467	248.17	13.9126	248.68	14.0799
247.16	13.5853	247.67	13.7499	248.18	13.9159	248.69	14.0832
247.17	13.5885	247.68	13.7532	248.19	13.9192	248.7	14.0865
247.18	13.5917	247.69	13.7564	248.20	13.9224	248.71	14.0898
247.19	13.5950	247.7	13.7597	248.21	13.9257	248.72	14.0931
247.2	13.5982	247.71	13.7629	248.22	13.9290	248.73	14.0964
247.21	13.6014	247.72	13.7661	248.23	13.9322	248.74	14.0997
247.22	13.6046	247.73	13.7694	248.24	13.9355	248.75	14.1030
247.23	13.6078	247.74	13.7726	248.25	13.9388	248.76	14.1063
247.24	13.6110	247.75	13.7759	248.26	13.9420	248.77	14.1096
247.25	13.6143	247.76	13.7791	248.27	13.9453	248.78	14.1128
247.26	13.6175	247.77	13.7824	248.28	13.9486	248.79	14.1161
247.27	13.6207	247.78	13.7856	248.29	13.9519	248.8	14.1194
247.28	13.6239	247.79	13.7889	248.30	13.9551	248.81	14.1227
247.29	13.6271	247.8	13.7921	248.31	13.9584	248.82	14.1260
247.3	13.6304	247.81	13.7954	248.32	13.9617	248.83	14.1293
247.31	13.6336	247.82	13.7986	248.33	13.9650	248.84	14.1326
247.32	13.6368	247.83	13.8019	248.34	13.9682	248.85	14.1359
247.33	13.6400	247.84	13.8051	248.35	13.9715	248.86	14.1393
247.34	13.6433	247.85	13.8084	248.36	13.9748	248.87	14.1426
247.35	13.6465	247.86	13.8116	248.37	13.9781	248.88	14.1459
247.36	13.6497	247.87	13.8149	248.38	13.9813	248.89	14.1492
247.37	13.6529	247.88	13.8181	248.39	13.9846	248.9	14.1525

247.38	13.6562	247.89	13.8214	248.40	13.9879	248.91	14.1558
247.39	13.6594	247.9	13.8246	248.41	13.9912	248.92	14.1591
247.4	13.6626	247.91	13.8279	248.42	13.9944	248.93	14.1624
247.41	13.6658	247.92	13.8311	248.43	13.9977	248.94	14.1657
247.42	13.6691	247.93	13.8344	248.44	14.0010	248.95	14.1690
247.43	13.6723	247.94	13.8376	248.45	14.0043	248.96	14.1723
247.44	13.6755	247.95	13.8409	248.46	14.0076	248.97	14.1756
247.45	13.6788	247.96	13.8441	248.47	14.0109	248.98	14.1789
248.99	14.1822	249.5	14.3517	250	14.5191	250.5	14.6878
249	14.1855	249.51	14.3550	250.01	14.5225	250.51	14.6912
249.01	14.1888	249.52	14.3583	250.02	14.5258	250.52	14.6946
249.02	14.1922	249.53	14.3617	250.03	14.5292	250.53	14.6980
249.03	14.1955	249.54	14.3650	250.04	14.5325	250.54	14.7014
249.04	14.1988	249.55	14.3684	250.05	14.5359	250.55	14.7048
249.05	14.2021	249.56	14.3717	250.06	14.5393	250.56	14.7082
249.06	14.2054	249.57	14.3750	250.07	14.5426	250.57	14.7116
249.07	14.2087	249.58	14.3784	250.08	14.5460	250.58	14.7150
249.08	14.2120	249.59	14.3817	250.09	14.5494	250.59	14.7183
249.09	14.2153	249.60	14.3850	250.1	14.5527	250.6	14.7217
249.1	14.2187	249.61	14.3884	250.11	14.5561	250.61	14.7251
249.11	14.2220	249.62	14.3917	250.12	14.5595	250.62	14.7285
249.12	14.2253	249.63	14.3951	250.13	14.5628	250.63	14.7319
249.13	14.2286	249.64	14.3984	250.14	14.5662	250.64	14.7353
249.14	14.2319	249.65	14.4018	250.15	14.5696	250.65	14.7387
249.15	14.2352	249.66	14.4051	250.16	14.5730	250.66	14.7421
249.16	14.2386	249.67	14.4084	250.17	14.5763	250.67	14.7455
249.17	14.2419	249.68	14.4118	250.18	14.5797	250.68	14.7489
249.18	14.2452	249.69	14.4151	250.19	14.5831	250.69	14.7523
249.19	14.2485	249.70	14.4185	250.2	14.5864	250.7	14.7557
249.2	14.2518	249.71	14.4218	250.21	14.5898	250.71	14.7591
249.21	14.2552	249.72	14.4252	250.22	14.5932	250.72	14.7625
249.22	14.2585	249.73	14.4285	250.23	14.5966	250.73	14.7659
249.23	14.2618	249.74	14.4319	250.24	14.5999	250.74	14.7693
249.24	14.2651	249.75	14.4352	250.25	14.6033	250.75	14.7727
249.25	14.2684	249.76	14.4386	250.26	14.6067	250.76	14.7761
249.26	14.2718	249.77	14.4419	250.27	14.6101	250.77	14.7795
249.27	14.2751	249.78	14.4453	250.28	14.6134	250.78	14.7829
249.28	14.2784	249.79	14.4486	250.29	14.6168	250.79	14.7863
249.29	14.2817	249.80	14.4520	250.3	14.6202	250.8	14.7897
249.3	14.2851	249.81	14.4553	250.31	14.6236	250.81	14.7931
249.31	14.2884	249.82	14.4587	250.32	14.6269	250.82	14.7965
249.32	14.2917	249.83	14.4620	250.33	14.6303	250.83	14.7999
249.33	14.2950	249.84	14.4654	250.34	14.6337	250.84	14.8033
249.34	14.2984	249.85	14.4687	250.35	14.6371	250.85	14.8067
249.35	14.3017	249.86	14.4721	250.36	14.6405	250.86	14.8101
249.36	14.3050	249.87	14.4754	250.37	14.6438	250.87	14.8135
249.37	14.3083	249.88	14.4788	250.38	14.6472	250.88	14.8169
249.38	14.3117	249.89	14.4822	250.39	14.6506	250.89	14.8204
249.39	14.3150	249.90	14.4855	250.4	14.6540	250.9	14.8238

249.4	14.3183	249.91	14.4889	250.41	14.6574	250.91	14.8272
249.41	14.3217	249.92	14.4922	250.42	14.6607	250.92	14.8306
249.42	14.3250	249.93	14.4956	250.43	14.6641	250.93	14.8340
249.43	14.3283	249.94	14.4989	250.44	14.6675	250.94	14.8374
249.44	14.3317	249.95	14.5023	250.45	14.6709	250.95	14.8408
249.45	14.3350	249.96	14.5057	250.46	14.6743	250.96	14.8442
249.46	14.3383	249.97	14.5090	250.47	14.6777	250.97	14.8476
249.47	14.3417	249.98	14.5124	250.48	14.6811	250.98	14.8511
249.48	14.3450	249.99	14.5157	250.49	14.6844	250.99	14.8545
249.49	14.3483	250.00	14.5191	250.5	14.6878	251.00	14.8579
251.00	14.8579	251.5	15.0292	252	15.2019	252.50	15.3759
251.01	14.8613	251.51	15.0327	252.01	15.2054	252.51	15.3794
251.02	14.8647	251.52	15.0361	252.02	15.2088	252.52	15.3829
251.03	14.8681	251.53	15.0396	252.03	15.2123	252.53	15.3864
251.04	14.8715	251.54	15.0430	252.04	15.2158	252.54	15.3899
251.05	14.8750	251.55	15.0464	252.05	15.2193	252.55	15.3934
251.06	14.8784	251.56	15.0499	252.06	15.2227	252.56	15.3969
251.07	14.8818	251.57	15.0533	252.07	15.2262	252.57	15.4004
251.08	14.8852	251.58	15.0568	252.08	15.2297	252.58	15.4039
251.09	14.8886	251.59	15.0602	252.09	15.2331	252.59	15.4074
251.10	14.8920	251.6	15.0637	252.1	15.2366	252.60	15.4109
251.11	14.8955	251.61	15.0671	252.11	15.2401	252.61	15.4144
251.12	14.8989	251.62	15.0706	252.12	15.2435	252.62	15.4179
251.13	14.9023	251.63	15.0740	252.13	15.2470	252.63	15.4214
251.14	14.9057	251.64	15.0775	252.14	15.2505	252.64	15.4249
251.15	14.9091	251.65	15.0809	252.15	15.2540	252.65	15.4284
251.16	14.9126	251.66	15.0843	252.16	15.2574	252.66	15.4319
251.17	14.9160	251.67	15.0878	252.17	15.2609	252.67	15.4354
251.18	14.9194	251.68	15.0912	252.18	15.2644	252.68	15.4389
251.19	14.9228	251.69	15.0947	252.19	15.2679	252.69	15.4424
251.20	14.9263	251.7	15.0981	252.2	15.2714	252.70	15.4459
251.21	14.9297	251.71	15.1016	252.21	15.2748	252.71	15.4494
251.22	14.9331	251.72	15.1051	252.22	15.2783	252.72	15.4529
251.23	14.9365	251.73	15.1085	252.23	15.2818	252.73	15.4564
251.24	14.9400	251.74	15.1120	252.24	15.2853	252.74	15.4599
251.25	14.9434	251.75	15.1154	252.25	15.2887	252.75	15.4634
251.26	14.9468	251.76	15.1189	252.26	15.2922	252.76	15.4669
251.27	14.9502	251.77	15.1223	252.27	15.2957	252.77	15.4704
251.28	14.9537	251.78	15.1258	252.28	15.2992	252.78	15.4739
251.29	14.9571	251.79	15.1292	252.29	15.3027	252.79	15.4774
251.30	14.9605	251.8	15.1327	252.3	15.3061	252.80	15.4809
251.31	14.9640	251.81	15.1361	252.31	15.3096	252.81	15.4844
251.32	14.9674	251.82	15.1396	252.32	15.3131	252.82	15.4880
251.33	14.9708	251.83	15.1431	252.33	15.3166	252.83	15.4915
251.34	14.9743	251.84	15.1465	252.34	15.3201	252.84	15.4950
251.35	14.9777	251.85	15.1500	252.35	15.3236	252.85	15.4985
251.36	14.9811	251.86	15.1534	252.36	15.3271	252.86	15.5020
251.37	14.9846	251.87	15.1569	252.37	15.3305	252.87	15.5055
251.38	14.9880	251.88	15.1603	252.38	15.3340	252.88	15.5090

251.39	14.9914	251.89	15.1638	252.39	15.3375	252.89	15.5125
251.40	14.9949	251.9	15.1673	252.4	15.3410	252.90	15.5161
251.41	14.9983	251.91	15.1707	252.41	15.3445	252.91	15.5196
251.42	15.0017	251.92	15.1742	252.42	15.3480	252.92	15.5231
251.43	15.0052	251.93	15.1777	252.43	15.3515	252.93	15.5266
251.44	15.0086	251.94	15.1811	252.44	15.3550	252.94	15.5301
251.45	15.0120	251.95	15.1846	252.45	15.3584	252.95	15.5336
251.46	15.0155	251.96	15.1880	252.46	15.3619	252.96	15.5372
251.47	15.0189	251.97	15.1915	252.47	15.3654	252.97	15.5407
251.48	15.0224	251.98	15.1950	252.48	15.3689	252.98	15.5442
251.49	15.0258	251.99	15.1984	252.49	15.3724	252.99	15.5477
253.01	15.5547	253.52	15.7350	254.03	15.9166	254.53	16.0960
253.02	15.5583	253.53	15.7385	254.04	15.9202	254.54	16.0996
253.03	15.5618	253.54	15.7421	254.05	15.9237	254.55	16.1032
253.04	15.5653	253.55	15.7456	254.06	15.9273	254.56	16.1068
253.05	15.5688	253.56	15.7492	254.07	15.9309	254.57	16.1104
253.06	15.5724	253.57	15.7527	254.08	15.9345	254.58	16.1140
253.07	15.5759	253.58	15.7563	254.09	15.9380	254.59	16.1176
253.08	15.5794	253.59	15.7598	254.10	15.9416	254.6	16.1212
253.09	15.5829	253.6	15.7634	254.11	15.9452	254.61	16.1248
253.1	15.5864	253.61	15.7669	254.12	15.9488	254.62	16.1284
253.11	15.5900	253.62	15.7705	254.13	15.9523	254.63	16.1320
253.12	15.5935	253.63	15.7740	254.14	15.9559	254.64	16.1356
253.13	15.5970	253.64	15.7776	254.15	15.9595	254.65	16.1392
253.14	15.6006	253.65	15.7811	254.16	15.9631	254.66	16.1428
253.15	15.6041	253.66	15.7847	254.17	15.9667	254.67	16.1464
253.16	15.6076	253.67	15.7882	254.18	15.9703	254.68	16.1501
253.17	15.6111	253.68	15.7918	254.19	15.9738	254.69	16.1537
253.18	15.6147	253.69	15.7954	254.20	15.9774	254.7	16.1573
253.19	15.6182	253.7	15.7989	254.21	15.9810	254.71	16.1609
253.2	15.6217	253.71	15.8025	254.22	15.9846	254.72	16.1645
253.21	15.6253	253.72	15.8060	254.23	15.9882	254.73	16.1681
253.22	15.6288	253.73	15.8096	254.24	15.9918	254.74	16.1717
253.23	15.6323	253.74	15.8131	254.25	15.9953	254.75	16.1753
253.24	15.6359	253.75	15.8167	254.26	15.9989	254.76	16.1789
253.25	15.6394	253.76	15.8203	254.27	16.0025	254.77	16.1826
253.26	15.6429	253.77	15.8238	254.28	16.0061	254.78	16.1862
253.27	15.6465	253.78	15.8274	254.29	16.0097	254.79	16.1898
253.28	15.6500	253.79	15.8309	254.30	16.0133	254.8	16.1934
253.29	15.6535	253.8	15.8345	254.31	16.0169	254.81	16.1970
253.3	15.6571	253.81	15.8381	254.32	16.0205	254.82	16.2006
253.31	15.6606	253.82	15.8416	254.33	16.0241	254.83	16.2043
253.32	15.6641	253.83	15.8452	254.34	16.0276	254.84	16.2079
253.33	15.6677	253.84	15.8488	254.35	16.0312	254.85	16.2115
253.34	15.6712	253.85	15.8523	254.36	16.0348	254.86	16.2151
253.35	15.6747	253.86	15.8559	254.37	16.0384	254.87	16.2187
253.36	15.6783	253.87	15.8595	254.38	16.0420	254.88	16.2224
253.37	15.6818	253.88	15.8630	254.39	16.0456	254.89	16.2260

253.38	15.6854	253.89	15.8666	254.40	16.0492	254.9	16.2296
253.39	15.6889	253.9	15.8702	254.41	16.0528	254.91	16.2332
253.4	15.6924	253.91	15.8737	254.42	16.0564	254.92	16.2368
253.41	15.6960	253.92	15.8773	254.43	16.0600	254.93	16.2405
253.42	15.6995	253.93	15.8809	254.44	16.0636	254.94	16.2441
253.43	15.7031	253.94	15.8844	254.45	16.0672	254.95	16.2477
253.44	15.7066	253.95	15.8880	254.46	16.0708	254.96	16.2513
253.45	15.7102	253.96	15.8916	254.47	16.0744	254.97	16.2550
253.46	15.7137	253.97	15.8951	254.48	16.0780	254.98	16.2586
253.47	15.7172	253.98	15.8987	254.49	16.0816	254.99	16.2622
253.48	15.7208	253.99	15.9023	254.50	16.0852	255	16.2658
253.49	15.7243	254	15.9059	254.51	16.0888	255	16.2658
253.5	15.7279	254.01	15.9094	254.52	16.0924	255.01	16.2695
253.51	15.7314	254.02	15.9130	254.53	16.0960	255.02	16.2731
255.03	16.2767	255.67	16.5100	256.18	16.6975	256.69	16.8864
255.04	16.2803	255.68	16.5137	256.19	16.7012	256.7	16.8901
255.05	16.2840	255.69	16.5173	256.2	16.7049	256.71	16.8939
255.06	16.2876	255.70	16.5210	256.21	16.7086	256.72	16.8976
255.07	16.2912	255.71	16.5247	256.22	16.7123	256.73	16.9013
255.08	16.2949	255.72	16.5283	256.23	16.7160	256.74	16.9050
255.09	16.2985	255.73	16.5320	256.24	16.7197	256.75	16.9087
255.1	16.3021	255.74	16.5357	256.25	16.7234	256.76	16.9125
255.11	16.3058	255.75	16.5393	256.26	16.7271	256.77	16.9162
255.12	16.3094	255.76	16.5430	256.27	16.7307	256.78	16.9199
255.13	16.3130	255.77	16.5467	256.28	16.7344	256.79	16.9236
255.14	16.3167	255.78	16.5503	256.29	16.7381	256.8	16.9273
255.15	16.3203	255.79	16.5540	256.3	16.7418	256.81	16.9311
255.16	16.3239	255.80	16.5577	256.31	16.7455	256.82	16.9348
255.17	16.3276	255.81	16.5613	256.32	16.7492	256.83	16.9385
255.18	16.3312	255.82	16.5650	256.33	16.7529	256.84	16.9422
255.19	16.3348	255.83	16.5687	256.34	16.7566	256.85	16.9460
255.2	16.3385	255.84	16.5724	256.35	16.7603	256.86	16.9497
255.21	16.3421	255.85	16.5760	256.36	16.7640	256.87	16.9534
255.22	16.3457	255.86	16.5797	256.37	16.7677	256.88	16.9572
255.23	16.3494	255.87	16.5834	256.38	16.7714	256.89	16.9609
255.24	16.3530	255.88	16.5871	256.39	16.7751	256.9	16.9646
255.25	16.3567	255.89	16.5907	256.4	16.7788	256.91	16.9683
255.26	16.3603	255.90	16.5944	256.41	16.7825	256.92	16.9721
255.27	16.3639	255.91	16.5981	256.42	16.7862	256.93	16.9758
255.28	16.3676	255.92	16.6018	256.43	16.7899	256.94	16.9795
255.29	16.3712	255.93	16.6054	256.44	16.7936	256.95	16.9833
255.3	16.3749	255.94	16.6091	256.45	16.7973	256.96	16.9870
255.31	16.3785	255.95	16.6128	256.46	16.8011	256.97	16.9907
255.32	16.3822	255.96	16.6165	256.47	16.8048	256.98	16.9945
255.33	16.3858	255.97	16.6201	256.48	16.8085	256.99	16.9982
255.34	16.3894	255.98	16.6238	256.49	16.8122	257	17.0019
255.35	16.3931	255.99	16.6275	256.5	16.8159	257.01	17.0057
255.36	16.3967	256.00	16.6312	256.51	16.8196	257.02	17.0094
255.37	16.4004	256.01	16.6349	256.52	16.8233	257.03	17.0131

255.38	16.4040	256.02	16.6385	256.53	16.8270	257.04	17.0169
255.39	16.4077	256.03	16.6422	256.54	16.8307	257.05	17.0206
255.4	16.4113	256.04	16.6459	256.55	16.8344	257.06	17.0243
255.41	16.4150	256.05	16.6496	256.56	16.8381	257.07	17.0281
255.42	16.4186	256.06	16.6533	256.57	16.8418	257.08	17.0318
255.43	16.4223	256.07	16.6570	256.58	16.8456	257.09	17.0356
255.44	16.4259	256.08	16.6606	256.59	16.8493	257.10	17.0393
255.45	16.4296	256.09	16.6643	256.6	16.8530	257.11	17.0430
255.46	16.4332	256.1	16.6680	256.61	16.8567	257.12	17.0468
255.47	16.4369	256.11	16.6717	256.62	16.8604	257.13	17.0505
255.48	16.4405	256.12	16.6754	256.63	16.8641	257.14	17.0543
255.49	16.4442	256.13	16.6791	256.64	16.8678	257.15	17.0580
255.5	16.4478	256.14	16.6828	256.65	16.8716	257.16	17.0618
255.51	16.4515	256.15	16.6864	256.66	16.8753	257.17	17.0655
255.65	16.5027	256.16	16.6901	256.67	16.8790	257.18	17.0692
255.66	16.5064	256.17	16.6938	256.68	16.8827	257.19	17.0730
257.20	17.0767	257.7	17.2647	258.2	17.4540	258.70	17.6447
257.21	17.0805	257.71	17.2685	258.21	17.4578	258.71	17.6485
257.22	17.0842	257.72	17.2722	258.22	17.4616	258.72	17.6524
257.23	17.0880	257.73	17.2760	258.23	17.4654	258.73	17.6562
257.24	17.0917	257.74	17.2798	258.24	17.4692	258.74	17.6600
257.25	17.0955	257.75	17.2836	258.25	17.4730	258.75	17.6638
257.26	17.0992	257.76	17.2873	258.26	17.4768	258.75	17.6677
257.27	17.1030	257.77	17.2911	258.27	17.4806	258.77	17.6715
257.28	17.1067	257.78	17.2949	258.28	17.4844	258.78	17.6753
257.29	17.1105	257.79	17.2987	258.29	17.4882	258.79	17.6792
257.30	17.1142	257.8	17.3024	258.3	17.4920	258.80	17.6830
257.31	17.1180	257.81	17.3062	258.31	17.4958	258.81	17.6868
257.32	17.1217	257.82	17.3100	258.32	17.4997	258.82	17.6907
257.33	17.1255	257.83	17.3138	258.33	17.5035	258.83	17.6945
257.34	17.1292	257.84	17.3176	258.34	17.5073	258.84	17.6983
257.35	17.1330	257.85	17.3213	258.35	17.5111	258.85	17.7022
257.36	17.1367	257.86	17.3251	258.36	17.5149	258.86	17.7060
257.37	17.1405	257.87	17.3289	258.37	17.5187	258.87	17.7098
257.38	17.1442	257.88	17.3327	258.38	17.5225	258.88	17.7137
257.39	17.1480	257.89	17.3365	258.39	17.5263	258.89	17.7175
257.40	17.1518	257.9	17.3403	258.4	17.5301	258.90	17.7214
257.41	17.1555	257.91	17.3440	258.41	17.5339	258.91	17.7252
257.42	17.1593	257.92	17.3478	258.42	17.5377	258.92	17.7290
257.43	17.1630	257.93	17.3516	258.43	17.5416	258.93	17.7329
257.44	17.1668	257.94	17.3554	258.44	17.5454	258.94	17.7367
257.45	17.1705	257.95	17.3592	258.45	17.5492	258.95	17.7406
257.46	17.1743	257.96	17.3630	258.46	17.5530	258.96	17.7444
257.47	17.1781	257.97	17.3668	258.47	17.5568	258.97	17.7482
257.48	17.1818	257.98	17.3705	258.48	17.5606	258.98	17.7521
257.49	17.1856	257.99	17.3743	258.49	17.5644	258.99	17.7559
257.50	17.1893	258	17.3781	258.5	17.5683	259.00	17.7598
257.51	17.1931	258.01	17.3819	258.51	17.5721	259.01	17.7636
257.52	17.1969	258.02	17.3857	258.52	17.5759	259.02	17.7675

APPENDIX I

BACKGROUND-TARGET RADIANCE and ATD COMPUTATIONS FOR UNPOLARIZED CASE

The method to calculate the field values of this table is given in Chapter 5 Section C.

Zenith Angle (Degree)	Range (km)	Path Rad.	Radiance From Background* (W/m^2-sr)	Bandwidth (micrometer)	Trans.	Radiance From Target* (W/m^2-sr)	ATD (C^o)
165	0.31	3.631	31.9615	8--9	0.8391	7.014	3.79
				9--10	0.9205	8.070	
				10--11	0.9225	8.012	
				11--12	0.8933	7.403	
				Total		30.500	
120	0.6	5.842	31.874	8--9	0.7618	6.368	4.00
				9--10	0.8693	7.621	
				10--11	0.8678	7.537	
				11--12	0.8203	6.798	
				Total		28.325	
105	1.159	9.353	31.47	8--9	0.6513	5.444	5.86
				9--10	0.7855	6.886	
				10--11	0.7759	6.739	
				11--12	0.7014	5.813	
				Total		24.883	
104	1.24	9.805	31.5145	8--9	0.6378	5.331	4.78
				9--10	0.7745	6.790	
				10--11	0.7637	6.633	
				11--12	0.6861	5.686	
				Total		24.441	
103	1.333	10.31	31.4058	8--9	0.6229	5.207	5.00
				9--10	0.7621	6.681	
				10--11	0.7499	6.513	
				11--12	0.6688	5.543	
				Total		23.944	
102	1.443	10.89	31.15807	8--9	0.6061	5.066	5.47
				9--10	0.7479	6.557	
				10--11	0.7341	6.376	
				11--12	0.6492	5.380	
				Total		23.379	
101.7	1.479	11.08	31.1859	8--9	0.6007	5.021	5.42
				9--10	0.7433	6.516	
				10--11	0.729	6.332	
				11--12	0.6429	5.328	
				Total		23.197	
101.6	1.492	11.14	31.1959	8--9	0.5989	5.006	5.41
				9--10	0.7417	6.502	
				10--11	0.7272	6.316	
				11--12	0.6407	5.310	
				Total		23.135	

101.5	1.505	11.2	31.2058	8--9	0.597	4.990	5.39
				9--10	0.7401	6.488	
				10--11	0.7254	6.300	
				11--12	0.6385	5.292	
				Total		23.071	
101.4	1.518	11.27	31.2169	8--9	0.5951	4.975	5.38
				9--10	0.7384	6.473	
				10--11	0.7236	6.285	
				11--12	0.6362	5.273	
				Total		23.005	
101.3	1.531	11.34	31.0277	8--9	0.5932	4.959	5.72
				9--10	0.7368	6.459	
				10--11	0.7218	6.269	
				11--12	0.634	5.254	
				Total		22.942	
101.2	1.545	11.41	31.0391	8--9	0.5912	4.942	5.70
				9--10	0.7351	6.444	
				10--11	0.7199	6.253	
				11--12	0.6317	5.235	
				Total		22.874	
101.1	1.558	11.47	31.051	8--9	0.5893	4.926	5.68
				9--10	0.7334	6.429	
				10--11	0.718	6.236	
				11--12	0.6293	5.216	
				Total		22.807	
100.5	1.647	11.91	31.1369	8--9	0.5769	4.822	5.55
				9--10	0.7226	6.335	
				10--11	0.7059	6.131	
				11--12	0.6146	5.094	
				Total		22.382	
100.2	1.694	12.14	31.1893	8--9	0.5703	4.767	5.46
				9--10	0.7167	6.283	
				10--11	0.6995	6.076	
				11--12	0.6068	5.029	
				Total		22.155	
100	1.728	12.3	31.2284	8--9	0.5658	4.730	4.99
				9--10	0.7127	6.248	
				10--11	0.695	6.036	
				11--12	0.6013	4.983	
				Total		21.997	
99.8	1.763	12.47	31.271	8--9	0.5612	4.691	5.32
				9--10	0.7086	6.212	
				10--11	0.6904	5.996	
				11--12	0.5957	4.937	
				Total		21.837	

99.4	1.837	12.81	31.354	8--9	0.5515	4.610	4.18
				9--10	0.6998	6.135	
				10--11	0.6806	5.911	
				11--12	0.584	4.840	
				Total		21.496	
99.2	1.877	13	31.396	8--9	0.5464	4.567	4.12
				9--10	0.6952	6.095	
				10--11	0.6755	5.867	
				11--12	0.5779	4.790	
				Total		21.319	
99	1.919	13.18	31.442	8--9	0.5412	4.524	5.04
				9--10	0.6904	6.052	
				10--11	0.6702	5.821	
				11--12	0.5715	4.736	
				Total		21.134	
98.5	2.031	13.68	31.47	8--9	0.5274	4.409	5.01
				9--10	0.6778	5.942	
				10--11	0.6561	5.699	
				11--12	0.5548	4.598	
				Total		20.647	
98.4	2.055	13.79	31.496	8--9	0.5246	4.385	4.97
				9--10	0.6751	5.918	
				10--11	0.6531	5.673	
				11--12	0.5513	4.569	
				Total		20.545	
98.3	2.079	13.9	31.523	8--9	0.5216	4.360	4.92
				9--10	0.6723	5.894	
				10--11	0.6501	5.646	
				11--12	0.5477	4.539	
				Total		20.440	
98.2	2.105	14	31.552	8--9	0.5187	4.336	4.42
				9--10	0.6696	5.870	
				10--11	0.647	5.620	
				11--12	0.5126	4.248	
				Total		20.074	
98	2.157	14.23	31.611	8--9	0.5126	4.285	4.77
				9--10	0.6638	5.819	
				10--11	0.6406	5.564	
				11--12	0.5365	4.446	
				Total		20.114	
97.5	2.3	14.82	31.777	8--9	0.4964	4.149	4.51
				9--10	0.6485	5.685	
				10--11	0.6236	5.416	
				11--12	0.5167	4.282	
				Total		19.533	

97.4	2.331	14.95	31.812	8--9	0.493	4.121	4.44
				9--10	0.6452	5.656	
				10--11	0.6199	5.384	
				11--12	0.5125	4.247	
				Total		19.409	
97.3	2.363	15.08	31.84924	8--9	0.4896	4.093	4.38
				9--10	0.6419	5.627	
				10--11	0.6162	5.352	
				11--12	0.5082	4.212	
				Total		19.284	
97.2	2.396	15.21	31.88712	8--9	0.4861	4.063	4.33
				9--10	0.6384	5.597	
				10--11	0.6125	5.320	
				11--12	0.5038	4.175	
				Total		19.155	
97.1	2.43	15.34	31.92621	8--9	0.4825	4.033	4.26
				9--10	0.635	5.567	
				10--11	0.6086	5.286	
				11--12	0.4994	4.139	
				Total		19.025	
97	2.464	15.48	31.96655	8--9	0.4789	4.003	4.19
				9--10	0.6314	5.535	
				10--11	0.6047	5.252	
				11--12	0.4949	4.102	
				Total		18.892	
96.8	2.537	15.76	32.05104	8--9	0.4714	3.940	4.05
				9--10	0.6241	5.471	
				10--11	0.5965	5.181	
				11--12	0.4856	4.025	
				Total		18.617	
96.6	2.613	16.05	32.14081	8--9	0.4636	3.875	3.90
				9--10	0.6164	5.404	
				10--11	0.588	5.107	
				11--12	0.4759	3.944	
				Total		18.330	
96.4	2.695	16.36	31.86249	8--9	0.4556	3.808	4.41
				9--10	0.6084	5.334	
				10--11	0.5791	5.030	
				11--12	0.4659	3.861	
				Total		18.033	
96.2	2.782	16.68	31.94008	8--9	0.4472	3.738	4.28
				9--10	0.5999	5.259	
				10--11	0.5698	4.949	
				11--12	0.4555	3.775	
				Total		17.721	

96.1	2.827	16.84	31.38594	8--9	0.4429	3.702	5.28
				9--10	0.5956	5.221	
				10--11	0.565	4.907	
				11--12	0.4501	3.730	
				Total		17.561	
96	2.874	17.01	31.43	8--9	0.4385	3.665	5.21
				9--10	0.5911	5.182	
				10--11	0.5601	4.865	
				11--12	0.4446	3.685	
				Total		17.397	
95.9	2.923	17.18	31.47705	8--9	0.434	3.628	5.14
				9--10	0.5865	5.142	
				10--11	0.555	4.820	
				11--12	0.439	3.638	
				Total		17.228	
95.8	2.974	17.36	31.52521	8--9	0.4295	3.590	5.05
				9--10	0.5818	5.100	
				10--11	0.5499	4.776	
				11--12	0.4333	3.591	
				Total		17.058	
95.6	3.08	17.72	31.6249	8--9	0.42	3.511	4.89
				9--10	0.5721	5.015	
				10--11	0.5391	4.682	
				11--12	0.4215	3.493	
				Total		16.702	
95.4	3.194	18.1	31.71769	8--9	0.4102	3.429	4.74
				9--10	0.5618	4.925	
				10--11	0.5278	4.584	
				11--12	0.4092	3.391	
				Total		16.330	
95.2	3.317	18.5	31.8171	8--9	0.4	3.344	4.58
				9--10	0.551	4.830	
				10--11	0.516	4.482	
				11--12	0.3964	3.285	
				Total		15.941	
95	3.45	18.92	31.9	8--9	0.3893	3.254	4.43
				9--10	0.5396	4.730	
				10--11	0.5035	4.373	
				11--12	0.3831	3.175	
				Total		15.533	
94	4.317	21.37	32.314	8--9	0.3278	2.740	3.74
				9--10	0.4714	4.133	
				10--11	0.4295	3.730	
				11--12	0.3068	2.543	
				Total		13.146	
93.6	4.801	22.55	32.662	8--9	0.2987	2.497	3.25
				9--10	0.4376	3.836	
				10--11	0.3933	3.416	
				11--12	0.2713	2.248	
				Total		11.998	

THIS PAGE INTENTIONALLY LEFT BLANK

APPENDIX J

COMPUTATIONS WITH POLARIZED FILTER

1. BREAKDOWN of BACKGROUND RADIANCE

When the horizontal polarizer is added to the sensor the fraction of radiance that enters the sensor will vary depending on the degree of polarization value (Dpol).

Range (km)	Sea emission	Dpol Value*	Incident Rad.Value	Sky Reflection	Dpol Value**	Incident Rad. Value	Path Rad.	DPol(%0)	Total
0.31	28.2065	0.1	14.089147	0.1235	11.6	0.06891	3.6314	1.8157	15.97376
0.319	28.1378	0.2	14.040762	0.1268	21	0.07671	3.70386	1.85193	15.96941
0.599	25.3283	3.7	12.195576	0.7033	76.6	0.62101	5.8429	2.92145	15.73804
1.728	14.9885	9.9	6.7523193	3.9385	26.7	2.49504	12.3013	6.15065	15.39801
2.157	12.8075	10.7	5.7185488	4.5758	22.2	2.79581	14.2279	7.11395	15.62831
2.874	10.2973	11.4	4.5617039	4.1221	20.4	2.4815	17.011	8.5055	15.54871
3.45	8.7899	11.8	3.8763459	4.1881	18.3	2.47726	18.9227	9.46135	15.81496
4.317	7.1319	12.2	3.1309041	3.8133	17	2.23078	21.369	10.6845	16.04618
4.801	6.4201	12.4	2.8120038	2.1471	16.2	1.24747	22.5454	11.2727	15.33217
5.408	5.6673	12.6	2.4766101	2.0202	15.4	1.16566	23.8613	11.93065	15.57292
5.773	5.2531	12.7	2.2929782	1.9306	15	1.1101	24.5774	12.2887	15.69177
6.677	4.3621	12.8	1.9018756	1.6999	14.2	0.97064	26.137	13.0685	15.94102
7.921	3.4151	13	1.4855685	1.3839	13.8	0.78744	27.875	13.9375	16.21051
8.738	2.9214	13.1	1.2693483	1.2167	13.4	0.68987	28.8093	14.40465	16.36387
9.748	2.443	13.3	1.0589538	1.0357	13.1	0.58569	29.7811	14.89055	16.53519
11.03	1.9244	13.4	0.8332652	0.8429	12.9	0.47582	30.7803	15.39015	16.69923
12.71	1.4354	13.5	0.6208105	0.643	12.6	0.36201	31.7865	15.89325	16.87607
15.03	0.9709	13.7	0.4189434	0.4436	12.4	0.2493	32.7657	16.38285	17.0511
18.47	0.554	13.8	0.238774	0.2574	12.3	0.14453	33.6628	16.8314	17.2147
20.92	0.3752	14	0.161336	0.1755	12.3	0.09854	34.054	17.027	17.28688
24.24	0.224	14.1	0.096208	0.1054	12.3	0.05918	34.3916	17.1958	17.35119
29.09	0.1072	14.3	0.0459352	0.0506	12.3	0.02841	34.6583	17.32915	17.4035
29.71	0.09771	14.3	0.0418687	0.0462	12.3	0.02594	34.68063	17.34032	17.40813
30.36	0.0886	14.3	0.0379651	0.0419	12.3	0.02353	34.70212	17.35106	17.41255
31.05	0.07991	14.3	0.0342414	0.0378	12.3	0.02122	34.72279	17.3614	17.41686
31.78	0.07166	14.4	0.0306705	0.0339	12.3	0.01903	34.74259	17.3713	17.421
32.56	0.06383	14.4	0.0273192	0.0302	12.3	0.01696	34.76155	17.38078	17.42505
33.39	0.05644	14.4	0.0241563	0.0267	12.3	0.01499	34.77967	17.38984	17.42898
34.28	0.04949	14.4	0.0211817	0.0234	12.4	0.01315	34.79701	17.39851	17.43284
35.23	0.04299	14.5	0.0183782	0.0203	12.4	0.01141	34.81353	17.40677	17.43655
36.26	0.03694	14.5	0.0157919	0.0174	12.4	0.00978	34.82927	17.41464	17.44021
37.38	0.03134	14.5	0.0133979	0.0148	12.4	0.00832	34.84424	17.42212	17.44384
38.6	0.02618	14.6	0.0111789	0.0124	12.4	0.00697	34.85853	17.42927	17.44741

* All the Dpol values for sea surface emission are vertical polarization

** All the Dpol values for Sky reflection component are horizontal polarization

2. ATD COMPUTATION

Range (km)	Target+Path Radlance Value*			Bckground Total Rad.	Target+Path.Rad.Temperature Value			Background Rad. Temp.value	ATD Values		
	Target has Dpol=0%	Target has Dpol=2%	Target has Dpol=8%		Target has Dpol=0%	Target has Dpol=2%	Target has Dpol=8%		Target has Dpol=0%	Target has Dpol=2%	Target has Dpol=8%
0.31	17.06532	17.37032	18.28531	15.97376	257.170	257.980	260.000	254.19	2.980	3.790	5.810
0.599	17.08326	17.36651	18.03392	15.73804	257.218	257.968	259.710	253.53	3.688	4.438	6.180
1.728	17.14936	17.36933	17.84187	15.398009	257.397	257.970	259.217	252.56	4.837	5.410	6.657
2.874	17.18623	17.37515	17.8599	15.548708	257.495	257.994	259.260	252.99	4.505	5.004	6.270
3.45	17.22743	17.38276	17.84874	15.814957	257.607	258.016	259.235	253.745	3.862	4.271	5.490
4.801	17.27131	17.39128	17.75121	15.332169	257.707	258.038	258.980	252.38	5.327	5.658	6.600
5.408	17.28835	17.39551	17.71698	15.572916	257.767	258.047	258.890	253.06	4.707	4.987	5.830
5.773	17.29672	17.39689	17.69738	15.691773	257.784	258.049	258.840	253.4	4.384	4.649	5.440
6.677	17.31773	17.40271	17.65766	15.941019	257.842	258.060	258.730	254.1	3.742	3.960	4.630
7.921	17.34032	17.40838	17.61255	16.210508	257.900	258.080	258.618	254.848	3.052	3.232	3.770
8.738	17.35257	17.41153	17.58841	16.363867	257.934	258.087	258.553	255.27	2.664	2.817	3.283
9.748	17.36554	17.41504	17.56354	16.535192	257.965	258.095	258.487	255.734	2.231	2.361	2.753
11.03	17.37923	17.41902	17.53837	16.699232	258.005	258.105	258.425	256.187	1.818	1.918	2.238
12.71	17.39385	17.42387	17.51392	16.87607	258.040	258.120	258.360	256.665	1.375	1.455	1.695
15.03	17.40818	17.42869	17.49024	17.051097	258.080	258.134	258.298	257.134	0.946	1.000	1.164
18.47	17.42257	17.4344	17.4699	17.214704	258.112	258.143	258.244	257.565	0.547	0.578	0.679
20.92	17.42967	17.43772	17.46188	17.286879	258.130	258.158	258.220	257.759	0.371	0.399	0.461
24.24	17.43048	17.43518	17.44928	17.35119	258.138	258.159	258.188	257.93	0.208	0.229	0.258
29.09	17.4457	17.44803	17.45503	17.403497	258.172	258.180	258.200	258.07	0.102	0.110	0.130
29.71	17.53651	17.53864	17.54501	17.408125	258.176	258.191	258.202	258.08	0.096	0.111	0.122
30.36	17.52852	17.53044	17.53619	17.412552	258.183	258.192	258.204	258.094	0.089	0.098	0.110
31.05	17.52137	17.52309	17.52828	17.416861	258.184	258.193	258.205	258.105	0.079	0.088	0.100
31.78	17.51461	17.51615	17.52079	17.421	258.187	258.194	258.207	258.115	0.072	0.079	0.092
32.56	17.50911	17.5105	17.51467	17.425052	258.190	258.195	258.208	258.124	0.066	0.071	0.084
33.39	17.50316	17.50439	17.50807	17.428983	258.192	258.196	258.209	258.133	0.059	0.063	0.076
34.28	17.49808	17.49916	17.5024	17.432838	258.194	258.200	258.210	258.143	0.051	0.057	0.067
35.23	17.49345	17.4944	17.49722	17.436552	258.197	258.202	258.213	258.152	0.045	0.050	0.061
36.26	17.48926	17.49007	17.49251	17.440206	258.200	258.204	258.216	258.1605	0.039	0.043	0.055
37.38	17.48513	17.48581	17.48786	17.443835	258.207	258.207	258.218	258.175	0.032	0.032	0.043
38.6	17.4819	17.48247	17.48418	17.447413	258.210	258.210	258.220	258.1807	0.029	0.029	0.039

* Target Dpol values were assumed as horizontally polarized.

APPENDIX K

ATD - DELTA W COMPARISON

Range (km)	Target+path.rad.value (0%)	Target+path.rad.value (2%)	Target+path.rad.value (8%)	Bckground Total Radiance	Delta W (0% Dpol)	Delta W (2% Dpol.)	Delta W (%8 Dpol.)
0.310	17.0653	17.3703	18.2853	15.9738	1.0916	1.3966	2.3115
0.599	17.0833	17.3665	18.0339	15.7380	1.3452	1.6285	2.2959
1.728	17.1494	17.3693	17.8419	15.3980	1.7513	1.9713	2.4439
2.157	17.1707	17.3719	17.9527	15.6283	1.5424	1.7436	2.3244
2.874	17.1862	17.3752	17.8599	15.5487	1.6375	1.8264	2.3112
3.450	17.2274	17.3828	17.8487	15.8150	1.4125	1.5678	2.0338
4.317	17.2574	17.3889	17.7832	16.0462	1.2112	1.3427	1.7371
4.801	17.2713	17.3913	17.7512	15.3322	1.9391	2.0591	2.4190
5.408	17.2884	17.3955	17.7170	15.5729	1.7154	1.8226	2.1441
5.773	17.2967	17.3969	17.6974	15.6918	1.6050	1.7051	2.0056
6.677	17.3177	17.4027	17.6577	15.9410	1.3767	1.4617	1.7166
7.921	17.3403	17.4084	17.6125	16.2105	1.1298	1.1979	1.4020
8.738	17.3526	17.4115	17.5884	16.3639	0.9887	1.0477	1.2245
9.748	17.3655	17.4150	17.5635	16.5352	0.8303	0.8799	1.0284
11.029	17.3792	17.4190	17.5384	16.6992	0.6800	0.7198	0.8391
12.711	17.3939	17.4239	17.5139	16.8761	0.5178	0.5478	0.6379
15.030	17.4082	17.4287	17.4902	17.0511	0.3571	0.3776	0.4391
18.469	17.4226	17.4344	17.4699	17.2147	0.2079	0.2197	0.2552
20.922	17.4297	17.4377	17.4619	17.2869	0.1428	0.1508	0.1750
24.240	17.4305	17.4352	17.4493	17.3512	0.0793	0.0840	0.0981
29.087	17.4457	17.4480	17.4550	17.4035	0.0422	0.0445	0.0515
29.707	17.5365	17.5386	17.5450	17.4081	0.1284	0.1305	0.1369
30.360	17.5285	17.5304	17.5362	17.4126	0.1160	0.1179	0.1236
31.050	17.5214	17.5231	17.5283	17.4169	0.1045	0.1062	0.1114
31.782	17.5146	17.5162	17.5208	17.4210	0.0936	0.0952	0.0998
32.559	17.5091	17.5105	17.5147	17.4251	0.0841	0.0855	0.0896
33.388	17.5032	17.5044	17.5081	17.4290	0.0742	0.0754	0.0791
34.276	17.4981	17.4992	17.5024	17.4328	0.0652	0.0663	0.0696
35.229	17.4935	17.4944	17.4972	17.4366	0.0569	0.0578	0.0607
36.259	17.4893	17.4901	17.4925	17.4402	0.0491	0.0499	0.0523
37.378	17.4851	17.4858	17.4879	17.4438	0.0413	0.0420	0.0440
38.603	17.4819	17.4825	17.4842	17.4474	0.0345	0.0351	0.0368

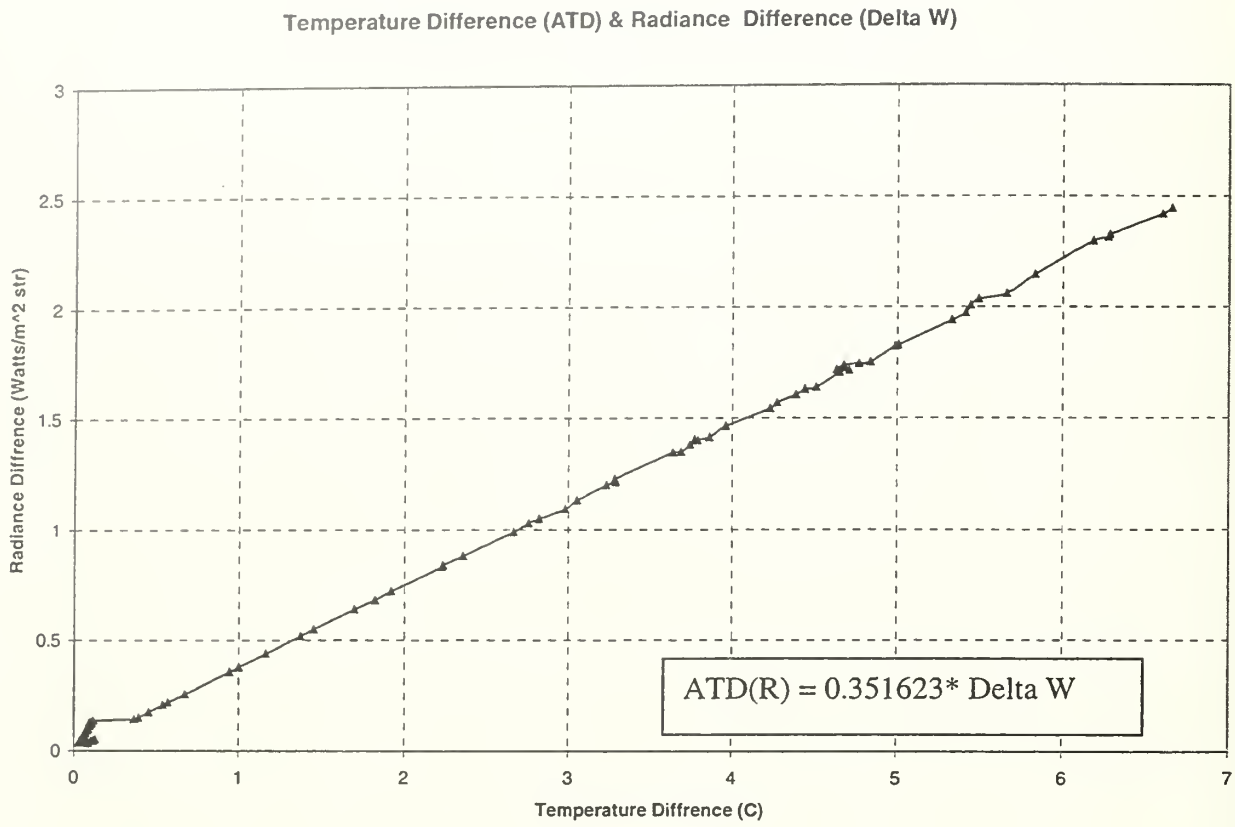
Temperature Difference (ATD) & Radiance Difference (Delta W)
Radiance Diffrence (Watts/m^2 str)
Temperature Diffrence (C)
ATD(R) = 0.351623* Delta W
0
0.5
1
1.5
2
2.5
3
0
1
2
3
4
5
6
7

LIST OF REFERENCES

1. Cooper A.W., "Polarization Issues in Infrared Imaging of Ships Against Background," *Proceedings of the DDR&E Electromagnetic/Electro-Optic Performance Prediction and Products Symposium*, Monterey, 1997
2. Cooper A.W. and Crittenden E.C., *Electro-Optic Sensors and Systems*, Manuscript, Naval Postgraduate School, September 1998
3. Kaplan H., *Practical Applications of Infrared Thermal Sensing and Imaging Equipment*, SPIE Optical Engineering Press, Washington, 1993
4. Wolfe L. W. and Zissis J. G., *The Infrared Handbook*, Office of Naval Research, Department of Navy, Washington, DC, 1978
5. Khalil S. and Hovanessian S.A., *Introduction to Electro-Optical Imaging and Tracking Systems*, Artech House, Inc., MA, 1993
6. Hackforth L.H., *Infrared Radiation*, McGraw-Hill Book Company, Inc., New York, 1960
7. Kruse P.W., McGlauchlin L.,and McQuistan R.B., *Elements of Infrared Technology*, John Willey & Sons, Inc. New York, 1962

8. Jamieson J.A., McFee R.H., Plass G.N., Grube R.H., and Richards R.G., *Infrared Physics and Engineering*, McGraw-Hill Book Company, 1963

9. Wollenweber G. F., "Thermal Background Modeling and Its Use in Science and Technology", *SPIE Proceedings*, Vol.1687, 1992

10. Zeisse C.R., *SeaRad, A Sea Radiance Prediction Code, Technical Report* 1702, Naval Command, Control, and Ocean Surveillance Center, RDT and E Division, November 1995

11. Accetta J.S., Shumaker D.L., *The Infrared and Electro-Optical Systems Handbook*, Vol.6, SPIE Optical Engineering Press and Infrared Information Analysis Center, 1996

12. Jordan D.L., Lewis G., "Infrared Polarization Signatures," *AGARD Meeting on Atmospheric Propagation Effects Through Natural and Man-made Obscurants for Visible to MM-Wave Radiation*, May 1993

13. Morey B., Ellis K., Perry D., and Gleichman K., *Infrared Signature Simulation of Military Targets*, Infrared Information Analysis Center Environmental Research Institute of Michigan, September 1994

14. Goksin C., *Evaluation of Tactical Decision Programs for Predictions of Field Performance of IR Sensors*, Master`s Thesis, Naval Postgraduate School, September 2000

15. Cooper A.W., Lentz W.J., Walker P.L., and Chan P.M., "Infrared Polarization Measurements of Ship Signatures and Background Contrast," *SPIE Proceedings*, Vol. 2223, 1994

16. Gregoris D.J., Yu S., Cooper A.W., and Milne E.A., "Polarization Measurements of Sun Glint from the Sea Surface", *SPIE Procedings*, Vol.1687, 1992

17. Nee S.M.F., Cole T., Yoo C., and Burge D., " Characterization of Infrared Polarizers", *SPIE Procedings*, Vol. 3121, 1997

18. Lagaras S. E., *Modeled Detection And Recognition Range For A Polarization Filtered FLIR Sensor*, Master's Thesis, Naval Postgraduate School, June 1999

19. Maxwell J.R., Beard J.L., and Due C., "Polarization In The Thermal Infrared", paper presented at the Workshop on Detection, Discrimination, and Classification of Targets in Clutter, 13-15 November 1990

20. Walker P.L., Lentz W.J., Cooper A.W., "Atmospheric and Sea State Dependence of Polarized Infrared Contrast", *SPIE Proceedings*, Vol. 2469, April 1995

21. Accetta J.S., Shumaker D.L., *The Infrared and Electro-Optical Systems Handbook*, Vol.4, SPIE Optical Engineering Press and Infrared Information Analysis Center, 1996

22. Shumaker D.L., Wood J.T. and Thacker C.R., *Infrared Imaging Systems Analysis,* The Environmental Research Institute of Michigan, 1993

23. Guimares F.C.E., *Investigation of Minimum Resolvable Temperature Difference Formulation For Polarized Thermal Imaging Range Prediction,* Master's Thesis, Naval Postgraduate School, September 1999

24. Driggers R., Cox P., and Edwards T., *Introduction to Infrared and Electro-Optical Systems,* Artech House Inc., MA, 1999

25. ThermoAnalytics Inc., "MuSES 5.0 Manual",94X Airport Road P.O. Box 66, Calumet, Mi 49913, May 2000

26. Cox C., and Munk W., "Bulletin of The Scripps Institution of Oceanography", Vol. 6, 1956

27. Yu C., *Estimate of Maximum Detection Range For FLIR From EOMET95 Measurement Data,* Master's Thesis, Naval Postgraduate School, December 1997

INITIAL DISTRIBUTION LIST

No. Copies

1. Defense Technical Information Center. 2
   87725 John J. Kingman Rd., STE 0944
   Ft. Belvoir, VA 22060-6218

2. Dudley Knox Library 2
   Naval Postgraduate School
   411 Dyer Rd.
   Monterey, CA 93943-5101

3. Engineering and Technology Curricular Office 1
   Code 34
   Naval Postgraduate School
   Monterey, CA 93943-5107

4. Professor Alfred W. Cooper, Code PH/Cr 3
   Department of Physics
   Naval Postgraduate School
   Monterey, CA 93943-5117

5. Professor Ron J. Pieper, Code EC/Pr 1
   Department of Physics
   Naval Postgraduate School
   Monterey, CA 93943-5117

6. Dr. Andreas K. Goroch 1
   Naval Research Laboratory
   Monterey, CA, 93943-5101

7. Kara Kuvvetleri Komutanligi 1
   Personel Daire Baskanligi
   06200 Bakanliklar, Ankara
   Turkey

8. Kara Kuvvetleri Komutanligi Kutuphanesi 1
   06200 Bakanliklar, Ankara
   Turkey

9. Kara Harp Okulu Komutanligi Kutuphanesi 1
   06654 Bakanliklar, Ankara
   Turkey

10. Kara Kuvvetleri Egitim ve Doktrin Komutanligi-EDOK-Kutuphanesi 1
Balgat, Ankara
Turkey

11. Mehmet Yildirim, 1st Lieutenant Turkish Army 2
Kara Kuvvetleri Komutanligi
Teknik ve Prj. Yon. D. Bsk.ligi
Tank Sb. Pl.Sb.
Bakanliklar, Ankara
Turkey